

INFORMATION TO USERS

This manuscript has been reproduced from the microfilm master. UMI films the text directly from the original or copy submitted. Thus, some thesis and dissertation copies are in typewriter face, while others may be from any type of computer printer.

The quality of this reproduction is dependent upon the quality of the copy submitted. Broken or indistinct print, colored or poor quality illustrations and photographs, print bleedthrough, substandard margins, and improper alignment can adversely affect reproduction.

In the unlikely event that the author did not send UMI a complete manuscript and there are missing pages, these will be noted. Also, if unauthorized copyright material had to be removed, a note will indicate the deletion.

Oversize materials (e.g., maps, drawings, charts) are reproduced by sectioning the original, beginning at the upper left-hand corner and continuing from left to right in equal sections with small overlaps. Each original is also photographed in one exposure and is included in reduced form at the back of the book.

Photographs included in the original manuscript have been reproduced xerographically in this copy. Higher quality 6" x 9" black and white photographic prints are available for any photographs or illustrations appearing in this copy for an additional charge. Contact UMI directly to order.

UMI

University Microfilms International
A Bell & Howell Information Company
300 North Zeeb Road, Ann Arbor, MI 48106-1346 USA
313/761-4700 800/521-0600

SEA LEVEL RISE AND COASTAL EROSION IN THE HAWAIIAN ISLANDS

**A DISSERTATION SUBMITTED TO THE GRADUATE DIVISION OF THE
UNIVERSITY OF HAWAII IN PARTIAL FULFILLMENT OF THE
REQUIREMENTS FOR THE DEGREE OF**

DOCTOR OF PHILOSOPHY

IN

OCEAN ENGINEERING

MAY 1995

By

Dongchull Jeon

Dissertation Committee:

**Franciscus Gerritsen, Chairperson
Charles H. Fletcher III
Edward D. Stroup
Hans-Jurgen Krock
Kwok Fai Cheung**

UMI Number: 9532594

UMI Microform 9532594

Copyright 1995, by UMI Company. All rights reserved.

**This microform edition is protected against unauthorized
copying under Title 17, United States Code.**

UMI

**300 North Zeeb Road
Ann Arbor, MI 48103**

ACKNOWLEDGEMENTS

I wish to thank Prof. Franciscus Gerritsen for giving me the chance to synthesize both scientific and engineering aspects of the oceans. Without his invaluable advice and guidance that he has given me throughout the years of my stay at Dept. of Ocean Engineering, Univ. of Hawaii, this study could not have been made.

I also wish to thank the following who deserve my heartfelt gratitude:

To my other committee members Drs. C. Fletcher, H. Krock, E. Stroup, and K.F. Cheung for giving me important suggestions to improve my manuscript.

To Dr. Klaus Wyrтки for teaching me the essence about a physical oceanographer's attitude and intuition.

To Dr. Charles Bretschneider for encouraging me to get fruitful results throughout my study.

To Mr. P. Caldwell at TOGA Sea Level Center, Univ. of Hawaii for offering me sea-level and wave data and computer programming which are the primary essence of this study.

To Dr. N. Wang for cordially offering me his computer program to strengthen this study in a modelling aspect.

Most especially to my dear wife, for I could not have continued and enjoyed my study without her enduring love and encouragement.

ABSTRACT

Time series and the power spectral distributions of relative sea levels are analyzed at selected tide-gauge stations in the western and central North Pacific between equator and about 30°N, in association with different time scales of motions. Coastal response to these sea-level dynamics is discussed in detail, based on the aerial photographs of shoreline changes. Wave climate around the Hawaiian Islands as well as surf conditions on Oahu are examined for simulating cross-shore beach erosion processes with an energetics-based sediment transport model.

Long-term trend of relative sea-level rise during the past several decades (+1 to +5 cm/decade at most of the tide-gauge stations) is primarily affected by the local tectonism such as volcanic loading, plate movement and reef evolution, and subduction at the plate boundaries. Continual volcanic loading at Kilauea, Hawaii results in consequential subsidence of the Hawaiian Islands. Secondary reason for sea-level rise is the thermal expansion of sea surface waters due to global warming by increasing greenhouse gases, which may be potentially more significant in the near future.

Interannual sea-level fluctuations, associated with *ENSO* (El Niño Southern Oscillation) phenomena, seem to be the primary factor to cause serious beach erosion (up to 10 times the long-term trend). Mean *annual* cycle of sea level ($H \approx 10$ cm) and alternate annual wave conditions are the main causes of the cross-shore oscillation of sediment transport, although there is still some loss of sediments to deep-water region.

Short-term change of beach profiles is basically caused by incoming wave conditions as well as sea-level height, sediment characteristics, and underlying geology. Simulations by a cross-shore sediment transport model show that higher waves result in faster offshore transport and deeper depth of active profile change, and that beach recovery process is usually much slower than the erosion process, especially after a storm surge. Deep erosion during a storm surge can not be recovered for much longer duration by mild post-storm waves, but may be partly recovered by non-breaking long waves such as longer-period swells.

TABLE OF CONTENTS

ACKNOWLEDGEMENTS	iii
ABSTRACT	iv
LIST OF TABLES	viii
LIST OF FIGURES	x
LIST OF ABBREVIATIONS AND SYMBOLS	xiii
1. INTRODUCTION	1
2. SEA-LEVEL RISE IN THE HAWAIIAN ISLANDS	17
3. METHODS AND ANALYSES	36
3.1. AVAILABLE DATA	36
3.1.1. Tide-gauge Records	36
3.1.2. Aerial Photographs	41
3.1.3. Waves	47
3.1.4. Beach and Sediment Characteristics	53
3.2. METHODS	54
3.2.1. Mean Sea Levels	54
3.2.1.1. Filling Gaps in MSL Data	54
3.2.1.2. Linear Regression	56
3.2.1.3. Averaging and Smoothing	56
3.2.1.4. Spectral Analyses	57
3.2.2. Models	58
3.3. ANALYSES OF SEA-LEVEL CHANGES	59
4. EFFECTS OF SEA-LEVEL CHANGE ON BEACH EROSION	68

5. EFFECTS OF STORMS ON BEACH EROSION	82
5.1. GENERAL REMARKS	82
5.2. SHORT-TERM BEACH EROSION MODELS	97
5.3. SHORT-TERM FLUCTUATION	107
6. SHORELINE CHANGES AND BEACH RECOVERY	115
6.1. SHORELINE CHANGES IN THE HAWAIIAN ISLANDS	115
6.2. CASE STUDIES	122
6.2.1. Waimea Bay Beach, Oahu	122
6.2.2. Hapuna Beach, Hawaii	136
6.3. BEACH RECOVERY	147
7. COASTAL ZONE MANAGERMENTS	160
7.1. ARTIFICIAL NOURISHMENT	161
7.2. HARD SOLUTIONS	163
7.3. MANAGEMENT STRATEGIES	165
8. CONCLUSIONS	167
APPENDICES.....	173
REFERENCES	181

LIST OF TABLES

1.1	Estimated contributions to sea level rise	12
2.1	Lengths of the coastlines and the beaches in the major Hawaiian Islands	18
2.2	Sea-level trend of rise in the Hawaiian Islands ...	29
2.3	Projected sea-level rise in 2040 in the Hawaiian Islands	30
2.4	Mean monthly sea-level values and standard deviations of the annual cycles in the Hawaiian Islands	31
3.1	Locations and lengths of tide-gauge data at selected island stations in the North Pacific	37
3.2	Locations and numbers of measured transects of aerial photographs in major Hawaiian Islands	42
3.3	The mean sea-level differences of the annual and interannual oscillations and the rate of sea-level rise in the Hawaiian Islands	60
5.1	Average wave heights and periods for different seasons and for different wave types	91
6.1	Average sediment size at Waimea Bay Beach, Oahu and at Hapuna Beach, Hawaii	124
6.2	Average sediment size of Hawaiian beach sands during winter and during summer	125
6.3	Changes of vegetation line from aerial photos and converted values with annual cycle of MSL	125
6.4	Interannual rising trends of sea-level at Honolulu Harbor, Oahu	128
6.5	Interannual rising trends of sea level at Hilo ...	139

6.6	Volume transports from measured beach profiles on Waimea Bay, Oahu and Hapuna Beach, Hawaii	142
6.7	Contributions of sea-level changes and waves to the shoreline retreat	158
6.8	Calculated shoreline retreat for different beach-face slopes	159
A.1	Temperature-dependency of the density of standard seawater at an atmospheric pressure	174
A.2	Mean annual trends of shoreline changes in the Hawaiian Islands	175

LIST OF FIGURES

1.1	Global mean temperature variations on three different time scales since Pleistocene	3
1.2	Southern oscillation index with annual mean atmospheric pressure, and schematic diagrams of the air-sea coupling before and during El Niño	5
1.3	Tilting of the Philippine Islands indicated by relative land movement at 6 tide-gauge stations	7
1.4	Concentrations of greenhouse gases	9
1.5	Predicted increase in global mean temperature and sea-level rise	11
2.1	Percentage of the trade winds as monthly averages from ship's observations	23
2.2	Long-term sea level trend, 12-month running mean, monthly sea levels in the Hawaiian Islands...	24
2.3	Model for island development on the Pacific plate	28
2.4	Power spectral density distributions of sea levels in the Hawaiian Islands	33
3.1	Standard deviation of monthly sea level differences as a function of distance in the Hawaiian Islands, and a time series of monthly sea level anomalies at Honolulu and Mokuoloe, Oahu	40
3.2	Locations of the selected tide-gauge stations, NOAA wave buoy (51001), and Waimea Bay Beach in Oahu and Hapuna Beach in Hawaii	48

3.3	Example of time series with low frequency drift and the spectrum of the record	52
3.4	Example of Weight-Folding Method for a time-series of monthly sea levels with a gap of 11 months	55
3.5	Long-term trend, 12-month running mean, and monthly sea levels at Truk, Kwajalein, Wake	62
3.6	Mean annual cycles of monthly sea levels in the selected western Pacific islands	66
4.1	Monthly average CO ₂ concentration in dry air observed at Mauna Loa, Hawaii, and relative trend of global mean temperature	69
4.2	Schematic diagram of the relationship between sea level rise and coastal erosion by Bruun Rule	71
5.1	Schematic diagram of cross-shore sediment transport under waves	82
5.2	Ranges and mean directions of the typical wind waves around the Hawaiian Islands	86
5.3	Surf height distributions on Oahu during winter and summer	88
5.4	Deep water wave climate as annual variations of wave height at the northwest of Kauai	90
5.5	Location of the points of origin of tropical cyclones during a 20-year period	94
5.6	Hurricane tracks around the Hawaiian Islands	96
5.7	Schematic diagram of Edelman's model for idealized beach profile, and the relationship between dune erosion and storm surge height	106

5.8	Relative wave height for a slow-moving hurricane and components of the storm surge	108
5.9	Schematic diagram of maximum potential response of equilibrium profile to sea level rise	111
5.10	Amplitude and phase lag of maximum erosion for different scales of erosion time	114
6.1	Mean annual trends of shoreline changes from aerial photos in the Hawaiian Islands	118
6.2	Mean annual cycles of monthly sea levels in the Hawaiian Islands	120
6.3	Geography and bottom topography of Waimea Bay	123
6.4	Beach profile changes and cross-shore transport rates on Waimea Bay Beach during winter	133
6.5	Beach profile changes and cross-shore transport rates on Waimea Bay Beach during summer	134
6.6	Geography and bottom topography of Hapuna Bay	137
6.7	Beach profile changes and cross-shore transport rates for different waves on Hapuna Beach	143
6.8	Schematic diagram of complex wave breaking over long reef bottom in the Hawaiian Islands	147
6.9	Beach profile changes and cross-shore transport rates after storm surge on Waimea Bay Beach	150
6.10	Beach profile changes and cross-shore transport rates after storm surge on Hapuna Beach	151
6.11	Seasonal fluctuations in beach sand reservoirs for selected beaches in the Hawaiian Islands	153

LIST OF ABBREVIATIONS AND SYMBOLS

ABBREVIATIONS

DWL	Design Water Level
ENSO	El Niño - Southern Oscillation
FFT	Fast Fourier Transform
HWL	High Water Line
IPCC	Intergovernmental Panel on Climate Change
MLLW	Mean Lower Low Water
MSL	Mean Sea Level
NEC	North Equatorial Current
NECC	North Equatorial Counter Current
NOAA	National Oceanic and Atmospheric Administration
NODC	National Oceanographic Data Center
PSMSL	Permanent Service for Mean Sea Level
RSL	Relative Sea Level
TOGA	Tropical Ocean Global Atmosphere Program
WFM	Weight Folding Method

SYMBOLS

$A, A(t)$	shape parameter in Dean's function
B	berm height
c	phase speed of waves
C_0	reference concentration of suspended sediment at the bottom
C_d	sediment concentration at mean water level
C_d, C_f	drag coefficient of beach bottom
D_{50}, D_{90}	characteristic sediment diameter (indices are for mass percentages)
d_c	closure depth with a seaward limit to extreme surf-related effects throughout a typical year
D_r	displacement error due to radial distortion
D_t	displacement error due to tilt
f	focal length of camera lens
F_{drag}	drag force
g	gravity
G_B	sediment-budget terms including sources and sinks
H, H_0	deep-water (significant) wave height
Hs_{50}	median annual significant wave height
h, h_b	water depth (index $_b$ for wave breaking) or ground elevation of an object on an aerial photograph
I	immersed weight (= weight - buoyancy of fluid)
k	wavenumber
K	arbitrary number in Dean's wave-sediment parameter
L	horizontal distance of active profile zone

L_o	deep-water wavelength ($= \lambda$)
m	linear beach-face slope ($= \tan \beta$)
M	mass flux between wave crest and trough
P	pressure or decimal fraction eroded material in the Bruun Rule
r	distance between isocenter of a photograph and the point
R	shoreline recession rate
$R(t)$	beach response function to steady-state forcing
R_m	maximum shoreline erosion potential
Re	Reynolds number
R_u	wave runup height
Q	photographic scale
q_t	sediment transport rate (index t for a moment)
$\langle \rangle$	time-averaged quantity
S	salinity or vertical rise of sea level
T	wave period
T_c	characteristic time-scale in beach recovery rate
T_s	characteristic time-scale in exponential beach response (Kriebel and Dean, 1993)
U	characteristic speed of tropical cyclones
u_3^*, u_5^*	wave velocity moments
u_t	total near-bottom fluid velocity
u_m, u_{m2}	harmonic components of oscillatory (wave) velocity
u_s, u_L	individual (short) wave and infragravity (long) wave velocities
w_o	fall speed of a single grain
w_s	sediment fall speed

x_b	surf-zone width
α	thermal expansion coefficient
β	angle of beach slope
γ	ratio of wave height to water depth at breaking depth ($= H_b/h_b$)
δ	relative mean flow speed ($= u/u_m$)
e_0	reference mixing coefficient
e_b	bedload efficiency factor
e_s	suspended load efficiency factor
ζ	flight altitude of the camera in aerial photography
κ	vertical mixing gradient
λ	wavelength
μ	kinematic viscosity
ν	dynamic viscosity ($= \mu/\rho$)
θ	angle from the principal line to the radial line (clockwise) between isocenter and the point within the plane of the photograph
θ	wave angle approaching to the orthogonal of the shoreline
θ_t	angle of tilt of the photograph
ϕ	Wentworth scale for sediment grain size ($= -\log_2 [\text{mm}]$) or internal angle of friction for sediment
ρ	density of seawater
ρ_s	density of sediments
σ_H	annual standard deviation of significant wave height
ξ	characteristic rate parameter ($= 1/T_s$)

χ beach recovery rate in response to sea-level fluctuation

ψ_1, ψ_2 wave velocity moments

ω_0 the frequency of a Hippy 120 sensor ($= 2\pi/120s$) for testing low-frequency drift

CHAPTER 1

INTRODUCTION

Relative sea-level changes, both in long- and short-term scales, play a significant role in producing beach erosion and in changing other coastal processes such as longshore and cross-shore sediment transport, nearshore circulation, and wave transformation.

The major causes of relative sea-level change may be primarily classified into two categories: eustatic (or geoidal) sea-level changes and isostatic land-level changes.

Climatic variations may cause volume changes in ocean water due to steric effects, melting/freezing of land ice or freshwater input from other sources like lakes and groundwater. Relative sea-level changes have occurred with different time scales.

On time scales of 10^5 years, climatic variations are strongly related to Cenozoic climatic effects documented in the sedimentary record, which address the orientation of the earth's axis of rotation and shape of its orbit and how these affect the insolation on the earth's surface

(*Milankovitch cycle*). Hence the glaciation and deglaciation events may reflect variations in solar insolation (Emery and Aubrey, 1991).

Over the last 21,000 years, there has been a gradual global warming of about 5°C, which led to a global sea-level rise of more than 100 meters. Because of either hydroisostacy or geoidal effects, the northern Hawaiian Islands experienced a general high stand of sea level between 6,000 and 4,000 years ago (Fletcher, pers. comm., Mitrovica and Peltier, 1991).

During the past several hundred years, the *Little Ice Age* (between about 1,500 and 1,800 A.D.) created a dramatic fluctuation in global climate by lowering temperatures (IPCC, 1990). The earth is still recovering from this Little Ice Age (Fig.1.1).

The prominent climatic fluctuation today is the El Niño Southern Oscillation (ENSO) -- a coupled ocean- atmospheric, global event with a period of about 2 to 7 years, which shows its strongest effects in the Pacific Ocean. El Niño, originally named from an abnormal warming phenomenon in the southeastern Pacific Ocean around the coast of Peru, is now recognized as a large-scale global teleconnection. The Southern Oscillation relates the pressure fluctuation in the

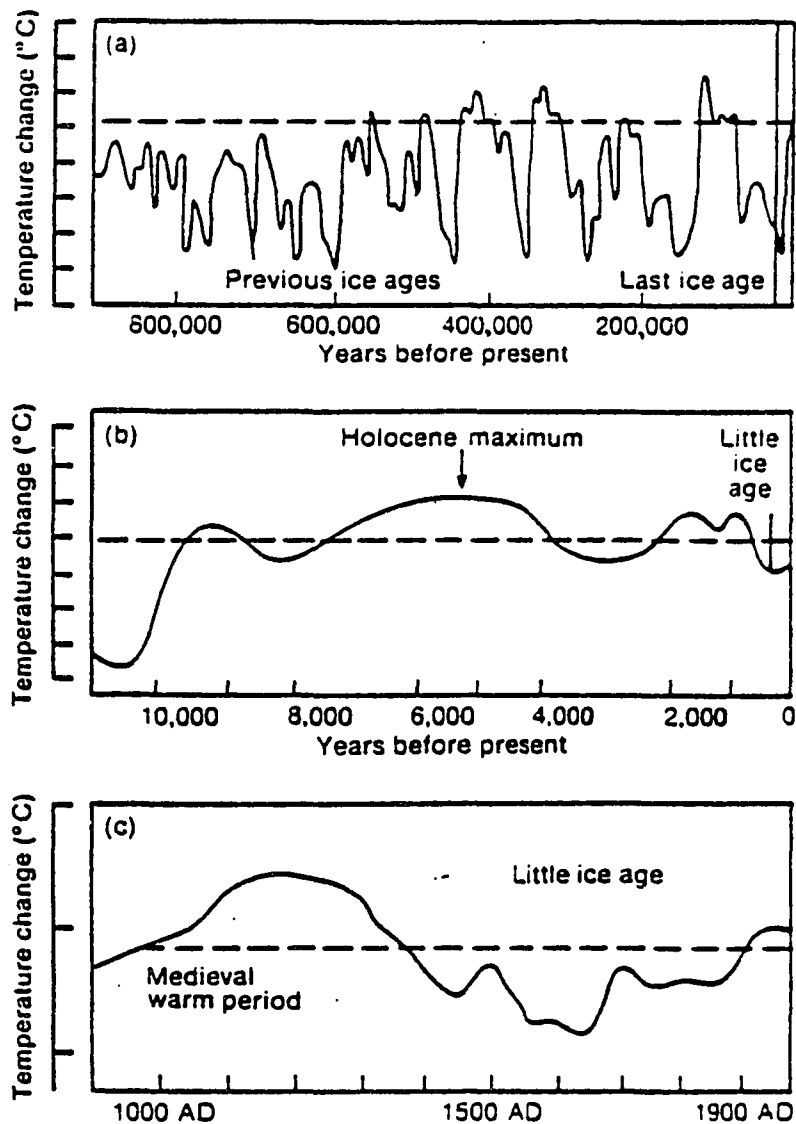
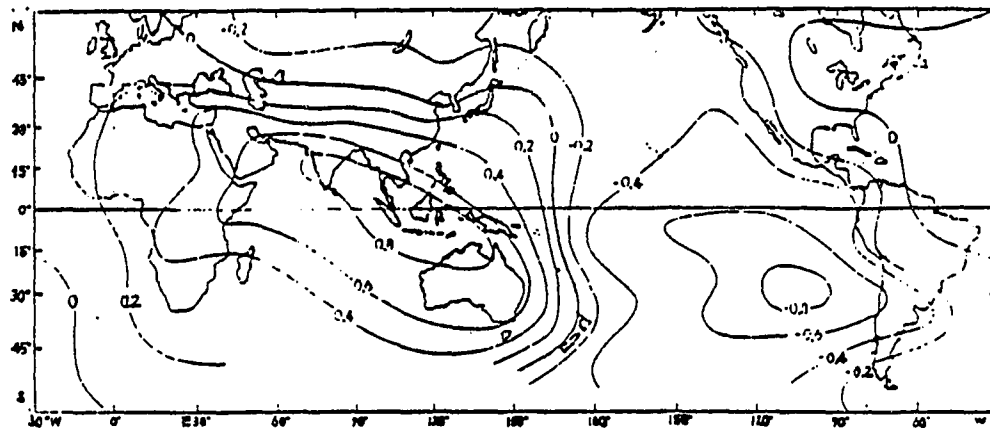


Fig.1.1. Schematic diagrams of global temperature variations since Pleistocene on three time-scales: (a) the last million years, (b) the last ten thousand years, and (c) the last thousand years. The dashed line normally represents condition near the beginning of the 20th century (after IPCC, 1990).

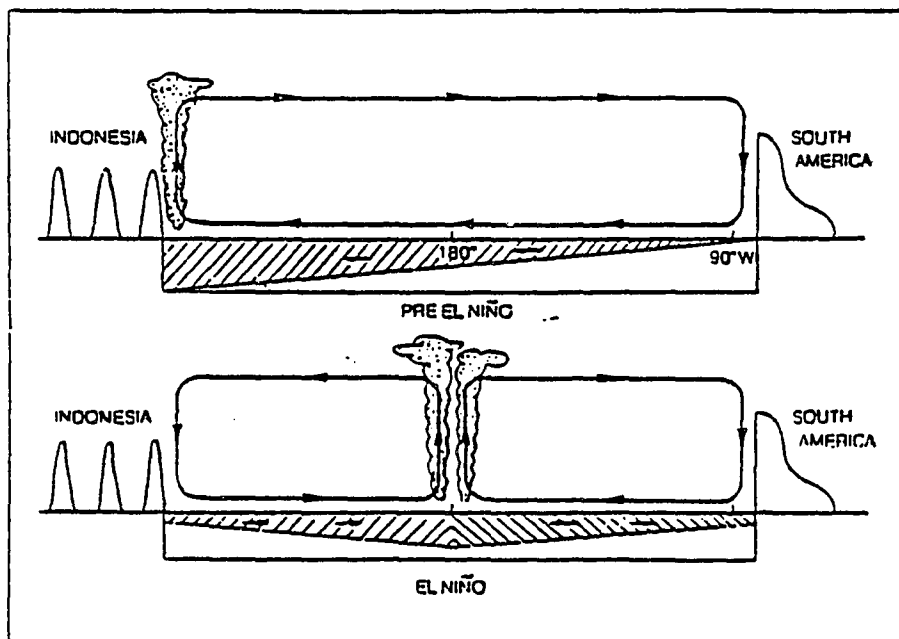
southeastern Pacific with alternating high or low pressure fields over southern Asia (Fig.1.2). The interannual variability of sea levels in response to ENSO may cause even greater impacts on coastal erosion (see Komar and Enfield, 1987) than long-term trend of sea-level rise. For instance, the 1982-83 El Niño raised the water level on the coast of Oregon by 60 cm within 12 months, which changed the shape of an inlet there due to erosion (Komar, 1986).

Atmospheric pressure and wind stress may be the major factors for changes in water level on time scales of days to months. In practice, the inverse barometric response of sea level to atmospheric pressure change is found to be a significant part of seasonal changes in high latitudes (Pattullo et al., 1955; Lisitzin, 1974).

An increase of atmospheric pressure by 1 mbar ($= 100 \text{ N m}^{-2}$) causes the depression of the sea level approximately by 1 cm. Tropical cyclones or hurricanes result in peaks of mean sea level by the combination of inverse barometric response and frictional processes. Since hurricanes are maintained by the energy that they extract from the heat in the ocean, thermal effects are very important and the input energy is redistributed within the ocean by stirring action of the storm in addition to advective effects (Gill, 1982).



(a)



(b)

Fig.1.2. (a) Southern oscillation expressed as the correlation of annual mean atmospheric pressure with Jakarta, and (b) schematic diagrams of the air-sea coupling before and during El Niño (after Wyrtki, 1975).

Isostatic land levels are changed by tectonic activities such as volcanism, sea-floor spreading, faults and subduction at the plate boundaries, glacial rebound, sediment compaction, land subsidence, and hydroisostasy on islands and continental margins. At active plate margins such as the East Pacific Rise or Mid-Atlantic Ridge, volcanic eruption from below the lithosphere, and the transform faults, may change the volume or shape of the local land masses. Due to the changes in spreading rate of the sea floor or different spreading rates of the plates, sea levels may be affected, although the effect is small over time scales of less than a million years. At active margins of the plates such as east of Japan and the Philippines, two plates collide and the oceanic plate is subducted beneath the continental plate, resulting in earthquakes and vertical movements from deformation of the land masses. Land tilting by different subsidence rates between eastern and western sides of the Philippines is shown in Fig.1.3.

One of the most important factors in determining global warming during the past century is the greenhouse effect: increasing the surface air temperature by enhanced trapping of longwaves radiated back from the earth's surface due to greenhouse gases such as CO_2 , CH_4 , N_2O , and CFCs (chlorofluorocarbons) in the atmosphere (Fig.1.4).

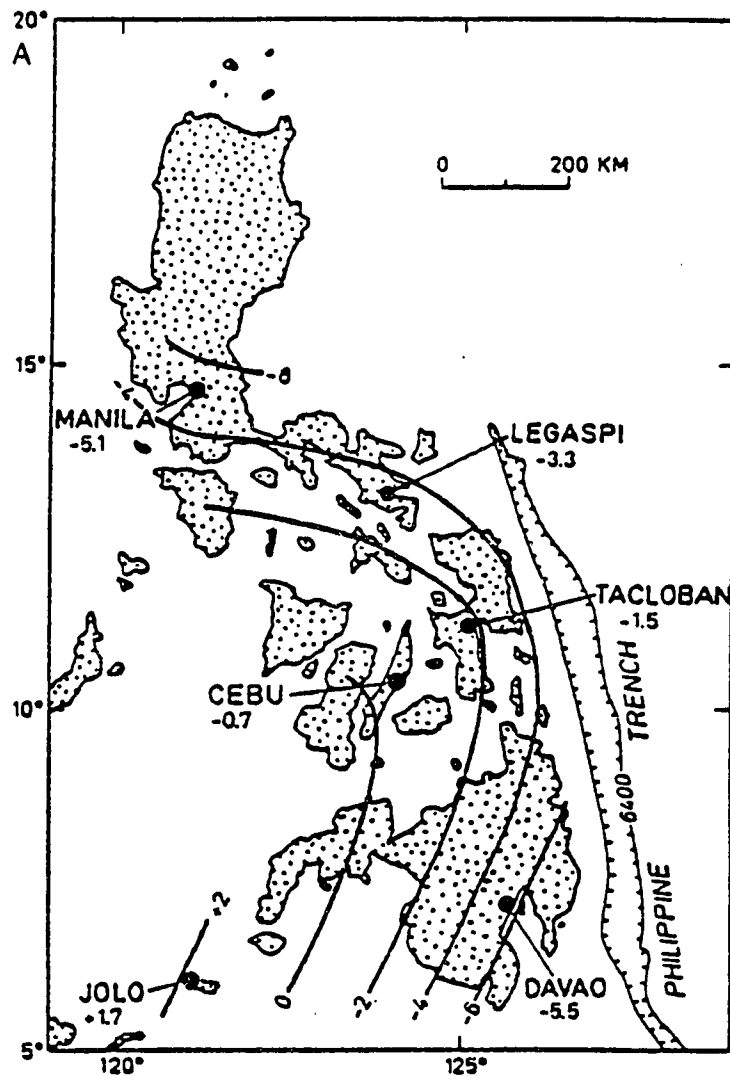


Fig.1.3. Tilting of the Philippine Islands indicated by relative land movement at 6 tide-gauge stations with 2 mm/yr intervals. (-) represents land subsidence and data are from PSMSL. (after Emery and Aubrey, 1991).

Since any body-material emits longwave radiation which is proportional to the fourth power of the body temperature¹, both the earth's surface and the glass of a greenhouse (or the atmosphere) will be heated up until an equilibrium is reached.

The most important factor causing the greenhouse effect in the atmosphere is water vapor, of which the concentration in the troposphere² is determined internally within the climate system and is not affected by human sources and sinks on a global scale. The concentration of ozone (O_3) as a second major greenhouse gas is changing in the atmosphere due to human activities, but the lack of adequate observations prevents us from accurately quantifying the climatic effect of the changes in tropospheric ozone (IPCC, 1990).

There is little doubt that global MSL (mean sea level) has risen by 10 to 30 cm during the past century. Some local tide-gauge records nonetheless have deviated from the global mean (from about 100 cm rise in 20 years in Tribeni, India, to about 160 cm fall in 14 years in Rorvik, Norway) (see Appendix I in Emery and Aubrey, 1991).

¹ Stefan-Boltzmann's law

² the lowest atmospheric layer which is characterized by temperature decrease from the ground (up to the height of 200 mbar or about 10 km) and strong vertical mixing; the other three upper layers are *stratosphere*, *mesosphere*, and *thermosphere* from the lowest.

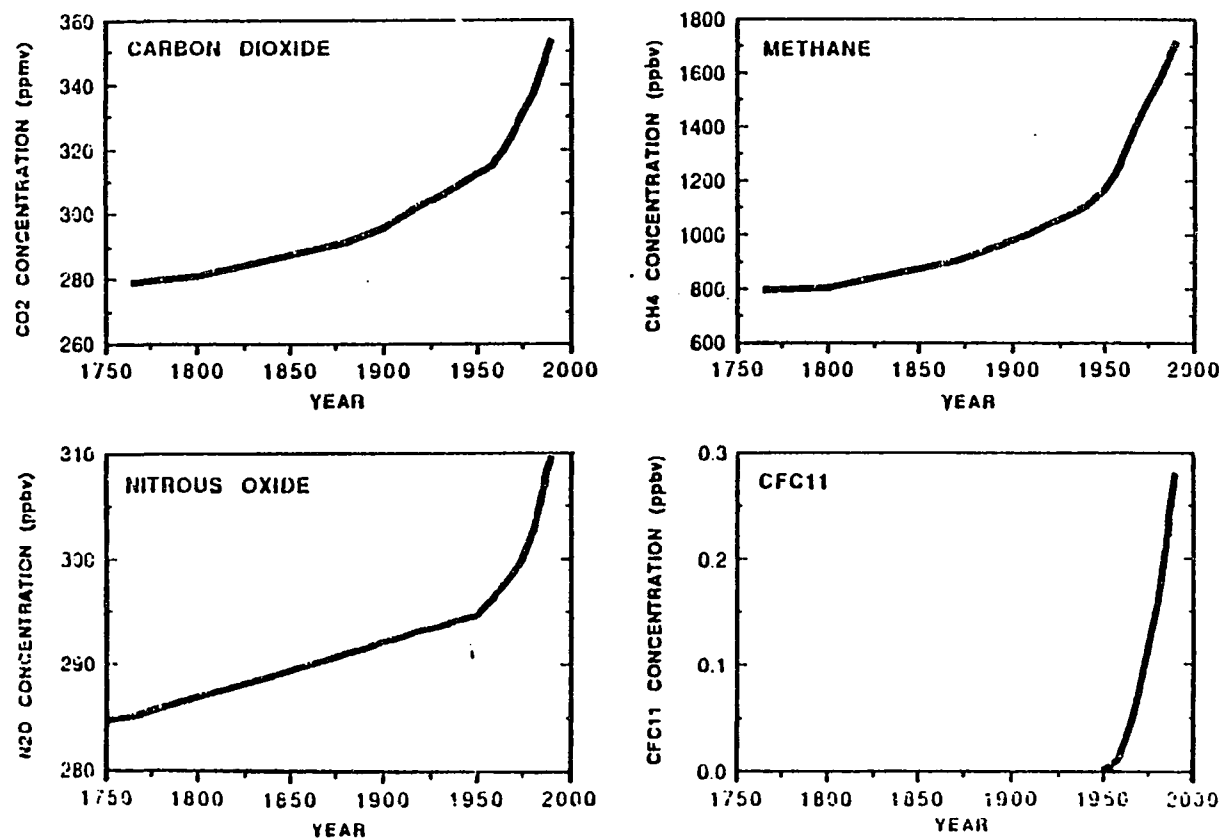


Fig.1.4. Concentrations of greenhouse gases -- carbon dioxide (CO_2), methane (CH_4), nitrous oxide (N_2O), and chlorofluorocarbons (CFCs) (after IPCC, 1990).

Due to uncertainties in the response of the atmosphere and oceans to the greenhouse effect, several scenarios have been suggested. Recently, the IPCC³ suggested that the average rate of increase of global mean temperature and the corresponding global MSL (mean sea level) rise are estimated to be about 3°C (2°C to 5°C) and about 60 cm, respectively, before the end of the next century, under the 'Business-as-Usual Scenario' (Fig.1.5). There will be significant regional deviations due to different contributing factors to sea-level rise.

But the complexities of the feedback mechanism of clouds regarding the increase of greenhouse gases in the atmosphere, the oceanic response to the increase of atmospheric temperature, and the interactions with snow and sea-ice and with the biosphere still leave the uncertainty range at least by about ± 30 cm in recent predictions of global mean sea level (see Wigley and Raper, 1992).

Four major climate-related contributing factors to global MSL rise on a time-scale of 100 years are 1) thermal expansion of the oceans, 2) glaciers and small ice caps, 3) the Greenland ice sheet, and 4) the Antarctic ice sheet.

If the IPCC predictions are correct, sea-level rise will accelerate over the next century. And the expansion of

³ Intergovernmental Panel on Climate Change, 1990

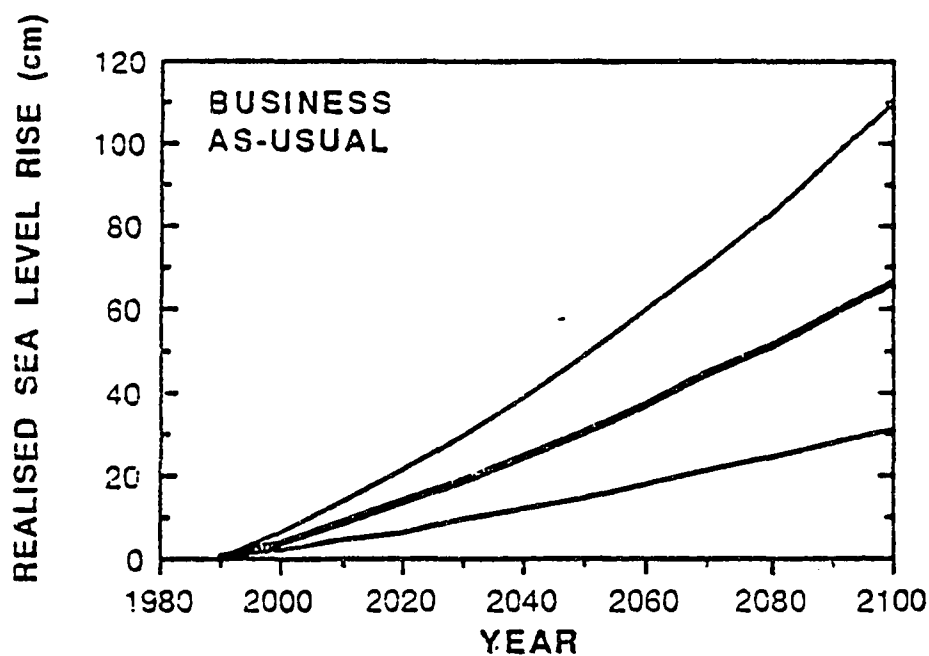
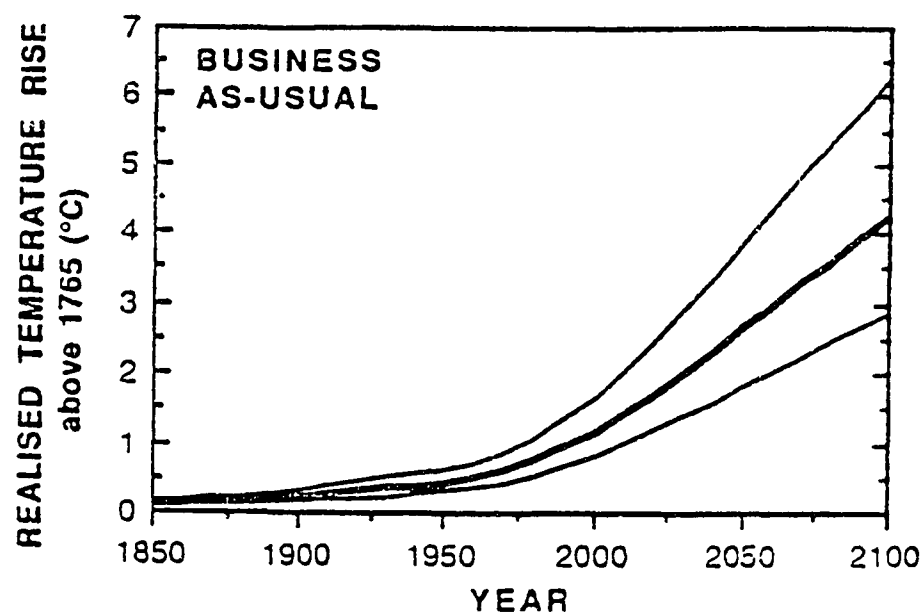


Fig.1.5. (a) Simulation of the increase in global mean temperature from 1850 to 1990 due to observed increases in greenhouse gases and predictions between 1990 and 2100, and (b) the predicted sea-level rise showing the best estimate and range, resulting from the Business-as-Usual emissions (after IPCC, 1990).

the tropics due to global warming may lead to an increase of the frequency and intensity of tropical storms and hurricanes (Wyrteki, 1990). Estimated contributions to sea level rise over the past 100 years and for the near future are shown in Table 1.1.

Table 1.1. Estimated contributions to sealevel rise during the past 100 years (upper) and between 1985 and 2030 (lower) in cm. Values in () are low and high estimates based on IPCC scenarios.

factors	past 100 years	1985 - 2030
thermal expansion	4 cm (2 to 6 cm)	10.1 cm (6.8 to 14.9 cm)
mountain glaciers	4 cm (1.5 to 7 cm)	7.0 cm (2.3 to 10.3 cm)
Greenland ice	2.5 cm (1 to 4 cm)	1.8 cm (0.5 to 3.7 cm)
Antarctic ice	0 (- 5 to 5 cm)	- 0.6 cm (- 0.8 to 0 cm)
Total	10.5 cm (-0.5 to 22 cm) (15 \pm 5 cm)*	18.3 cm (8.7 to 28.9 cm)

* observed values of global MSL rise during the past 100 years

There have been extensive efforts to reduce the range of uncertainty in the prediction of future climate and sea-

level changes. Estimates by IPCC working groups (IPCC, 1990) are the most recent collaborative outputs, and hence assumed to be the best predictions presently available. Based on these estimates of global mean sea-level rise, local rates of relative sea-level change in the Hawaiian Islands, as well as in other selected North Pacific islands, may be interpreted as to their possible causes.

The impact of short-term events such as hurricanes and tropical storms are also significant on coastal erosion. Storm waves are usually associated with wave set-up and higher tides, and may erode part of the dunes. But it may take fairly long (up to several years) to be recovered. The erosional effect by storm waves could be enhanced by the raised sea level; the beach erosion is maximized by the storm waves at the maximum phase of sea level fluctuations from daily to interannual time-scales. But quantitative analysis of beach erosion due to storm waves has been carried out mostly by model results, not by measurements.

Shoreline changes due to cross-shore and longshore sediment transport are a response of the coast to oceanic forcing such as wind waves, tidal fluctuations, and storm surges. Shoreline changes in this study will be examined by:

- 1) historical aerial photographic analysis,
- 2) analysis of previous measurements of waves, and sediment characteristics at Hawaiian beaches,
- 3) beach profile response models, based on the Bruun Rule, for long-term trend and interannual oscillation (Bruun, 1962; Dean and Maurmeyer, 1983) as well as for short-term variation such as due to storm surges (Kriebel and Dean, 1993),
- 4) cross-shore sediment transport rates and beach profile changes on a few selected beaches with an energetics-based transport model by Bailard (1984),
- 5) beach recovery rates for model storm waves and sea-level fluctuation,
- 6) quantitative analysis of contributing factors to beach erosion with different time scales,

From tide-gauge records and aerial photographs, interannual trends of sea-level fluctuation and mean annual oscillation superimposed on a linear long-term trend, from monthly mean sea-level values, and the corresponding land responses as shoreline changes are discussed in detail.

Time-series of daily MSL, winds and wave heights for short-time scale fluctuations of sea level and land responses are examined. Correlation between storms and shoreline changes are also calculated before and after storm events.

The Bruun Rule is applied to long-term trend, interannual and annual sea-level fluctuations, due to its simple relationship between sea-level rise and coastal erosion. The concepts of equilibrium beach profiles (Bruun, 1954; Dean, 1977; Bodge, 1992; Pruszek, 1993) and closure depths are discussed.

Short-term beach erosion was simulated by Bailard's model (1984) at selected Hawaiian beaches. This model does not need any information about vertical profile of sediment concentration in seawater but needs only near-bottom flow velocity, which can be calculated from the input forcing function (wave height and period). Therefore, it seems attractive to use the energetics-based sediment transport model (Bagnold, 1966; Bailard, 1984) when we want to know the short-term relationship between input energy flux and bottom profile change, although there are many assumptions in the model. There has been no verification of the model results by field measurements.

Based on the above measurements and computations, local information regarding the rate of relative sea-level rise and its impact on coastal erosion is described for Hawaiian beaches. Calculation of cross-shore sediment transport processes for selected Hawaiian beaches will further illuminate the importance of characteristic time scales for the erosive and regenerative developments.

CHAPTER 2
SEA-LEVEL RISE
IN THE HAWAIIAN ISLANDS

The Hawaiian Archipelago stretches about 1,500 miles from west-northwest, Kure Island, to east-southeast, the Island of Hawaii, which is the youngest island and still growing. They have been formed by successive volcanic activity, which is believed to be driven by the northwestward drift of the Pacific lithospheric plate while the *hot spot* in the asthenosphere⁴ stays fixed. Continual volcanic loading at Kilauea, Hawaii, has made both the island itself and the neighboring islands subside from isostatic adjustment. Hence the subsidence rate is the largest at the Island of Hawaii (+2.51 mm/yr at Hilo), second largest at the Island of Maui (+1.04 mm/yr at Kahului), and relatively smaller at the Islands of Oahu (+0.15 mm/yr at Honolulu) and Kauai (+0.33 mm/yr at Nawiliwili), although these values are subject to a large uncertainty.

⁴ one of the earth's interior layers classified by the plate tectonic processes, which is at a depth range from about 100 to 1,000 km in between *lithosphere* (upper rigid plate) and *mesosphere* (inner earth).

The total lengths of coastlines and beaches in the six major Hawaiian Islands are as follows:

Table 2.1. The lengths (in miles) of the coastlines and the beaches, and the ratio of beaches to coastline in the major six Hawaiian Islands.

island	coastline	total beaches	beach ratio
Kauai	85	35	41%
Oahu	129	50	39%
Molokai	106	23	22%
Lanai	52	18	35%
Maui	159	31	19%
Hawaii	306	19	6%

Many drowned river valleys are found around the coasts of Kauai. Oahu has more coastal plain and reefs and fewer sea cliffs than the other islands. About half of the coastline of Molokai is bedrock and sea cliff, and 25% of the island is mud flat mangrove swamps, gravel, and artificial structure. Most of the coastlines are composed of bedrock -- about 70% (110 miles) in Maui and 90% (275 miles) in Hawaii (Walker, 1974).

Coral reefs grow in tropical waters where seawater temperature exceeds about 18°C and water depth is limited to less than a few tens of meters due to the need of sunlight. Even in low latitudes, it is difficult for coral reefs to grow along the west coasts of continents where upwelling is prevailing and hence surface water is filled with subsurface cold water lower than 18°C for part of the year. This is because the earth's rotation effect (or *Coriolis effect*) causes the wind-driven surface layer of the eastern boundary currents (e.g., California Current, Peru Current in the Pacific Ocean; Canary Current and Benguela Current in the Atlantic Ocean) to move seawards and then subsurface cold water rises to replace the surface water.

Corals are tolerant for a wide range of salinity ($30 \text{ psu} < S < 38 \text{ psu}$) unless there is a freshwater input such as near an estuary where the salinity drops below 30 psu (i.e., practical salinity unit). Some corals may grow even in the Red Sea where the salinity is very high ($S > 40 \text{ psu}$) (Guilcher, 1988).

While hermatypic corals construct the framework of the reef, other organisms such as coralline algae, molluscs, and crustaceans contribute to the reef fabric. Coral reefs are highly productive ecosystems (in the order of $2,000 \text{ g-Carbon m}^{-2} \text{ yr}^{-1}$) but energy demands are high, so that net production

is in fact quite low (about a few percent) (Carter, 1988). The primary production is linked to the calcification process of reef construction, and the food chains allow for efficient recycling.

corals are rather minor contributors to the coral reef communities in the Hawaiian Islands as a whole.

Foraminifera, mollusks, red (coralline) algae, and echinoids (sea urchins) are more abundant. There are two common mineral forms of calcium carbonate -- the fragments of the skeletal parts of foraminifera and echinoids, and fragments of red algae are found as the mineral calcite while those of corals, mollusks, and green algae *Halimeda* are found as the mineral aragonite.

Fringing reefs are the most common type of reefs in the Hawaiian Islands. They are generally wide on the windward and narrow on the leeward coasts of the islands of Kauai and Oahu, respectively. Reefs fringing the west and north shores are more irregular and deeper than the reefs on windward or south shores, and have the well-sorted sandy beaches with large annual changes (Noda, 1989).

A significant cause of relative sea level change and sediment loss in the nearshore region of the Hawaiian Islands results from the formation of beachrock, i.e.,

stratified calcarious sandstones or conglomerates common along many tropical lime-sand beaches (Moberly et al., 1963). Beachrock may form rapidly. As beachrock forms it removes the sand, thus cemented, from the shoreline budget. Once beach sands are transported to the offshore region, some of the offshore sands are prevented from transporting onshore by the reefs or trapped and cemented in the pores of reef communities during the transport processes.

Meanwhile, reefs are protecting beaches from large waves and are a source of sediments. Contrary to the continental beach sands, Hawaiian beach sands are primarily produced by some fishes eating, grinding, and puffing out coral reefs (pers. comm., Krock, 1993). So the growth of coral reefs also has substantial positive effects.

The effect of thermal expansion on sea-level rise in the Hawaiian Islands is not expected to be large because of small change in temperature and shallow depth of the mixed layer in the tropical region, despite a relatively large value of the thermal expansion coefficient which increases from 0.8×10^{-3} at freezing temperatures to 3.4×10^{-3} at 30°C (Wyrтки, 1990). Wyrтки estimates that the sea-level rise in the tropics is only about one-tenth of that in polar regions.

However, continuing long-term response to glacial unloading causes global sea-level rise problems only at mid-

and low-latitudes because the land continues to rebound and hence relative sea level sinks at high latitudes (Barnett, 1984; Lambeck and Nakiboglu, 1984; Emery and Aubrey, 1991).

Northeasterly trade winds are predominant over the Hawaiian Islands, as much as about 86% of the year (Fig.2.1). The rest of the year is primarily affected by southerly Kona winds. Short-term changes of beach systems are basically governed by the wind waves. A local atmospheric eddy over the lee side of the Island of Hawaii due to trade winds (northeasterlies) may contribute to form an oceanic eddy. This orographic eddy may grow up to a certain range (diameter > 100 km) and then start to drift westward as Rossby waves with a speed of a few miles per day (Patzert, 1969). The eddy forms a low (*cyclonic*) or a high (*anticyclonic*) stand of sea level at its center, but it is expected that the eddy may not significantly affect the local coastal regions due to its slow rotation.

In the Hawaiian Islands, the long-term rising trend of relative sea level decreases from Hilo (+4.0 mm/yr), Hawaii to the northwest islands (Fig.2.2). Continual volcanic loading on Kilauea, Hawaii results in the subsidence of not only the island Hawaii itself but also the neighboring islands due to isostasy. The subsiding rate of the island Oahu was estimated as about +1 to +2 mm/yr from the shallow

core measurements of a fringing reef crest at Hanauma Bay, Oahu, (Nakiboglu et al., 1983), which is comparable to the RSL rising rate of +1.6 mm/yr obtained from the tide-gauge records at Honolulu Harbor, Oahu.

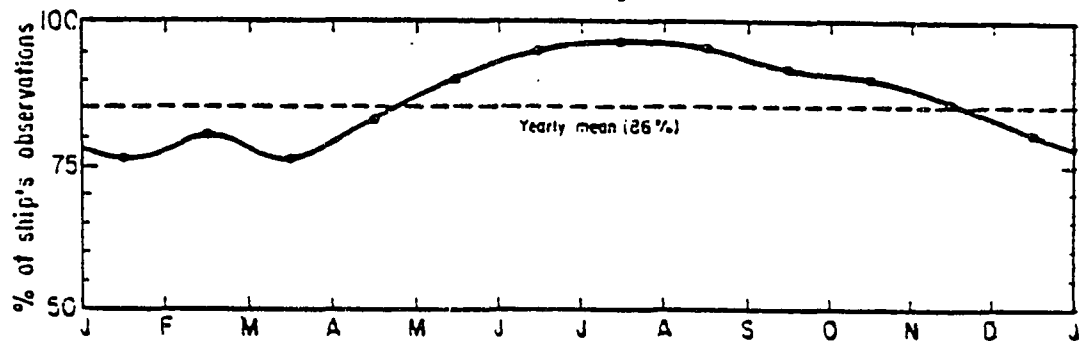


Fig.2.1. Percentage of the trade winds (NE, E, and SE) for the 5° squares between 15°N and 25°N latitude at 150°W to 155°W longitude plotted as monthly averages from ship's observations. Data from U.S. Navy Hydrographic Office Pilot Charts (H.O. 560). (after Patzert, 1969).

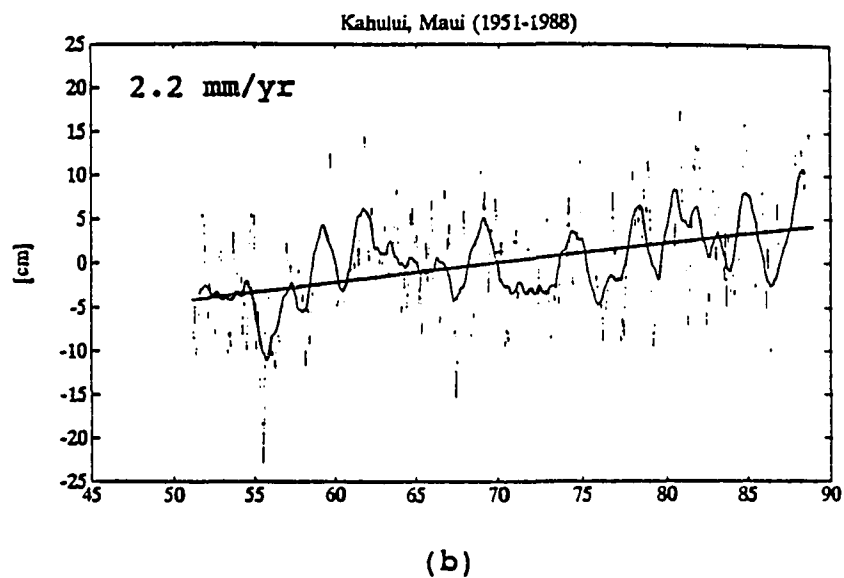
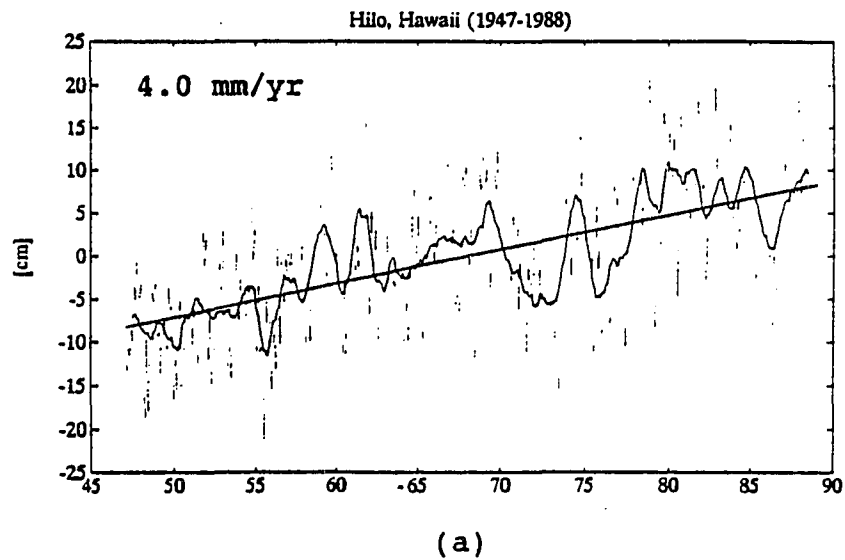


Fig.2.2. Long-term sea level trend (solid), 12-month running mean (solid curve), and monthly sea level values (dotted curve) at (a) Hilo, Hawaii, (b) Kahului, Maui, (c) Honolulu, Oahu, (d) Nawiliwili, Kauai, (e) Johnston, (f) Midway, and (g) Mokuoloe, Oahu.

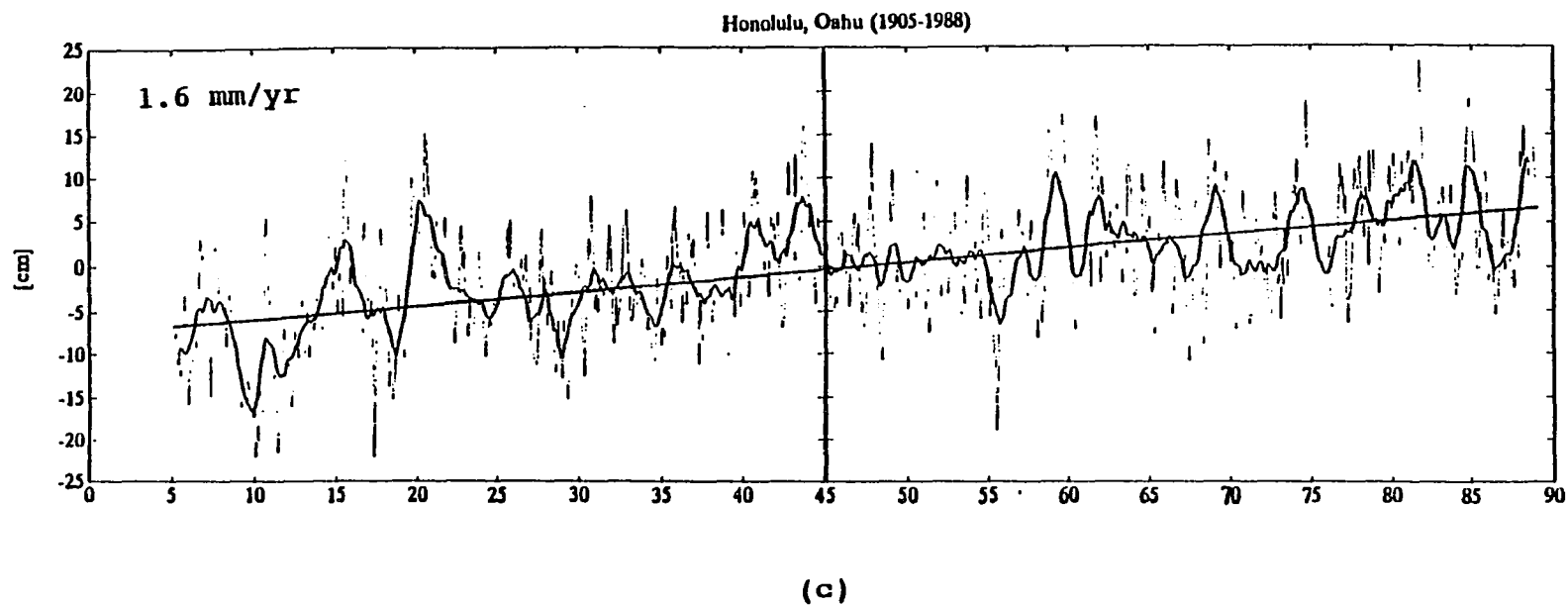
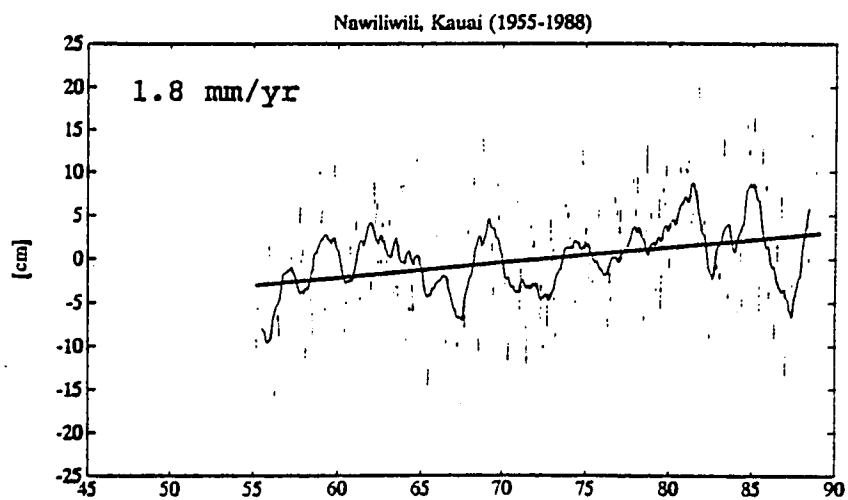
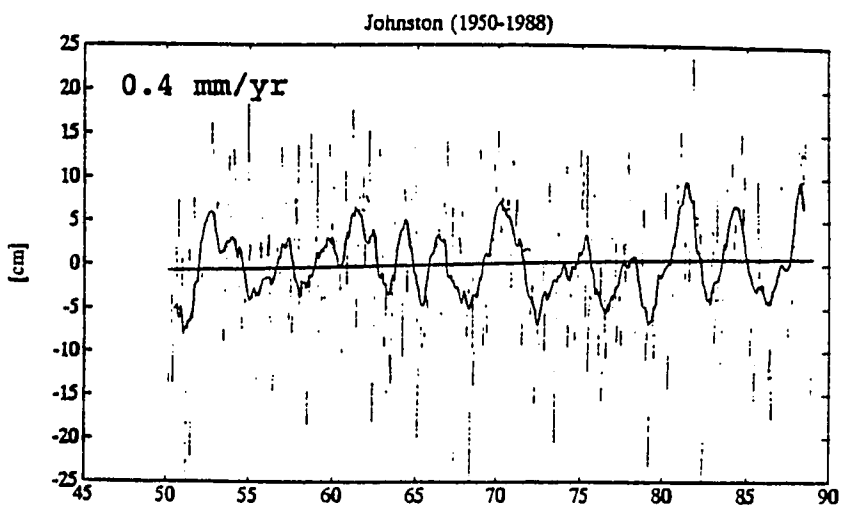


Fig.2.2. (continued) Long-term sea level trend (solid), 12-month running mean (solid curve), and monthly sea level values (dotted curve) at (a) Hilo, Hawaii, (b) Kahului, Maui, (c) Honolulu, Oahu, (d) Nawiliwili, Kauai, (e) Johnston, (f) Midway, and (g) Mokuoloe, Oahu.

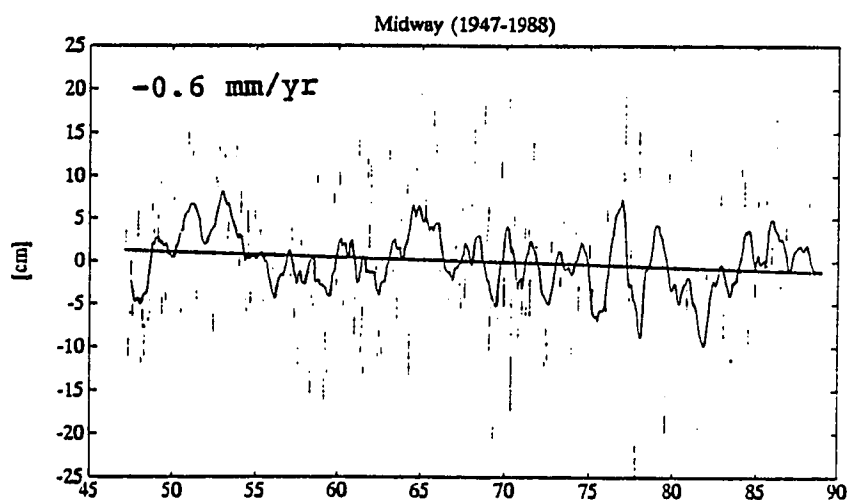


(d)

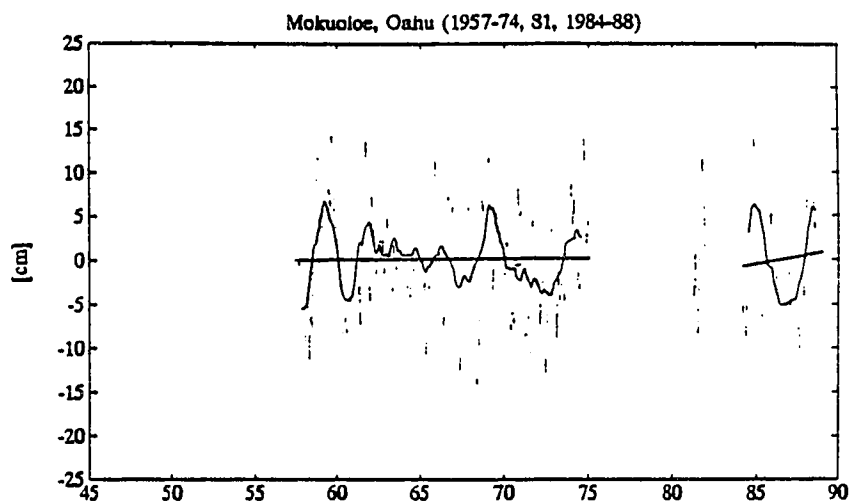


(e)

Fig.2.2. (continued) Long-term sea level trend (solid), 12-month running mean (solid curve), and monthly sea level values (dotted curve) at (a) Hilo, Hawaii, (b) Kahului, Maui, (c) Honolulu, Oahu, (d) Nawiliwili, Kauai, (e) Johnston, (f) Midway, and (g) Mokuoloe, Oahu.



(f)



(g)

Fig.2.2. (continued) Long-term sea level trend (solid), 12-month running mean (solid curve), and monthly sea level values (dotted curve) at (a) Hilo, Hawaii, (b) Kahului, Maui, (c) Honolulu, Oahu, (d) Nawiliwili, Kauai, (e) Johnston, (f) Midway, and (g) Mokuoloe, Oahu.

At Midway Island station, the trend is even slightly falling by about -0.4 mm/yr (Fig.6.3.(f)). This might be related to the reef evolution in the Hawaiian Island chain, running in a southeast and northwest direction. Scott and Rotondo (1983) propose a general reef evolution model for the Pacific plate; the 'moat and arch effect' acting at the passage over an asthenospheric bump may result in a raised atoll, which will sink later, leading to submerged atolls and seamounts (Fig.6.4).

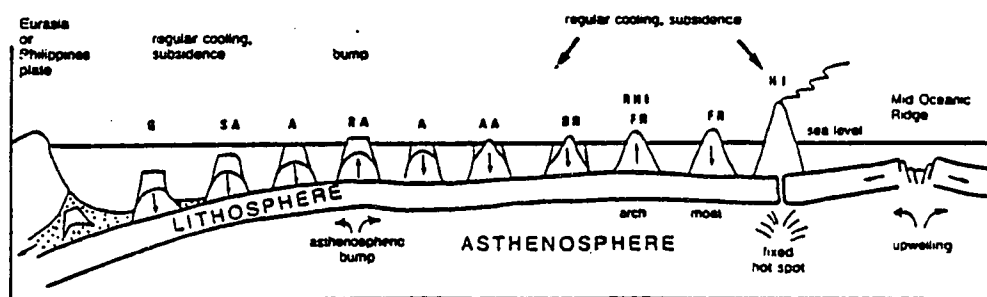


Fig.2.3. Proposed model for island development on the Pacific plate. Arrows indicate subsidence (↓) or emergence (↑). HI: high island; FR: fringing reef; RHI-FR: raised high island with fringing reef; BR: barrier reef; AA: almost-atoll; A: atoll; RA: raised atoll; SA: submerged atoll; G: guyot (simplified by Guilcher, 1988; originally from Scott and Rotondo, 1983)

The island of Maui subsides faster than the islands of Oahu and Kauai, because it is closer to Hawaii and hence more affected by isostatic subsidence due to volcanic loading at Kilauea, Hawaii.

Hwang and Fletcher (1992) summarize the island subsidence and the projected future submergence rates from the tide-gauge records (Table 2.2).

Table 2.2. Sea level trends of rise in the Hawaiian Islands. The numbers after \pm represent standard deviations. The unit is in cm/decade (from Hwang and Fletcher, 1992).

station	net submergence	subsidence rate	future submergence
Hilo	3.94 \pm 0.23	2.51 \pm 0.53	8.51 \pm 4.09
Kahului	2.46 \pm 0.23	1.04 \pm 0.53	7.04 \pm 4.09
Honolulu	1.57 \pm 0.08	0.15 \pm 0.38	6.15 \pm 3.94
Nawiliwili	1.75 \pm 0.30	0.33 \pm 0.61	6.32 \pm 4.17

Their estimates of the linear trend from tide-gauge records are a little higher than those analyzed in this study. They assume that the subsidence rate of the islands is the net submergence from the records minus the average ($= 1.42 \pm 0.30$ cm/decade) of the different estimates of global mean

sea level rise (see Table 2, Hwang and Fletcher, 1992). The corresponding island-specific subsidence rates then become 64% of the total submergence rate at Hilo, Hawaii, 42% at Kahului, Maui, 10% at Honolulu, Oahu, and 19% at Nawiliwili, Kauai, respectively. And the projected submergence rate is assumed as the island-specific subsidence rate plus the projected rate of future global sea-level rise, according to the IPCC (Intergovernmental Panel on Climate Change) best estimate scenario ($= 6.0 \pm 3.6$ cm/decade) (IPCC, 1990).

If this is correct even when applying to the Hawaiian Islands and linearly extrapolated for the next several decades, the relative sea-level rise on the major Hawaiian Islands is as follows (Table 2.3):

Table 2.3. Projected relative sea-level rise in 2040 on the major four Hawaiian Islands:

island	projected RSL rise in 2040
Hawaii	42.6 ± 20.5 cm
Maui	35.2 ± 20.5 cm
Oahu	30.8 ± 19.7 cm
Kauai	31.6 ± 20.9 cm

Table 2.4. Mean monthly sea-level values and the standard deviations of the annual cycles at the four major stations in the Hawaiian Islands. Units are in cm, and the mean values are relative to the minimum values.

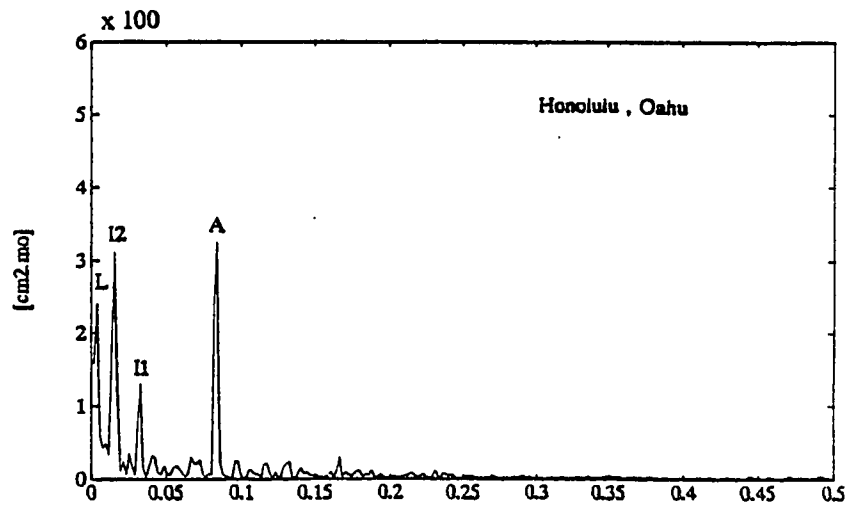
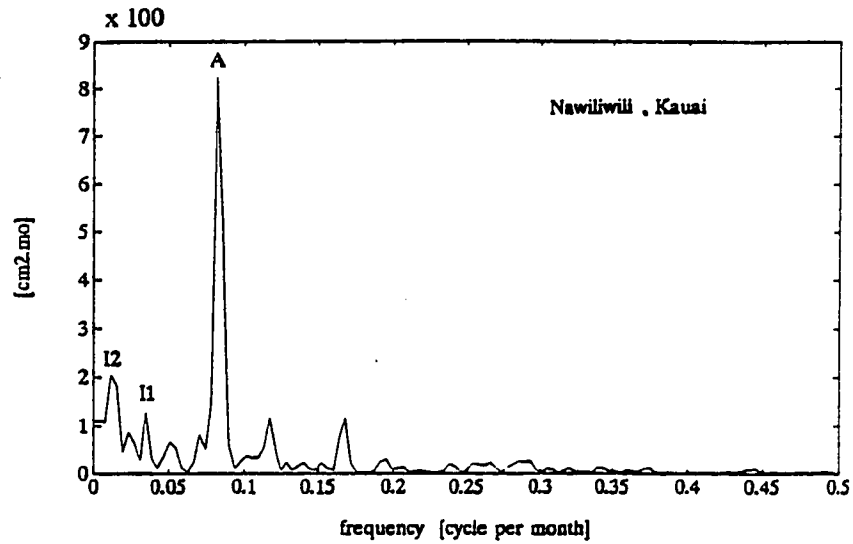
month	Nawiliwili Kauai	Honolulu Oahu	Kahului Maui	Hilo Hawaii
Jan	4.9 ± 6.3	3.0 ± 6.8	4.1 ± 5.6	4.3 ± 7.6
Feb	3.7 ± 6.4	2.4 ± 6.5	3.2 ± 4.7	2.2 ± 6.9
Mar	2.1 ± 5.8	1.3 ± 5.9	1.8 ± 4.3	1.8 ± 7.1
Apr	1.1 ± 5.2	0 ± 6.1	0.3 ± 4.5	0.9 ± 6.2
May	0 ± 5.0	0.3 ± 5.8	0 ± 4.5	0 ± 6.8
Jun	0.7 ± 5.4	1.2 ± 6.2	1.8 ± 6.0	0.7 ± 7.3
Jul	4.7 ± 6.4	4.1 ± 6.8	5.2 ± 5.8	5.0 ± 7.1
Aug	8.5 ± 6.7	7.1 ± 7.0	8.1 ± 5.4	9.6 ± 7.6
Sep	10.7 ± 5.5	8.6 ± 6.3	10.5 ± 5.2	10.4 ± 7.4
Oct	9.8 ± 5.0	8.3 ± 6.2	9.5 ± 5.1	10.0 ± 7.4
Nov	7.9 ± 4.0	6.6 ± 6.2	7.9 ± 5.3	8.2 ± 6.8
Dec	5.9 ± 4.8	4.6 ± 6.4	5.1 ± 5.0	5.3 ± 7.2

Therefore, it is encouraged that the engineers constructing coastal structures in the Hawaiian Islands should adjust the *design water level* (DWL)⁵ due to sea-level rise at least by +50 to +60 cm, in addition to the other effects, for the life-time of projects of 50 years.

The fluctuation pattern of the monthly mean sea levels in the Hawaiian Islands shows the annual and the interannual oscillations. The interannual fluctuation shows typically about 4-year period at Hilo (Hawaii), Honolulu (Oahu), Kahului (Maui), Nawiliwili (Kauai) in the power spectral density distribution (Fig.2.4). The mean annual cycle in four major islands shows the difference of about 10 cm between minimum (April to May) and maximum (September) sea-levels. The standard deviations of the mean annual cycle range from 4.0 to 7.6 cm (Table 2.4).

⁵ $DWL = MLLW + AsT + InB + WiS + WaS + WaR + LoT^* + IaF^{**}$
 MLLW : Mean Lower Low Water
 AsT : Astronomical Tide
 InB : Inverse Barometric Effect
 WiS : Wind Setup (storm surge or piling-up by Coriolis effect)
 WaS : Wave Setup
 WaR : Wave Runup (It is usually not included in DWL, but added later, if appropriate.)
 LoT* : Long-term Trend
 IaF** : Interannual Fluctuation
 (The last two terms in the righthand side are suggested by the author.)

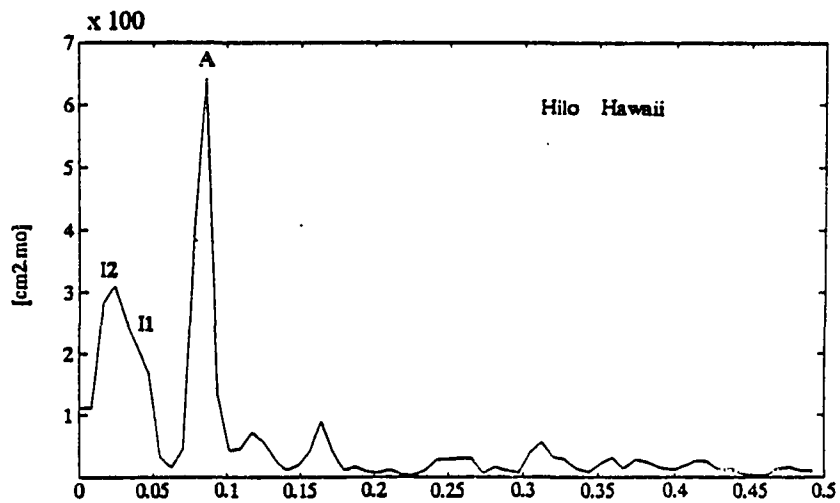
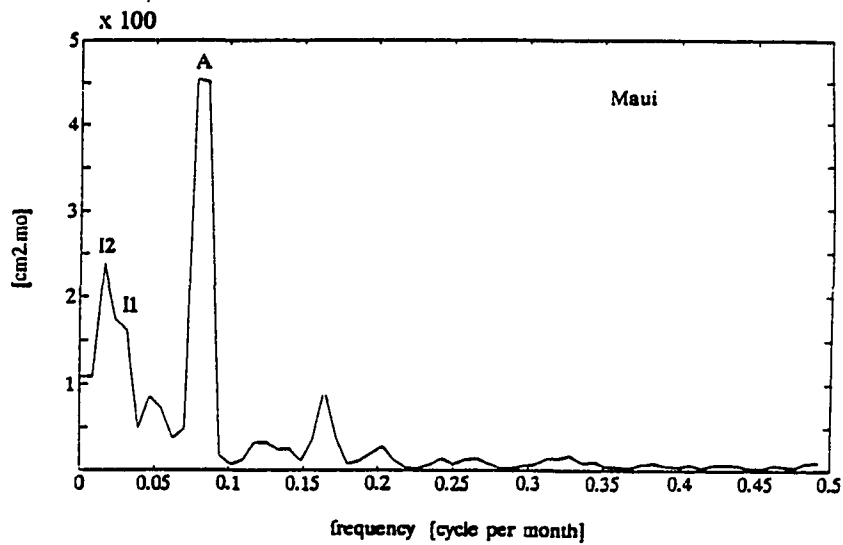
(a)



(b)

Fig.2.4. Power spectral density distributions at (a) Nawiliwili, Kauai, (b) Honolulu, Oahu, (c) Kahului, Maui, (d) Hilo, Hawaii, (e) Johnston Island, and at (f) Midway.

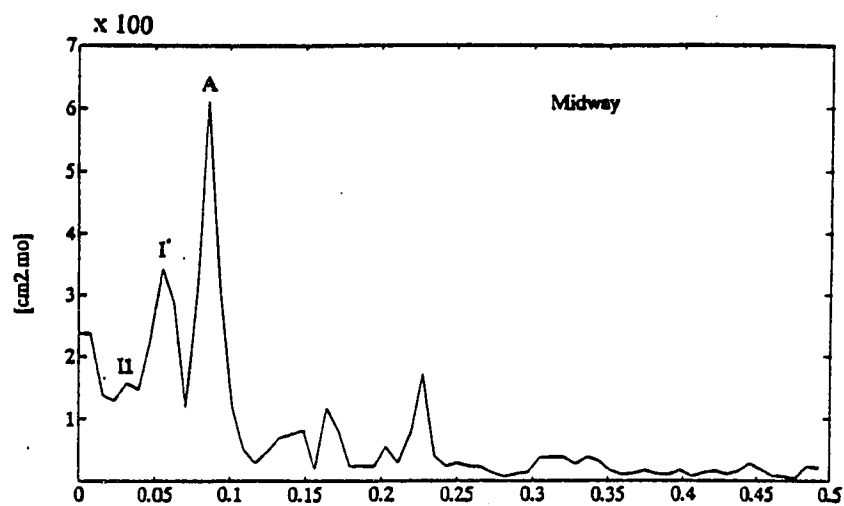
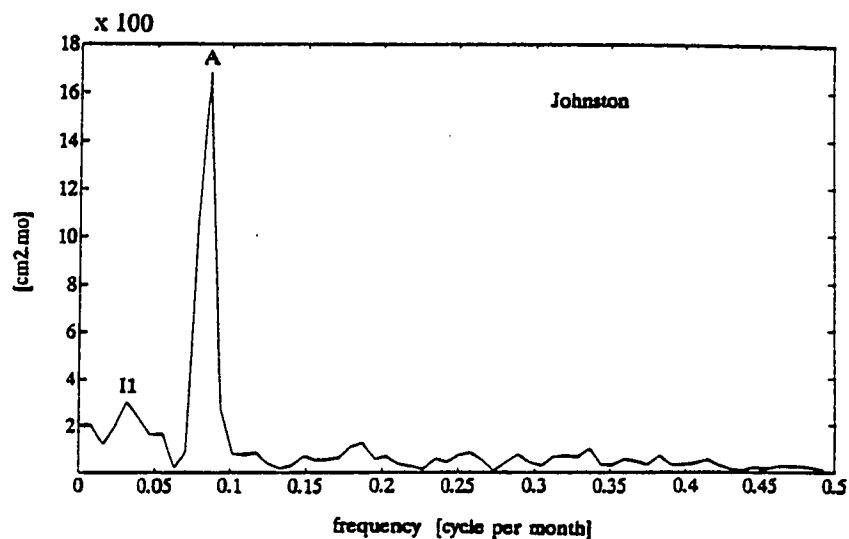
(c)



(d)

Fig.2.4. (continued) Power spectral density distributions at (a) Nawiliwili, Kauai, (b) Honolulu, Oahu, (c) Kahului, Maui, (d) Hilo, Hawaii, (e) Johnston Island, and at (f) Midway.

(e)



(f)

Fig.2.4. (continued) Power spectral density distributions at (a) Nawiliwili, Kauai, (b) Honolulu, Oahu, (c) Kahului, Maui, (d) Hilo, Hawaii, (e) Johnston Island, and at (f) Midway.

CHAPTER 3

METHODS AND ANALYSES

3.1. AVAILABLE DATA

3.1.1. Tide-gauge Records

Two sources of sea level data -- PSMSL (Permanent Service for Mean Sea Level⁶) and TOGA (Tropical Ocean and Global Atmosphere⁷) program -- are used. Fourteen island stations in the North Pacific between the equator and 35°N are selected for monthly sea level values from PSMSL, among which seven stations in the Hawaiian Islands are chosen both from PSMSL (monthly means) and TOGA (daily means). The locations and the durations of the data are shown in Table 3.1.

TOGA daily data at the 7 stations in the Hawaiian Islands are calculated using a two-step filtering operation. First, the dominant diurnal and semidiurnal tidal components are removed from the quality-controlled hourly values. Secondly, a 119-point convolution filter (Broomfield, 1976)

⁶ Bidston Observatory, Birkenhead, Merseyside, L43 7RA, U.K.

⁷ TOGA Sea Level Center, University of Hawaii, 1000 Pope Road, Honolulu, HI 96822, U.S.A.

Table 3.1. The locations and the lengths of the PSMSL (monthly MSL) and TOGA (daily MSL) data at the selected island stations in the North Pacific between the equator and 30°N.

station	latitude	longitude	period	years
Hilo, Hawaii	19°44'N	155°04'W	1947-86 (1973-90)	40 (18)
Kahului, Maui	20°45'N (20°54'N)	156°28'W	1947-86 (1973-90)	40 (18)
Honolulu, Oahu	21°19'N (21°18'N)	157°52'W	1905-86 (1973-90)	82 (18)
Mokuoloe, Oahu	21°26'N	157°47'W (157°48'W)	1957-86 (1981-90)	30 (10)
Nawiliwili, Kauai	21°58'N	159°21'W	1955-86 (1973-90)	32 (18)
French Frigate Shoal	23°52'N	166°17'W	(1975-89)	(15)
Midway Island	28°13'N	177°22'W	1947-86 (1974-90)	40 (17)
Johnston Island	16°45'N	169°31'W	1950-86 (1973-90)	37 (18)
Wake Island	19°17'N	166°37'E	1950-86	37
Eniwetok Island	11°22'N	162°21'E	1951-72	22
Kwajalein Island	8°44'N	167°44'E	1946-86	41
Truk Island	7°27'N	151°51'E	1947-86	40
Guam Island	13°26'N	144°39'E	1948-88	41
Legaspi, Philippines	13°09'N	123°45'E	1947-88	42
Davao, Philippines	7°05'N	125°38'E	1948-88	41

Values in () are for the locations or duration of TOGA data, when different from PSMSL data, in the Hawaiian Islands.

centered on noon is applied to remove the remaining high-frequency energy and to prevent aliasing when the data are computed to daily mean values (Caldwell et al., 1989).

TOGA monthly data are calculated by simply averaging all the daily mean values in a month. If a missing period is longer than seven days in a month, the monthly values are not calculated and but substituted either by linear interpolation or by weight-folding method (WFM) within a time-series (see Section 3.2).

Historically, sea level has been simply measured by reading the relative height of water level to a convenient bench-mark, e.g., a vertically mounted scale on a pier or wharf etc. There are a few different types of tide-gauge; float-type with a stilling well, bubbler-type with an air tank, and pressure sensor.

Typical pressure-sensor and field accuracies are reported as ± 2 cm and ± 5 cm, respectively (Rayner and Archer, 1985). Wyrтки et al. (1988) estimate monthly mean sea level values as representative with an accuracy of ± 2 cm from calculating the standard deviations of monthly mean sea level between pairs of stations at 5 stations in the Hawaiian Islands for about 20 years (Fig.3.1.(a)). Time-series of monthly sea level anomalies between Honolulu and Mokuoloe during 1957 to 1975 shows almost no phase lag with

the same amplitudes (Fig.3.1.(b)) (refer to the map on Fig.3.2, page 46).

Tide-gauge records used in this study are from two sources; the Permanent Service for Mean Sea Levels (PSMSL) and the Tropical Ocean - Global Atmosphere (TOGA) program. Monthly means are from both sources and daily means from TOGA are for the stations in the Hawaiian Islands only. PSMSL data have been collected from all the cooperative countries over the world and hence data quality may be subjective to the conditions in each country. However, the error range of measurements may be greatly reduced by averaging into monthly means. TOGA data have relatively higher quality since the satellite-transmitted data are directly controlled by comparing with the predictive tides using a least-square harmonic analysis from the calculated harmonic constituents.

In order to reduce aliasing, a monthly value is calculated if only 7 days or less are missing and rejected otherwise. The average data gap from the seven stations in the Hawaiian Islands is about 6.4% of the total data and the questionable fluctuations in the residual time-series is less than 0.5% (Caldwell et al., 1989). But subjective analysis for these residual fluctuations may still increase the error ranges unless the reasons are correctly determined.

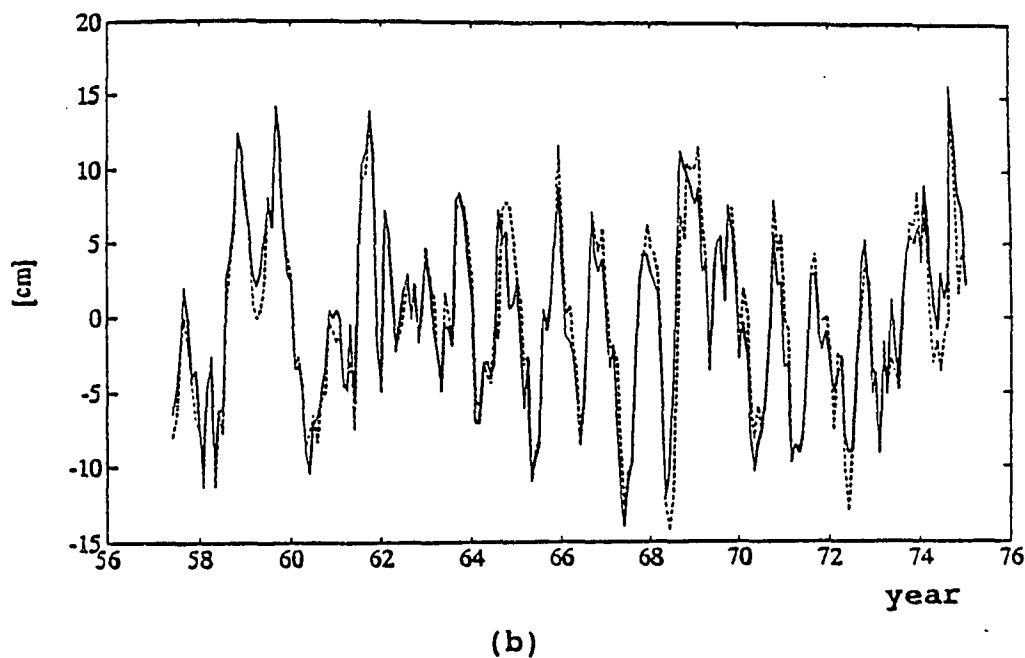
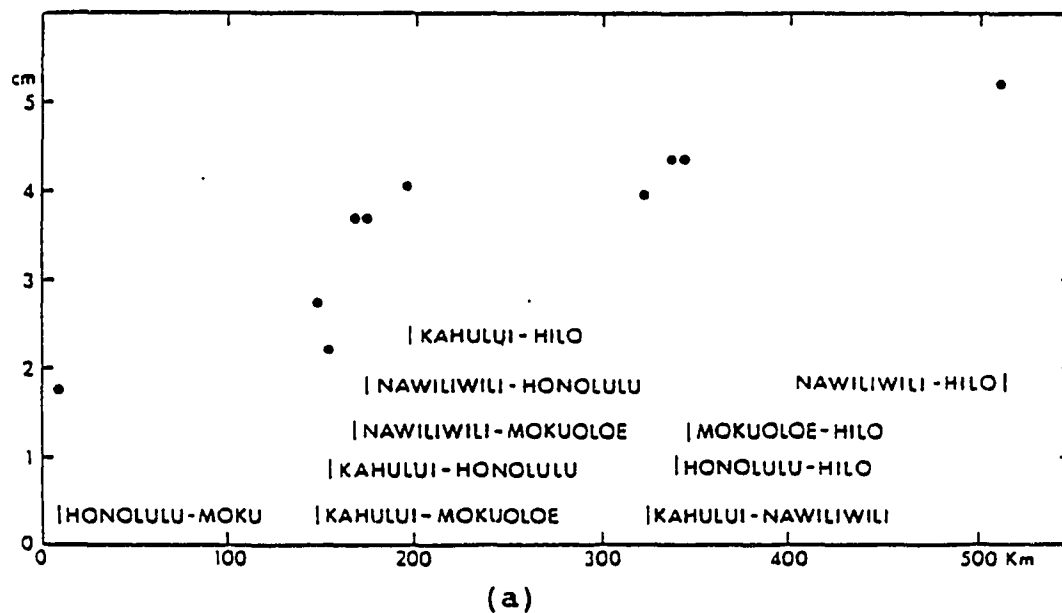


Fig.3.1. (a) Standard deviation (in cm) of the difference of monthly mean sea level among five stations in the Hawaiian Islands for about 20 years as a function of distance (in km) (after Wyrтки et al., 1988), and (b) monthly sea level anomalies at Honolulu (solid curve) and Mokuoloe (dashed curve), Oahu.

For the purpose of this study, data gaps are filled either linearly or by using WFM (*Weight-Folding Method*) as described in the next section (Section 3.2). Although WFM is based on the assumption that the nearer (missing) datum may have a higher correlation than the farther one, which seems to be more reasonable than the linear interpolation, this must not be always true and may be more biased than the linear interpolation in some cases. However, one obvious intention of this method is to create a continuous time-series not biased from the real time-series with a fortnight (≈ 14 days) tidal component in daily values and with an annual component in monthly values, respectively.

3.1.2. Aerial Photographs

Pre-analyzed aerial photographs on Oahu (Hwang, 1981) and on Maui, Kauai, and Hawaii (Makai Ocean Engineering, Inc., 1991) are primarily used to examine beach erosion and shoreline changes in the Hawaiian Islands. The time difference between first and last photos at each site is approximately from 25 to 40 years (3 to 5 photos with about a 10 year interval). The average numbers of transects at each site are as follows: 4 to 7 transects on Oahu, 3 to 5 on Kauai, 3 on Maui, 4 on Molokai, 2 to 3 on Hawaii. They were measured by the deviations of vegetation line and water

line from those in the base year (i.e., cross-shore beach distance between water line and vegetation line), using the method of photogrammetry. The locations and number of data selected from the previous analyses are as follows (Table 3.2):

Table 3.2. The location and the number of transects (or number of sites) of the aerial photographs in the four major Hawaiian Islands. Data selected (or averaged) from Makai Ocean Eng.(1991) and Hwang (1981).

island	location	no. of photographs	no. of transects	period
Kauai	KA (southwest)	4	11	1953-88
	KB (southeast)	4	9	1953-88
	KC (east)	3 - 4	36	1950-88
	KD (northeast)	3	13	1960-88
	KE (north)	4	10	1950-88
	KF (north)	3 - 4	6	1950-88
Oahu	north	3 - 7	82 (12)	1928-79
	windward	4 - 7	133 (14)	1928-80
	south	3 - 6	52 (11)	1928-79
	leeward	4 - 6	41 (10)	1949-79
Maui	MA (west)	3 - 4	25	1949-88
	MB (southwest)	4	19	1949-88
	MC (southwest)	4 - 5	23	1949-88
	MD (north)	4	21	1950-88
Hawaii	HA (northwest)	4	11	1950-88
	HB (west)	4 - 6	18	1950-88

Shoreline changes from aerial photographs, based on the previous analyses by Makai Ocean Engineering and Sea Engineering (1991) and Hwang (1981), were carefully re-analyzed, including an annual oscillation of sea level with the average slope of beach profile.

The traditional way of interpreting aerial photographs for long-term change of shoreline is to determine vegetation line or water line by eye, which involves some level of subjectivity and inconsistency in the detection process since the coastline as a transition zone between land and sea forms a complex system of brightness variation in the panchromatic spectrum (Shoshany and Degani, 1992).

In general, errors come from two typical sources; those are

1) errors due to photographic processes such as lens distortion, camera tilt, film development, differential scale change from the center to the margins, and relief displacement, etc., and

2) errors due to geometrical adjustment between photographs and base map.

Relief displacement changes radially from the center of the photo, which is coincident with the nadir point (the

point vertically below the camera) for a truly vertical photo. Since most coastal features have low relief, *radial distortion* due to elevation differences is not serious.

Lens distortion and *camera tilt* may result when an airplane and camera are not exactly parallel to the mean plane of the earth's surface at the instant of exposure. About half of near-vertical air photos taken for domestic mapping purposes are tilted less than 2 degrees, and few are tilted more than 3 degrees (Wong, 1980).

Scale change may result from the shifts in altitude along the photographic flight line, especially with light aircraft. The possible decrease of the aircraft elevation may significantly increase the scale of the air photos. An interesting example of the error by changing scale was reported by Anders and Byrnes (1991):

If an air photo were used to measure a shoreline distance by 10 cm for an assumed scale of 1:20,000, ground distance would be calculated at 2,000 m. However, if the actual scale were 19,934 m resulting from the decrease of the aircraft elevation by 10 m at the moment of camera exposure, which is common in small light planes, then the distance would be 1,993.4 m. This produces 6.6 m difference in location of the shoreline point.

Thus exact scale should be determined for digitizing data from each air photo. Photographic scale (Q) is calculated by

$$Q = \frac{f}{\zeta} \quad (3.1)$$

where

f = focal length of the camera lens

ζ = flight altitude of the camera above the mean elevation of the terrain

Correct interpretation of the HWL (high water line) and careful annotation are required to avoid large miscalculations. For a 1:20,000 scale, a 0.2 mm line drawn with a very thin drafting pen makes a ground line with 4 meter width. Therefore, in order to minimize error associate with shoreline annotation, photographic scale Q should be maximized, that is, measurement altitude must be low and camera lens should be large.

Displacement of an image due to *radial distortion* resulting from elevation changes (D_o) can be calculated as,

$$D_o = \frac{r h}{\zeta} \quad (3.2)$$

where

- r = distance from the center of the image to the top of the object,
- h = ground elevation of the object,
- = flight altitude of the camera

Lastly, displacement of a point on an aerial photograph due to tilt (D_t) from its actual ground position can be calculated by

$$D_t = \frac{r^2 \sin \theta_t \cos^2 \theta}{f - r \sin \theta_t \cos \theta} \quad (3.3)$$

where

- r = distance from the point to the isocenter,
- f = focal length of the lens,
- θ_t = angle of tilt of the photograph,
- θ = angle from the principal line to the radial line (clockwise) between isocenter and the point within the plane of the photograph

3.1.3. Waves

Twelve-year wave data from NODC⁸ (January 1981 - August 1992) are to be used, which had been measured by NOAA⁹ environmental buoy (no. 51001) at the northwest of Kauai (23°24'N, 162°18'W) (Fig.3.2).

Significant wave heights were corrected for low frequency noise, and wind speeds and directions with the original 8.5 minute interval were averaged for an hourly interval by TOGA Sea Level Center, University of Hawaii (pers. comm., Caldwell, 1993).

Maximum estimates of visual surf observations at five locations (Sunset Beach, Makaha, Ala Moana, Diamond Head, and North Beach) on Oahu during 1988 to 1992 are also used for examining the correlation between deep-water wave heights and surf heights. Since the data sources are the radio, National Weather Services, and personal observations, they are subjective to the observers.

⁸ National Oceanographic Data Center

⁹ National Oceanic and Atmospheric Administration

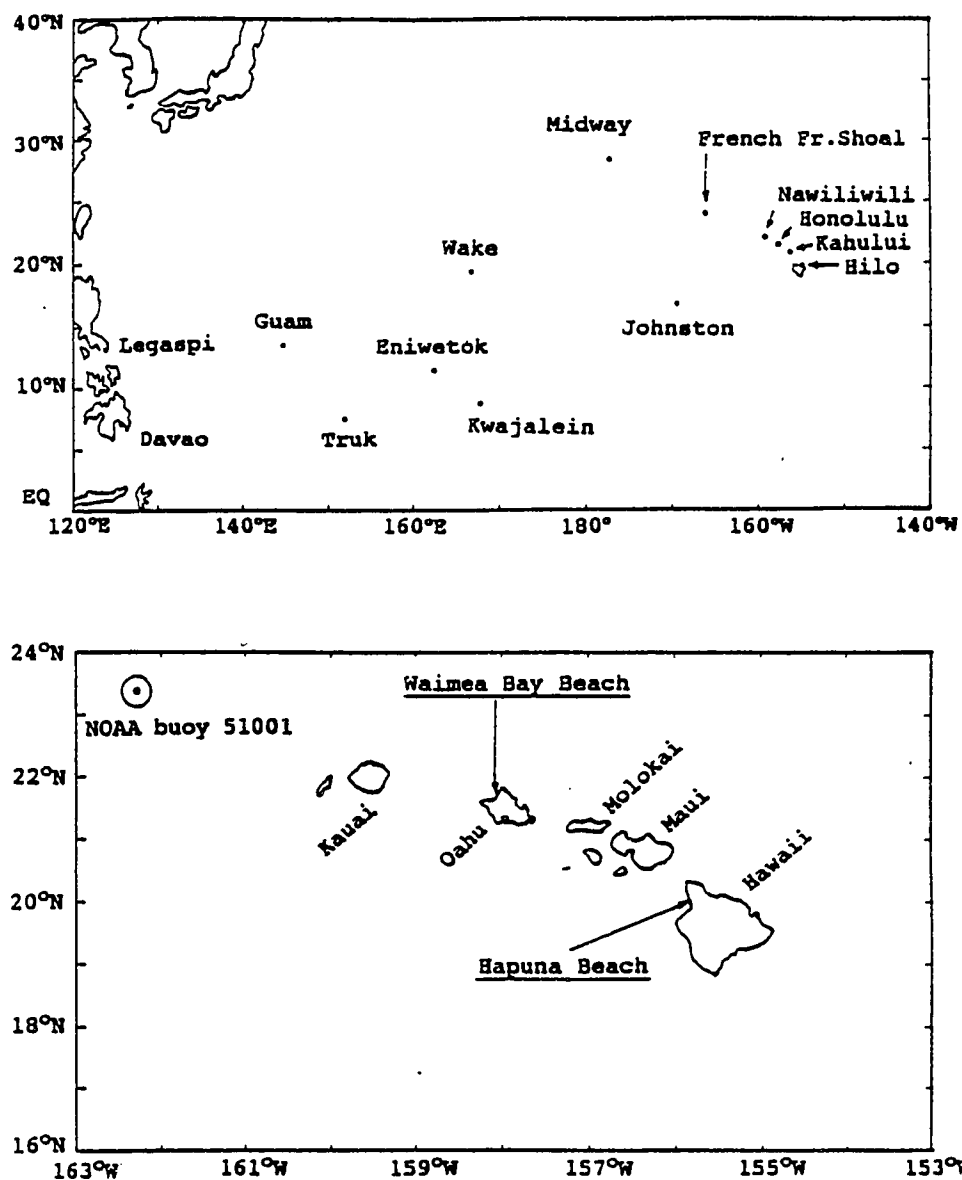


Fig.3.2. Location map of tide-gauge stations, NOAA environmental buoy (no. 51001), and Waimea Bay Beach, Oahu and Hapuna Beach, Hawaii.

The basic problem in measuring waves is that of sampling a time-varying process which is spread out on a two-dimensional surface. Buoys have been typically used for measuring waves. So the quality of the measurements has been dependent on the buoy's ability to follow the sea surface faithfully. A directional buoy is often used in recent days, which provides the information of wave-approaching directions and allows us to decompose wave energy with respect to both frequency and angle. However, the mooring line may still give a significant effect on buoy motion.

NOAA environmental buoy (no.51001) moored at a location northwest of Kauai ($23^{\circ}24'N$, $162^{\circ}18'W$) is an accelerometer-type wave measuring device, which obtains vertical displacement information of the buoy by electrically integrating vertical acceleration twice.

The total observational error may include several components as follows:

- 1) *static instrument measurement error ... residual error after calibration*
- 2) *dynamic measurement error ... error from the induced motion of the sensor due to buoy motion, the effect of*

the dynamic response or instability of the instrument to environmental changes

- 3) *physical disturbance error* ... error due to the superstructure or subsurface data line of the buoy
- 4) *data manipulation and processing error* ... data distortion in transferring, storing, retrieving or digitizing
- 5) *transform error* ... effect due to averaging or converting the environmental parameter
- 6) *dislocation error* ... error from temporal and spatial dislocations of the sensor due to response time, currents, weather, imprecise navigation etc.

Folkert and Woodle (1973) reported the representative error estimate of wave height from the accelerometer-type wave-rider buoy as 0.39 m, which includes the error contributions from transducer (= 0.2 m), signal conditioning (= 0.22 m), calibration (= 0.22 m), platform motion (= 0.13 m).

Other authors presented the estimate of error as ± 15 cm in 5 m (or ± 3 %) by typical instrument sensor and ± 20 cm in field accuracies, for this type of wave sensor (Rayner and Archer, 1985).

The calibration of wave-height sensing systems, e.g., the accelerometer transducer which is one of the most significant and principal error sources, is difficult but must be very precise since the measurement of wave height involves the double integration of low frequencies . But the more significant problem in performing adequate calibration is the lack of a true measure of the sea surface elevation. Apart from the problems with sensor calibration, the suspension platform of the buoy may be set into oscillation causing a low frequency drift in the signal (Fig.3.3).

Averaging wave heights and periods into hourly values, which was done by TOGA Sea Level Center, University of Hawaii, smooths the measured time-series from the wave buoy to a great degree. And daily mean values for obtaining the wave climate in this study will be even much smoother than the measured time-series, which will completely remove high frequency peaks.

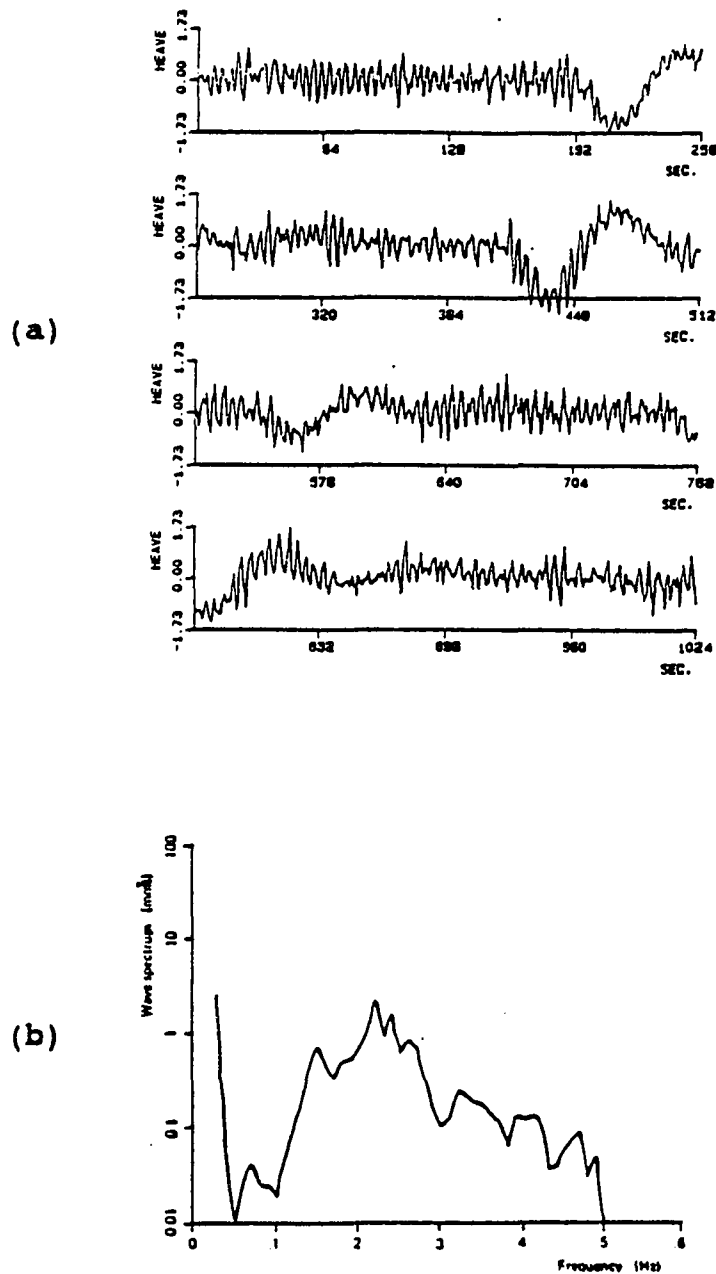


Fig.3.3. (a) Example of a time series with low frequency drift and (b) the spectrum of the record. This series was recorded with a Hippy 120 sensor ($\omega_0 = 2\pi/120s$). In this case the spectra will be correspondingly compressed towards 0 Hz. (after Barstow et al., 1985)

3.1.4. Beach Profiles and Sediment Characteristics

Measured beach profiles, sediment characteristics such as sand size, seasonal change of the size (Moberly and Chamberlain, 1964; Gerritsen, 1978; Parker, 1987) and sand volumes and widths of beach reservoirs (Chamberlain, 1968) in the past are also important data to be calculated with cross-shore sediment transport models, and compared with other data such as aerial photographs, as mentioned above.

3.2. METHODS

3.2.1. Mean Sea Levels

3.2.1.1. Filling Gaps in MSL Data

Data gaps are treated by three different ways:

- 1) gaps shorter than 6 months in monthly mean values (or 7 days in daily mean values) are linearly interpolated.
- 2) gaps equal or longer than 18 months in monthly mean values (or 21 days in daily mean values) are left as they are.
- 3) gaps in between 1) and 2), that is, equal or longer than 6 months but shorter than 18 months in monthly mean values (or equal or longer than 7 days but shorter than 21 days in daily mean values) are interpolated by the *Weight-Folding Method* (WFM).

WFM is carried out by three steps: take the same lengths of the neighboring data as that of a gap from both sides, and fold the neighboring data into the gap from endpoints (B_0 and A_0). Then, subtract these data values from the doubles of the data at endpoints ($2B_0 - B_1$ and $2A_0 - A_{L-1}$). Lastly, multiply linearly different weighting factors from both ends to the above values and add up the two resultant values to create a gap datum (Fig.3.4). This can be expressed as the following simple relationship such that

$$C_i = (2B_0 - B_i) * \frac{(L-i)}{L} + (2A_0 - A_{L-i}) * \frac{i}{L} \quad (3.4)$$

where B_0, A_0 = endpoints before and after the gap
 B_i = i -th data backward before the gap
 A_{L-i} = $(L-i)$ -th data after the gap
 C_i = created data for the gap by WFM
 L = the length of the gap

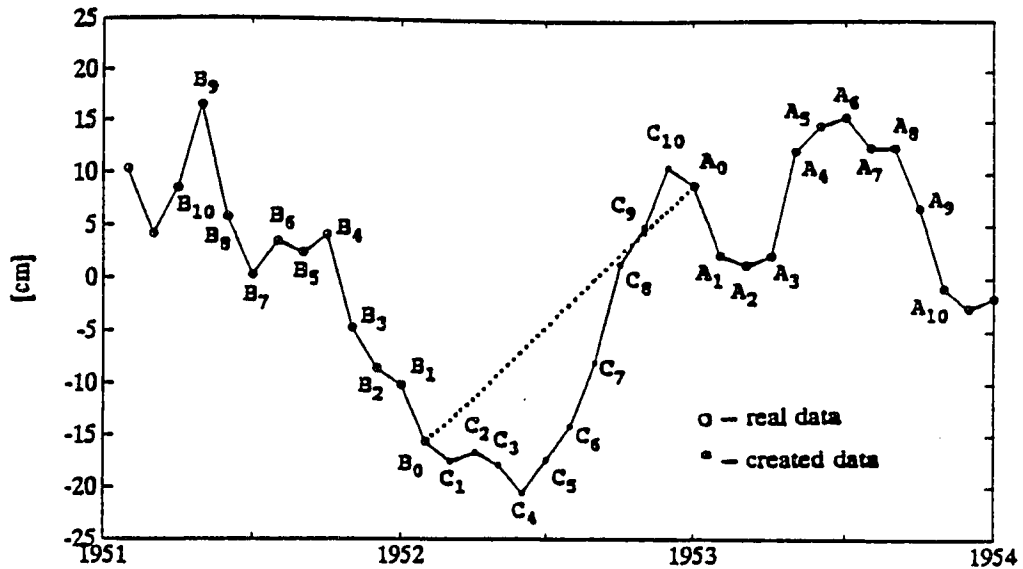


Fig.3.4. Example of *Weight-Folding Method* for a case of monthly time-series with a gap of 11 months. Dotted line between B_0 and A_0 is a linear interpolation, and C_i 's are created data from B_0, B_i 's and A_0, A_i 's with linearly interpolating weights.

3.2.1.2. Linear Regression

The whole time-series of data at each sea-level station is linearly fitted by the least squares method in order to determine the long-term linear trend. When the data gaps are too large and hence not filled, each data segment is linearly fitted, independently, such as at Mokuoloe, Oahu. Even for a continuous time series, rising or falling trends in an interannual scale by parts are selectively analyzed by linear regression.

3.2.1.3. Averaging and Smoothing

In order to obtain the mean annual cycle at each station, all the data in each month during the whole period are simply averaged after they are detrended, i.e., the mean and the linear long-term trend are removed. For analyzing interannual fluctuations, smoothing with twelve-month-running-means is applied. Hanning's filter (a bell-shaped window) is also used for obtaining the power spectral distribution of a time-series. This smoothing filter is applied before the time-series is transformed by *Fast Fourier Transform* (FFT).

3.2.1.4. Spectral Analyses

It is difficult to identify the frequency components from looking at the original signal. Fourier transform (or Fourier integral) of any signal in a time-series gives the distribution of signal strength with frequency.

Fast Fourier Transform (FFT) is applied to get a power spectral density distribution of monthly sea level values after they are smoothed by Hanning's filter with the width of 12 months. FFT is substantially faster in computer analysis than direct Fourier transform and hence popularly used now for a time-series of any power of two. If the length of a time-series is not an exact power of two, it is padded with trailing zeroes.

3.2.2. Models

Models for long-term trend and interannual variation of beach profiles are basically governed by the relative sea-level changes while the short-term response models are controlled by waves.

Beach profile response model by Bruun (1962) is applied to long-term trends (> 20 years) and to several-year-period fluctuations of sea level and beach profile changes. Based on observed long-term sea-level rise and interannual oscillations, the relationship between shoreline retreat and beach erosion will be examined.

Equilibrium profiles suggested by Dean (1977) and Bodge (1992) are also discussed, as well as Pruszek (1993) who introduces a time-dependent parameter for Dean's function (see next section in this chapter). Short-term response models by Edelman (1968), by Kriebel and Dean (1993), and by Steetzel (1990) are to be reviewed, despite the response time to establish an equilibrium profile.

An energetics-based model by Bailard (1984) is used to simulate beach profiles at Waimea Bay, Oahu and at Hapuna Beach, Hawaii for different wave heights in a time-scale of a few months. This model is represented by the beach profile changes and cross-shore sediment transport rates with one-week intervals.

3.3. ANALYSES OF SEA-LEVEL CHANGES

Major reasons of the long-term trend of relative sea level height are thermal expansion of ocean surface waters, changes in the Greenland and Antarctic ice sheets, and the melting of mountain glaciers (Gornitz and Lebedeff, 1987; Barnett, 1988; Peltier and Tushingham, 1989; Trupin and Wahr, 1990; Douglas, 1991). In addition to the eustatic sea level rise due to global warming and glacial melting as mentioned above, there are other factors; land fall/rise or tilting due to *local tectonism* such as volcanic activity, sea floor spreading, subduction of a plate into another plate at the plate boundary, *volume change in ocean basin* due to the above tectonic effect, *land transformation* due to long-term sediment transport, coral reef formation/growth and so on.

Annual oscillation and interannual fluctuation as well as long-term trend of relative sea levels would contribute altogether to coastal erosion. Although some author, e.g., Pruszek (1993), includes another signal of the sea-level fluctuation with a period of 20 to 30 years, it is excluded in this study because of data lengths. Long-term linear trend is considered with the Bruun Rule; a simple geometric conversion of shoreline retreat from sea-level rise and beach-slope with some restrictions in the sediment transport processes. Annual oscillation and interannual fluctuation are analyzed to deduce

the hypothesis of beach recovery; alternate rise and fall of sea levels would contribute more to coastal erosion as the time-scale of the fluctuation becomes longer. In reality, the erosional effect will be higher when high waves attack shores on the rising mode of sea-level fluctuation.

The height of oscillations of the annual and interannual sea-level components and the linear trend of sea-level rise at the stations in the Hawaiian Islands are shown in Table 3.3.

Table 3.3. The height of sea-level oscillations and the rate of sea-level rise at the stations of the Hawaiian Islands

	annual	interannual	long-term
Nawiliwili Kauai	10.7 \pm 5.5 cm	11.7 \pm 3.1 cm	1.8 cm/decade
Honolulu, Oahu	8.6 \pm 6.3	12.4 \pm 4.3	1.6
Kahului, Maui	10.5 \pm 5.2	10.8 \pm 2.0	2.2
Hilo, Hawaii	10.4 \pm 7.4	12.9 \pm 2.1	4.0

Since the interannual fluctuation of sea levels are often associated with El Niño events, which are stronger in the western Pacific than in the central Pacific region, three island stations in the western Pacific are selected for examining the possible relationship between the two.

At the 3 western Pacific island stations, Truk, Wake, and Kwajalein, the long-term linear trend varies at about +1 to +2 mm/yr (Fig.3.5). But the fluctuations of the averaged time-series data smoothed by 12 month running mean show quasi-periodic oscillations with several-year period, which correspond to the peaks of a low-frequency signal larger than the annual signal in the power spectral distribution (Fig.3.7). They seem to respond to the historic El Niño events with certain time lags, according to the time-series of the monthly mean sea-level heights.

At Truk Island, the two peaks with the periods of about 2 to 3 years are larger than the annual peak, and the semi-annual and 7-year signals are slightly less than the annual signal.

At Kwajalein, the 7-year signal is predominant and an annual signal is not clearly shown in the power spectra. In other words, the signals with semiannual, 10 months, annual, and biannual periods are comparable but much smaller than the peak with the 7-year period. At Wake Island, there exist many spectral peaks, which makes it difficult to analyze the mechanism of the sea level changes. A 10 to 11 year peak and an annual signal are comparably dominant, and there are several other smaller peaks with the periods from 5 years to 3 months.

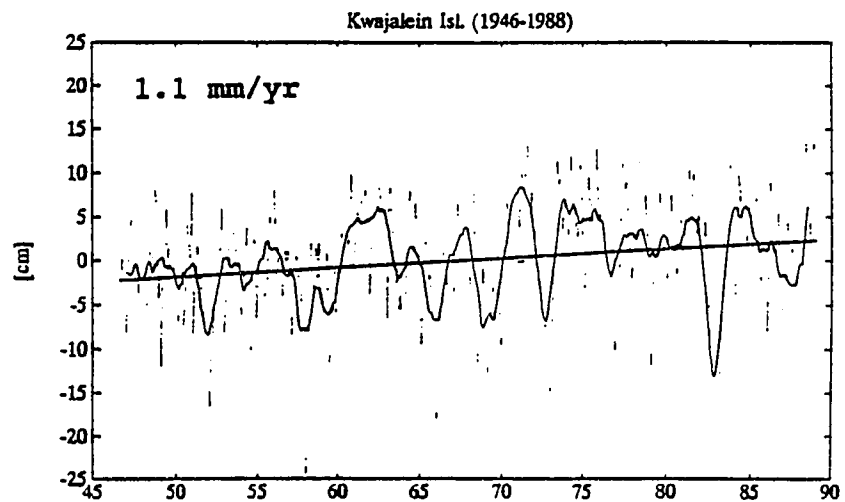
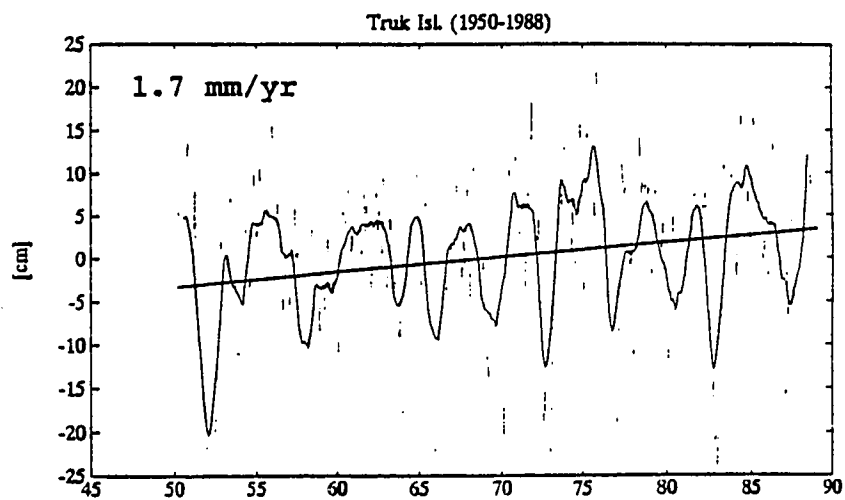
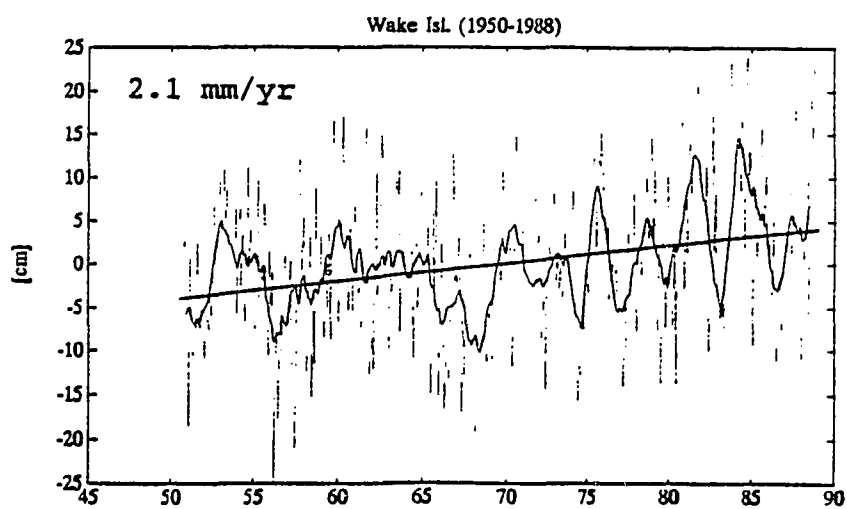


Fig.3.5. Long-term sea level trend (solid line), 12-month running mean (solid curve), and monthly sea level values (dotted curve) at (a) Truk, (b) Kwajalein, and (c) Wake Islands in the western Pacific Ocean.



(c)

Fig.3.5. (continued) Long-term sea level trend (solid line), 12-month running mean (solid curve), and monthly sea level values (dotted curve) at (a) Truk, (b) Kwajalein, and (c) Wake Islands in the western Pacific Ocean.

The mean annual difference of sea level height at the island stations of the western Pacific is about 10 cm, as is seen in the Hawaiian Islands. The maximum and minimum levels at Truk Island (about 7.5°N , 152°E) and Kwajalein (about 9°N , 168°E) occur in April and in January, respectively (Fig.3.6.(a),(b)). Surprisingly, at Kwajalein the monthly mean sea level height is almost flat (approximately 2 cm below the maximum level) from June to October after the maximum in April.

The annual pattern of the monthly mean sea level height is drastically different at Wake Island (about 19°N , 166.5°E), which shows a maximum in August and a minimum in May (Fig.3.6.(c)). There exists a slight secondary peak (about 3 cm higher than minimum level) between April and June. The secondary peak at Truk and the maximum level at Wake occur in the same month, October.

At Guam (about 13°N , 144°E) and at Eniwetok (about 11°N , 162°E), the patterns of the mean annual cycle are nearly sinusoidal and have almost the same phase as the sun's altitude, that is, maximum in June to July and minimum in December (Fig.3.6.(d),(e)). But the reason for this coincidence of phase is not clear; if there is no other contributing factors than the solar insolation, maximum sea surface temperature in annual cycle occurs in about 3 months after the date of the highest sun's altitude (summer solstice

in the Northern Hemisphere) due to high heat capacity of sea water.

Clear annual cycles of the monthly mean sea level height in the Hawaiian Islands follow the near-sinusoidal patterns in Guam and Eniwetok, except the phase lag: maximum level is about 3 months out of phase (between September and October) and minimum is even more lagged (April to May). While the high heat capacity of seawater and the steric effect might be the major causes of the annual cycle in the Hawaiian Islands, the annual variations of the monsoon winds and the surface current system in the western Pacific may result in the complex signals in the annual sea-level cycle.

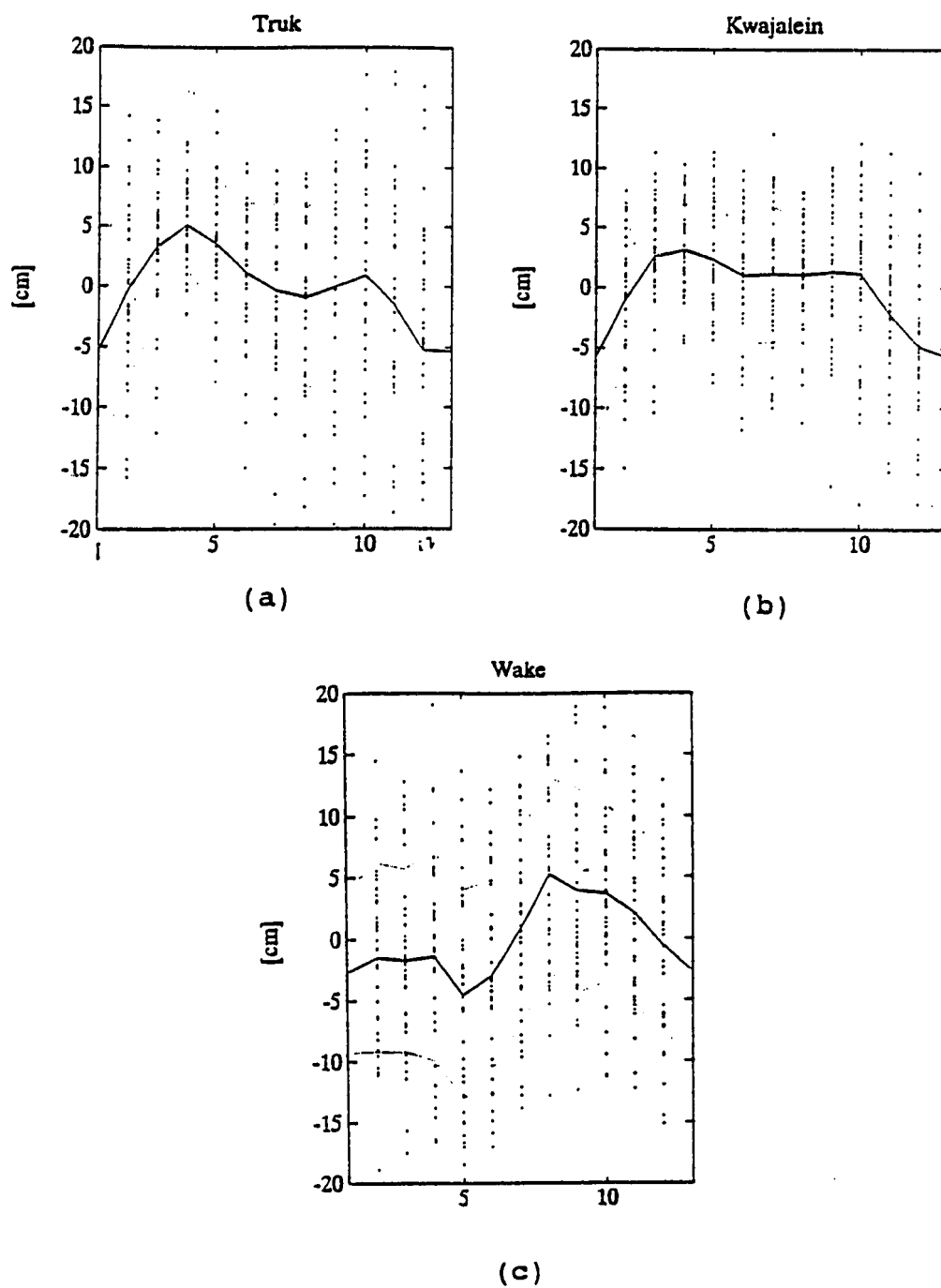


Fig.3.6. Mean annual cycle of monthly sea levels at (a) Truk, (b) Kwajalein, (c) Wake, (d) Guam, and (e) Eniwetok. Data are from PSMSL.

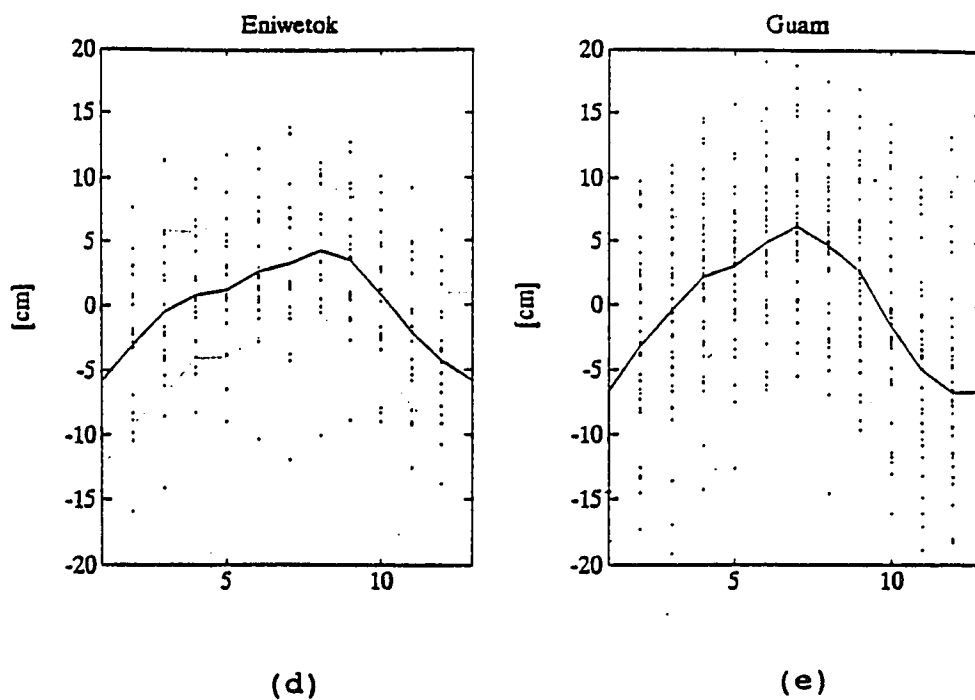


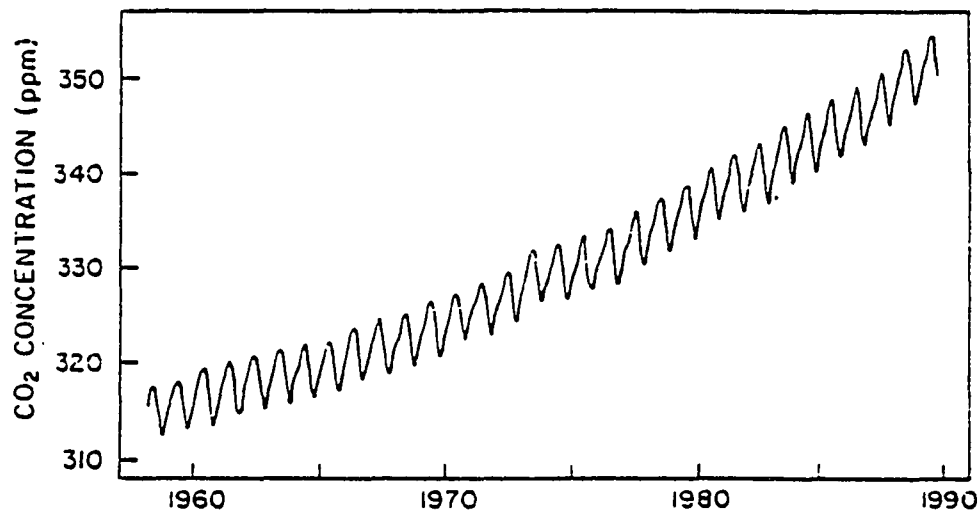
Fig.3.6. (continued) Mean annual cycle of monthly sea levels at (a) Truk, (b) Kwajalein, (c) Wake, (d) Guam, and (e) Eniwetok. Data are from PSMSL.

CHAPTER 4
EFFECTS OF SEA-LEVEL CHANGE
ON BEACH EROSION

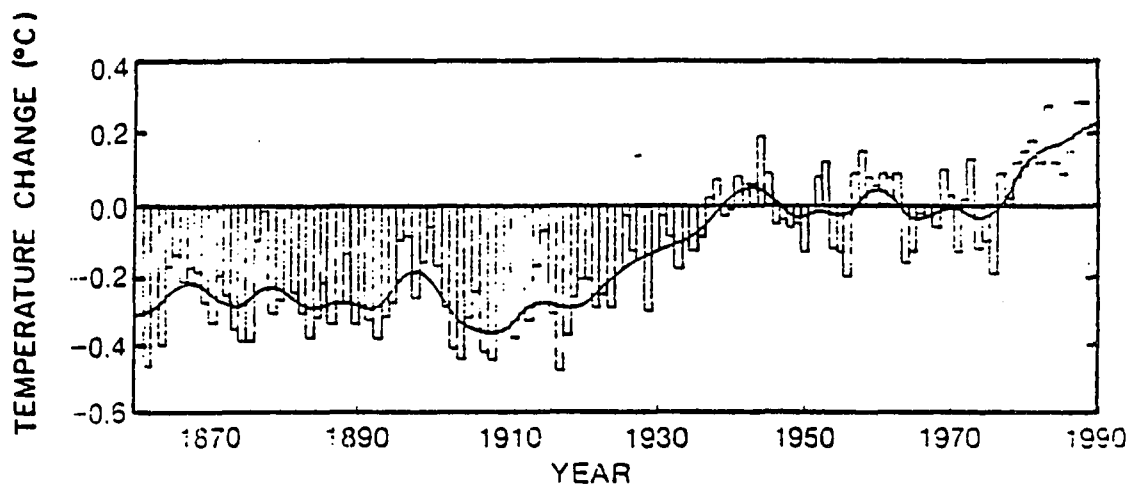
Glaciation/deglaciation due to climatic change, tectonic instability such as plate movements or volcanic activities, and global warming due to increasing greenhouse gases are all primary factors causing relative sea level rise as described in CHAPTER 1.

As a primary index of global warming, atmospheric CO₂ concentration has been increased by about 10% during the past 30 years and may be doubled in the next 50 years or so (Moberly and Mackenzie, 1985; IPCC, 1990) (Fig.4.1). According to the result of the general circulation model (IPCC, 1990), the increasing rate of greenhouse gases will result in the thermal expansion of the global, especially tropical, ocean surface layer. Although the IPCC scenario excludes the uncertainty due to the feedback mechanism of the atmospheric clouds, it seems now commonly accepted that the rate of sea level rise is increasing, i.e., accelerating at least for the next century.

Rise in mean sea level results in receding shorelines and in drowning low-lying coastal areas, which causes in turn submerged beach sediments to be transported both in



(a)



(b)

Fig.4.1. (a) Monthly average CO₂ concentration in parts per million of dry air observed at Mauna Loa, Hawaii, and (b) global mean temperature relative to the average for the period from 1951 to 1980 (after IPCC, 1990).

longshore and cross-shore directions by nearshore currents and waves. At most Hawaiian beaches surrounded by wide fringing reefs, longshore sediment transports, in general, are not so significant since waves usually break over the wide and shallow nearshore reefs before they approach the beaches. At beaches between headlands, such as Waimea Beach, the longshore transport causes a reorientation of the beach with changing wave conditions (Gerritsen, 1978).

A simplified two-dimensional 'relationship between sea level rise and cross-shore sediment transport' was first suggested by Bruun (1954) (*the Bruun Rule*), and widely tested and modified by other authors and by himself (Schwartz, 1965, 1967; Dubois, 1975; Dean and Maurmeyer, 1983; Bruun, 1988). For long-term change of sea level and coastal erosion due to cross-shore sediment transport, the *Bruun Rule* is a widely accepted concept despite its limitations in three-dimensional situations (Bruun, 1988).

Bruun (1962) proposed a simple two-dimensional relationship between shoreline retreat and an increase in local sea level along the cross-shore direction (Fig.4.2). It is assumed that

- 1) the upper beach is eroded due to the landward translation of the profile,
- 2) the material eroded from the upper beach is transported and deposited offshore,

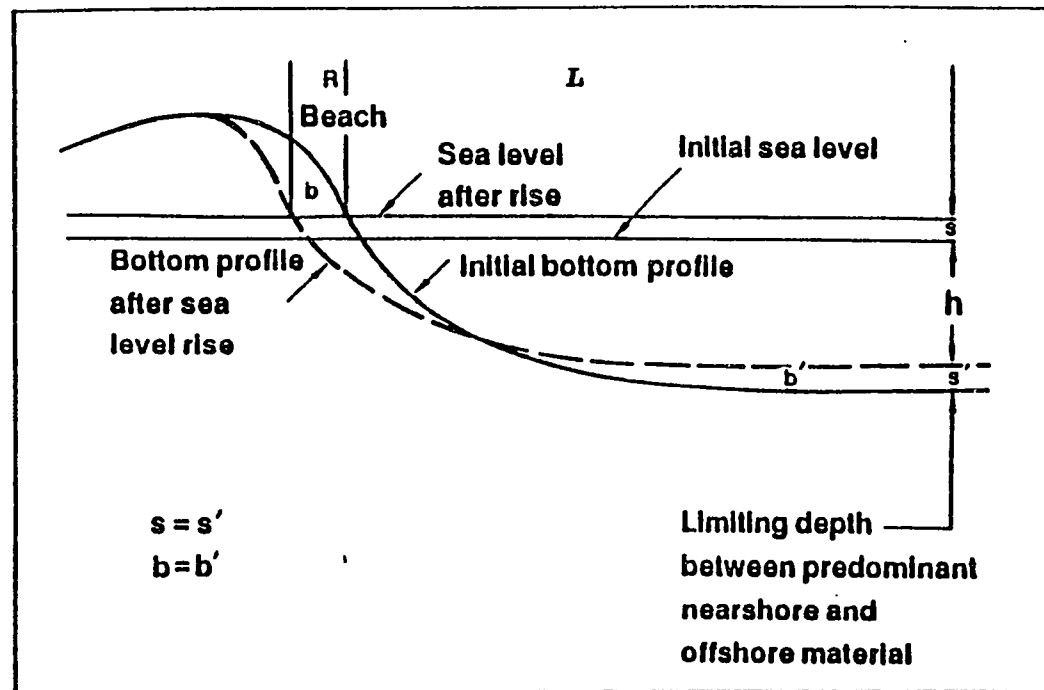


Fig.4.2. Schematic diagram of the relationship between sea level rise and coastal erosion by the Bruun Rule.

3) the rise in the nearshore bottom as a result of this deposition is equal to the rise in sealevel, thus maintaining a constant water depth.

When the gradient of longshore sediment transport is negligible, the eroded volume of sediments must be balanced by the volume to elevate the active width of the profile L , and a vertical distance (i.e., sea-level rise) S such that

$$R = \frac{L}{B+h} * S \approx \frac{S}{\tan \phi} \quad (4.1)$$

where R = the shoreline retreat rate,

S = an increase of sealevel,

L = the cross-shore distance to the water depth (h) of effective motion,

B = berm height,

$\tan \phi$ = $(B + h)/L$; the average slope of the nearshore along the cross-shore width L .

Meanwhile, Dubois (1975) defines $\tan \phi$ as the nearshore slope seaward from breaking waves, instead of the slope from the shore to the 'depth of effective motion'. In general, the bottom profile is not smooth and the 'depth of effective motion' may be variable, especially depending on the time scale of interest. But Dubois' definition does not seem to be a reasonable alternative, although it is validated by his

quantitative analysis, because a great portion of sediment transport occurs within the surf zone and hence the bottom profile in the surf zone may be more important than the slope seaward from the breaker line. Definitely, it must be the average slope, that is, 'effective vertical dimension over effective horizontal dimension of active profile'.

Dean and Maurmeyer (1983) suggested the modified Bruun Rule by considering the third dimension in the longshore direction:

$$P (B+h) R = L*S + G_b \quad (4.2)$$

where P = decimal fraction of eroded material that is compatible with the surfzone sediment, and
 G_b = sediment-budget terms including contributions from rivers or offshore, losses due to sediment being blown inland or transported offshore, and the longshore gradient of the littoral drift.

That is, the amount of littoral sediment driven from shoreline recession is balanced by the sum of the quantity required to maintain the equilibrium profile relative to a sealevel rise ($L*S$) and the sediment-budget terms (G_b).

A basic assumption of the Bruun model is the existence of an 'equilibrium beach profile', and that this profile is maintained or eventually achieved following a change in water level. The concept of 'equilibrium beach profile' (Bruun, 1954; Dean, 1977; Bodge, 1992; Pruszek, 1993) may be defined as an idealization of conditions which occur in nature for particular sediment characteristics and steady wave conditions (Dean and Maurmeyer, 1983). If a beach has a specific grain size and is exposed to constant forcing conditions, the beach may develop a profile shape that displays no net change in time (Larson, 1991). But 'the profile shape with no net change in time' may be different from beach to beach even for the same grain size and for the same wave conditions if the underlying geology, i.e., the bottom resistance against the forcing, as described by Pilkey et al. (1993), is different or if the component of the beach sediments is carbonate rather than silicate. In order to reach the same equilibrium state in beach profile, whether kinetic or dynamic, not only the forcing (in waves and sea level fluctuations) but also the response (in grain size, origin of sediments, and underlying geology etc.) should be the same. In reality, the equilibrium profile is dependent on wave conditions, and the evolution of a beach profile from one state to another does not occur with a constant profile form because the changes of profile are initiated where the profile is the most out of equilibrium.

Bruun (1954) and Dean (1977) propose an equilibrium beach profile given by

$$h(x) = A x^m \quad (4.3)$$

where $h(x)$ = water depth

x = horizontal distance from shoreline

A = dimensional shape parameter

Dean (1977) shows that eq.(4.4), with $m = 2/3$, is consistent with uniform energy dissipation per unit volume across the surf zone, applied to the U.S. east coast and the Gulf of Mexico.

Bodge (1992) suggests an alternative expression for the equilibrium beach profile given by

$$h(x) = B(1 - e^{-bx}) \quad (4.4)$$

where two parameters B and b have dimensions of depth and distance⁻¹, respectively. He compared eq.(4.3) and eq.(4.4) for various profile data and for hypothetical profiles, and concluded that the exponential expression eq.(4.3) is a better approximation to fit the data, especially for beaches with decreasing grain size in the offshore direction.

Bruun's (1954) empirical relationship (eq.(4.3)) from the beach profiles at Mission Bay, California and on the Danish North Sea coast was the first formulation for the equilibrium beach profile. By applying a least squares procedure, Dean (1977) proved that eq.(4.3), with $m = 2/3$, statistically well represented about 500 beach profiles (Hayden et al., 1975) along the U.S. east coast and the Gulf of Mexico. This empirical relationship for equilibrium beach profile has been used as the basis for the design of most coastal engineering projects on the continental beaches. In fact, the Bruun Rule (Bruun, 1962) is basically a simple equilibrium profile model that assumes the constant profile bounded by a 'closure depth'. The concept of a 'closure depth' (or a depth of effective sediment motion) is a critical assumption such that there is no net transport of sediment beyond the depth. The offshore current activity capable of transporting sediment beyond the closure depth was recognized as an insignificant and probably slow process (Bruun, 1962). But Pilkey et al. (1993) claimed that the concept of a closure depth is not valid since the offshore transport of sands beyond the closure depth is not insignificant during the last 20 year history of sand replenishment from Wrightsville Beach, North Carolina. Instead, they suggest the 'regime profile' concept to fit reality for certain beaches.

Pruszek (1993) examines beach changes in terms of Dean's (1977) function, eq.(4.3) with $m = 2/3$, and empirical orthogonal function. His basic assumption is that the dynamics and shape of the cross-shore profile must be analyzed at different time-scale. Thus parameter A as a function of time is given by the sum of several components with different time-scale such that

$$A(t) = \bar{A} + A_1 + A_2 + A' \quad (4.5)$$

where

$$\bar{A} = f(\text{sediment characteristics}) \approx \text{constant}$$

$$A_1 = f(\text{long-term cyclic change})$$

$$A_2 = f(\text{seasonal cyclic change})$$

$$A' = f(\text{short-term random change})$$

Since A_1 and A_2 are the cyclic changing terms with different time-scales, they are expressed by the Fourier components such that

$$A_{1,2} = \sum_{j=1}^2 a_j \cos\left(2\pi \frac{t}{T_j} + \phi_j\right) \quad (4.6)$$

where a_j , T_j , and ϕ_j represent amplitude, period, and phase of long-term and seasonal changes for $j = 1$ and $j = 2$, respectively.

A wave-based profile zonation comes from the exponential distribution form of wave statistics. And the peak near-bottom velocity that is exceeded 12 hours per year ($\approx 0.14\%$) is given by

$$[u_{\max(-d)}]_{s_{0.14}} = \left[0.03 \left(\frac{\rho_s - \rho}{\rho} \right) g d_c \right]^{\frac{1}{2}} \quad (4.7)$$

where d_c = closure depth with a seaward limit to extreme surf-related effects throughout a typical year

ρ_s = density of sands

ρ = density of seawater

The closure depth (d_c) for quartz sand in sea water with small-amplitude wave theory is approximated by

$$d_c = 2 H_{s50} + 12 \sigma_H \quad (4.8)$$

In any case, a closure depth must be the key concept in equilibrium profile models, which were developed for *siliceous* continental beaches. However, calculating a closure depth for *calcareous* Hawaiian beaches with the equilibrium profile model is still useful.

The maximum and minimum values of significant wave heights throughout a typical year at the NOAA buoy location are 6.9 m and 1.1 m, respectively, and the median and standard deviation are as follows:

$$\begin{aligned} H_{S_{50}} &= 4.0 \text{ m} \\ \sigma_{H_S} &= \pm 0.95 \text{ m} \end{aligned}$$

Then, the closure depth by eq.(4.8) is obtained as

$$\begin{aligned} d_c &= 2 H_{S_{50}} + 12 \sigma_{H_S} \\ &\approx 20 \text{ meters} \end{aligned}$$

This value is larger than the annual depth of effective motion which was estimated roughly twice the extreme nearshore wave height exceeded 12 hours per year (Hallermeier, 1981a). At Waimea Bay Beach, Oahu and at Hapuna Beach, Hawaii, the approximate depth of seaward limit to intense cross-shore sand transport was about 15 meters for model-storm waves in this study. This value of the closure depth is about 25% smaller than that calculated by eq.(4.8). The discrepancy may come from either underestimate by the Bailard's model or overestimate by eq.(4.8) because nearshore wave height is usually higher than deep-water wave height due to shoaling.

In reality, the depth of effective motion may depend on the time scale of interest. For example, at some locations on the east coast of the U.S. the effective depth associated with periods of interest of 1 year, 5 years, and 20 years may be about 4.5 m, 6 m, and 7.5 m, respectively (Dean and Maurmeyer, 1983). For longer time-scale of interest, not only waves but also sea-level fluctuations should be considered as forcing functions to the beach erosion. Moreover, the longer the period of sea-level fluctuations the more effective it may be on beach erosion if longshore sediment transport and all the other factors are negligible (that is, if cross-shore transport is the only significant erosion/acretion process).

Komar et al. (1991) argue that, if water-level is rapidly changed such as an abnormal sea level rise during an El Niño, the response of the beach may be too slow to maintain the equilibrium profile. Some other authors (Edelman, 1968; Dean, 1977; Kriebel and Dean, 1992) applied the Bruun Rule for shorter time-scale change of beach profiles. Therefore, it is controversial whether the Bruun Rule may be justified for investigating short-term variations.

Sea-level rise never occurs in a steady manner but in fluctuations with different time-scales. In fact,

interannual sea-level fluctuations seem to be very important to coastal processes and shoreline retreats since the RSL fall after the rise in this time-scale cannot usually restore the lost amount of the sediments as is the case of the mean annual oscillation of the cross-shore transports. Hence the computation of only long-term shoreline recession according to the Bruun Rule definitely underestimates the real amount of coastal erosion. Moreover, longshore sediment transport often plays a significant role in local shoreline changes. Thus, the relationship between sea-level rise and coastal erosion must be examined at least for an isolated beach or a littoral cell where there is little net longshore sediment transport to and from neighboring beaches. Despite the controversy of the validity of a closure depth in equilibrium profile models, a seaward limit to the effective sand motion by waves has been applied to many engineering problems.

CHAPTER 5
THE EFFECTS OF STORMS ON BEACH EROSION

5.1. GENERAL REMARKS

The cross-shore sediment transport due to waves is caused by

- 1) onshore transport by asymmetry of wave form in shallow water,
- 2) offshore transport by the return flow under the trough of wave form due to continuity, and
- 3) offshore transport as a bedload due to gravity at the bottom.

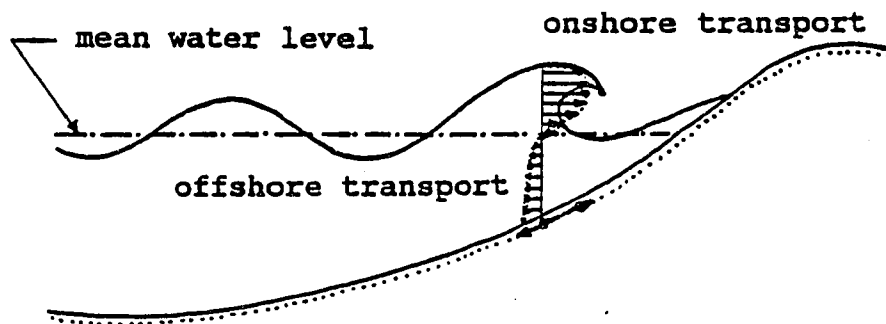


Fig.5.1. Schematic diagram of cross-shore sediment transport processes under waves. Arrows represent average transports over a wave period.

Linear gravity wave theory gives the phase speed of a small-amplitude deep-water wave as

$$c^2 = \frac{g}{k} \quad (5.1)$$

The second order Stokes wave moves slightly faster than the linear small-amplitude wave, which can be expressed in terms of the wave steepness, i.e., the ratio of wave height to wavelength ($= H/\lambda$) (see Fig.5.2-1, Kinsman, 1984),

$$c^2 = \frac{g}{k} [1 + \pi^2 (H/\lambda)^2] \quad (5.2)$$

The real trajectory of a fluid particle is not a closed circle such as described by pure linear wave theory but an open circle resulting in a nonzero mean second-order drift arising from the nonlinear solution (*Stokes drift*), which represents the difference between Lagrangian and Eulerian velocities.

Actual wave fields in shallow water show an extreme asymmetry (or *nonlinearity*) of wave form. The consequence of it is that the onshore fluid velocity under the crest of the wave is greater than the offshore-directed velocity

underneath the wave trough, resulting in an onshore sediment transport.

Return flow (or undertow) occurs between wave trough and the bottom, forming a vertical circulation cell due to the conservation of mass, while rip-currents form a part of a horizontal circulation cell. Thieke and Sobey (1990) considered the conservation of mass, momentum, and energy to describe cross-shore mean flow circulation with the horizontal flow velocity in terms of three components: a time-averaged quantity, turbulence and waves. They show that the return flow is rather less intense and directed offshore while the wave-induced mass transport velocity between trough and crest of the wave is relatively intense and directed towards the beach.

Once the near-bottom flow velocity exceeds the sediment threshold velocity, bottom sediments move as bedload by the resultant forces of gravity and friction.

During high and steep wave conditions, sediments move offshorewards due to the relatively stronger return flow than the onshore transport by wave asymmetry (*erosion*). The eroded sediments often form longshore bar(s) to the offshore region. During low and mild wave conditions, sediments move in the reverse direction (*accretion*) due to the wave

asymmetry and the relatively weaker return flow. The longshore bar is basically unstable and often migrates with the nodal point of infragravity waves (or *surf beat*), the uncoupled low-frequency waves in the nearshore region (Gerritsen and Jeon, 1991).

Waves around the Hawaiian Islands can be generated by both local and remote wind fields in any part of the Pacific Ocean. Trade winds (northeasterlies to southeasterlies) are predominant over almost the whole year since the Hawaiian Islands are located in the middle of the trade wind belt, which generates *trade-wind waves*. Kona storms (southerly to southwesterly) due to the passage of extratropical low-pressure systems associated with the westerlies during winter (from October to April), although not frequent, cause *Kona-storm waves*. Remote storms from the Aleutians or mid-latitudes in the North Pacific and from the Southern Hemisphere generate *North Pacific swell* and *Southern swell*, respectively. Each swell is usually frequent during the winter time of each hemisphere (Inman et al., 1963; Moberly and Chamberlain, 1964) (Fig.5.2).

The surf condition on the north shore, Oahu is extremely variable, usually very low during summer and very high during winter. The mean surf heights in summer (June, July, and August) and in winter (December, January, and February) on Sunset Beach were 0.11 ± 0.11 m, and $2.35 \pm$

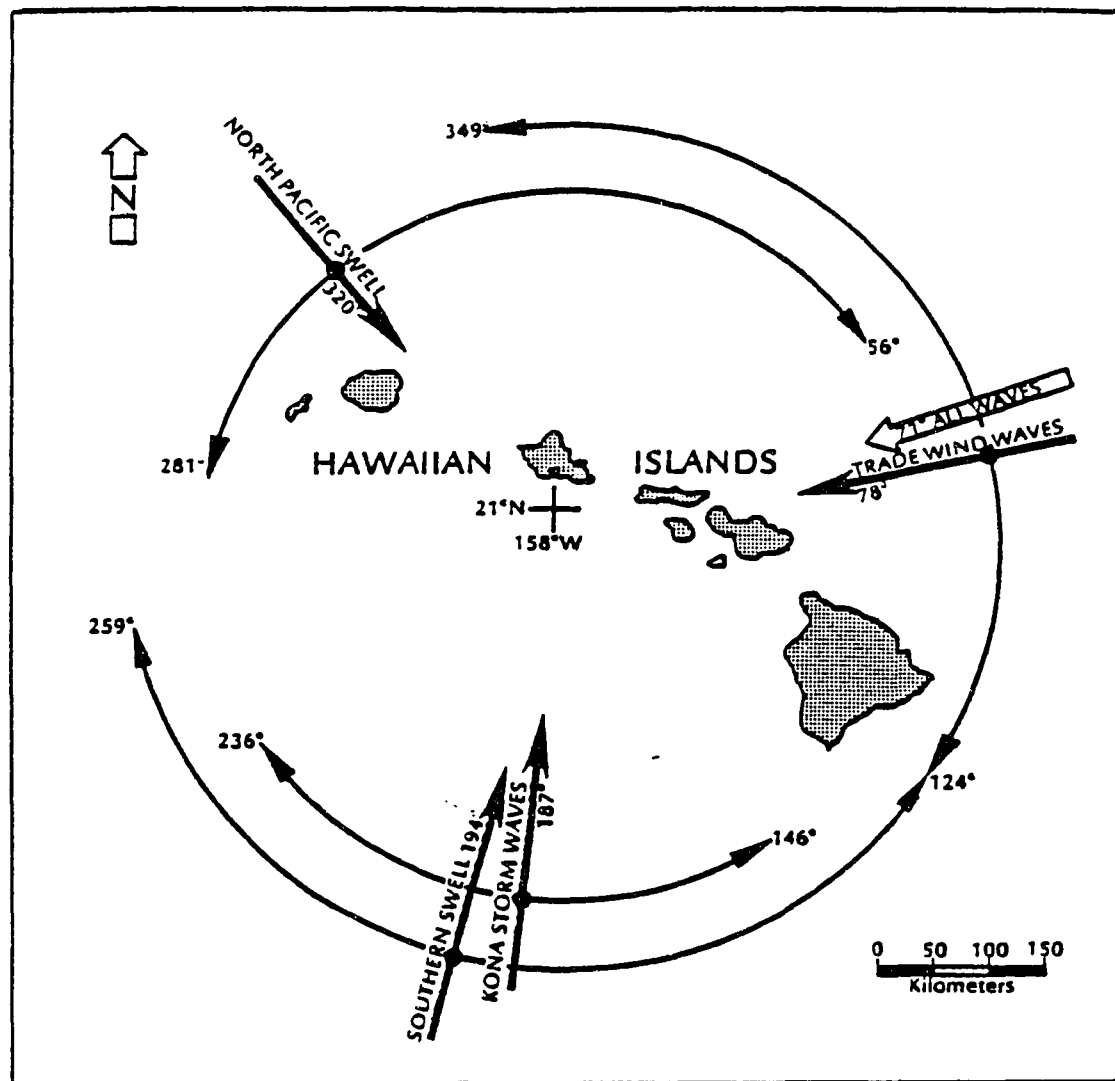


Fig.5.2. The ranges and mean directions of the typical wind waves approaching to the Hawaiian Islands (Inman et al., 1963).

1.35 m, respectively, during 1988 to 1992. Maximum surf height was reported over 7 m during the same period. On the contrary, mean surf heights on the south shore, Oahu are fairly low in both seasons but a little higher in summer ($H_b = 0.90 \pm 0.33$ m) than in winter ($H_b = 0.63 \pm 0.27$ m). Maximum wave height off Diamond Head, Oahu during this period was reported about 2.1 m. Meanwhile, the condition on the west shore, Oahu is in between north and south shores. Mean surf height on Makaha Beach was 0.35 ± 0.35 m in summer and 1.31 ± 0.90 m in winter, and maximum height was 6.1 m during the same period (Fig.5.3). This is because the surf condition is highly correlated with the winds -- the North Pacific storms in winter and the trade winds during the rest of the year -- in the Hawaiian Islands.

Wave-induced longshore currents due to breaking result in longshore sediment transport, which will not be discussed in this study since longshore transport is often not significant at Hawaiian beaches. Shallow coral-reef environments often play a role as offshore breakwaters and wave energy is greatly reduced before it arrives at the shore. This study is strictly limited to the shoreline change due to cross-shore sediment transport. However, edge waves and surf beats (or infragravity waves) are often responsible for many coastal features such as beach cusps, crescentic bars, caps, and bays.

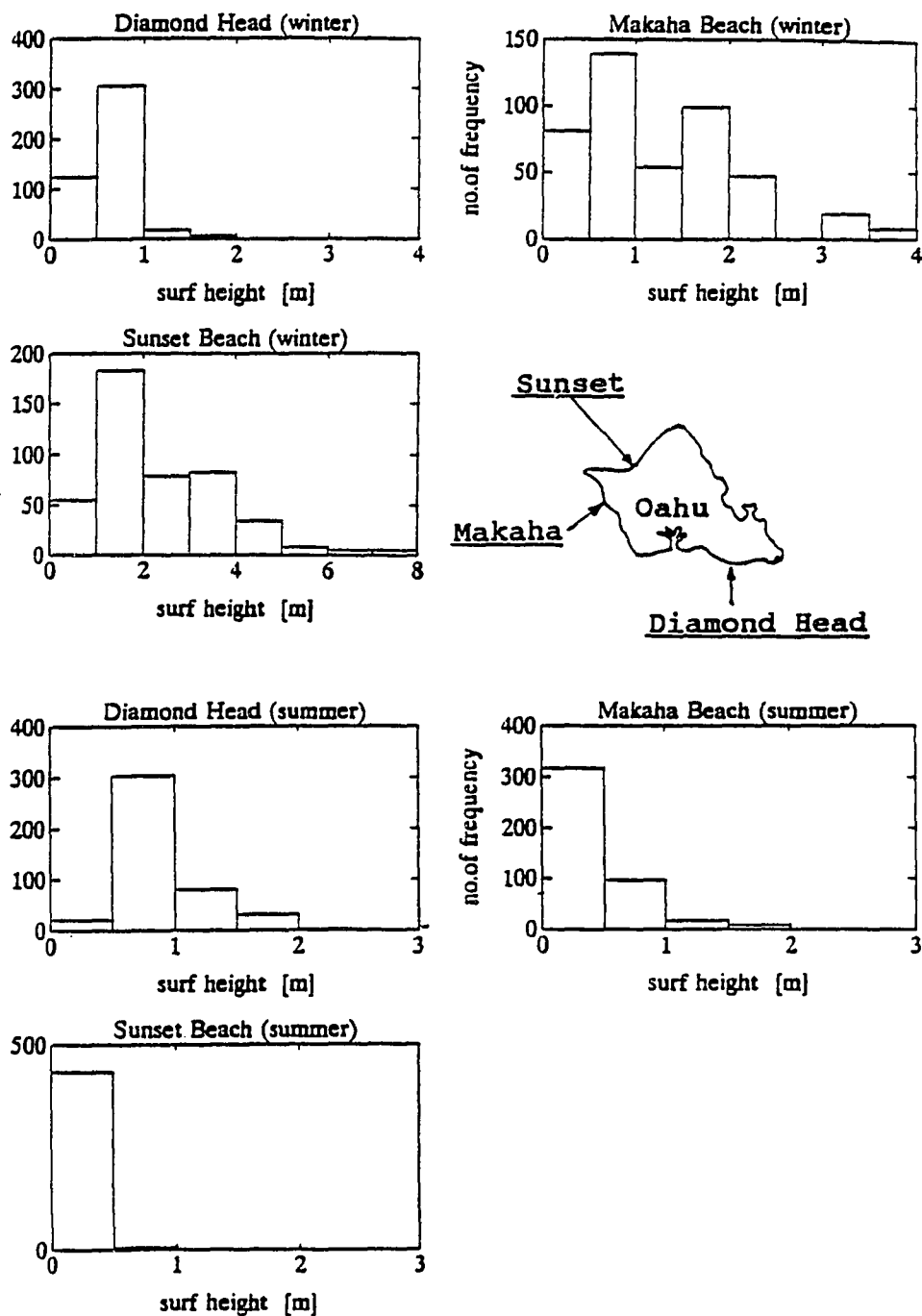


Fig.5.3. Surf height distributions on Diamond Head, Makaha Beach, and Sunset Beach, Oahu in winter (December, January, February) and in summer (June, July, August). Data are from P. Caldwell, TOGA Sea Level Center, Univ. of Hawaii.

Rip currents play an important role as a secondary return flow in nearshore circulation. They carry water back to the offshore region through the breaker zone in horizontal circulation, often with an undulating shoreline. They appear most noticeable when long and high waves produce wave setup on the beach (U.S.Army Corps of Engineers, 1984).

Wave climate northwest of Kauai (see Fig.3.2. for the location of the NOAA buoy) is shown as annual variations of daily mean significant wave heights for 12 years in Fig.5.4 (each curve represents an annual time-series each year). The average of significant wave height in winter (December, January, and February) exceeds 3 m, while it is reduced to less than 2 m during summer (June, July, and August). The corresponding average wave period is about 2 seconds longer in winter than in summer (Table 5.1). This is because stronger North Pacific swells affect the wave climate during winter and milder trade-wind waves prevail during the rest of a year (Inman et al., 1963; Moberly and Chamberlain, 1964; Patzert, 1969). From the crude correlation analysis between local wind directions and waves at the NOAA buoy station, North Pacific swells occur only about 5% of the annual time-series of waves while trade-wind waves occupy about 80% of the year. Southern swells and Kona-storm waves occur during the remaining 15% of the year.

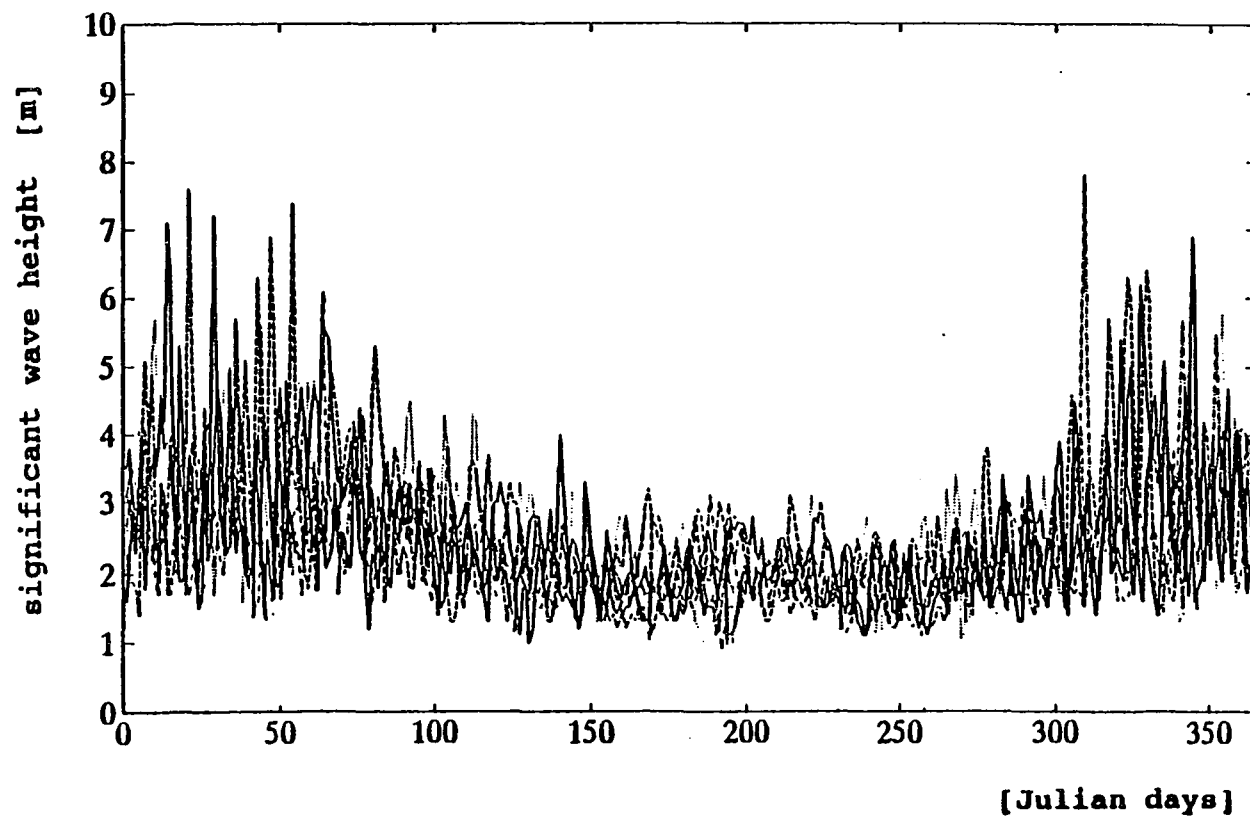


Fig.5.4. Wave climate as annual variations of daily mean significant wave height for 12 years at the northwest of Kauai ($23^{\circ}24'N$, $162^{\circ}18'W$), measured from the NOAA environmental buoy (no. 51001). Data are from NODC.

Table 5.1. Averaged significant wave height and wave period by season and by wave type: winter (December, January, February) and summer (June, July, August) seasons data are averaged from 1981 to 1992, and different wave types are taken in 1985 and 1990, at the NOAA buoy (51001) location (23°24'N, 162°18'W).

season or wave type	averaged sig. wave height (H_o)	averaged sig. wave period
winter	3.1 ± 0.17 m	7.7 ± 0.5 sec
summer	1.9 ± 0.11 m	5.7 ± 0.4 sec
Trade-wind waves	2.4 m	6.5 sec
Southern swells & Kona-storm waves	2.8 m	7.7 sec
North Pacific swells	3.5 m	8.0 sec

Disastrous damages as well as erosion of low-lying coastal areas may result from tropical cyclones and tsunamis (or seismic sea waves).

The typical horizontal dimension of a hurricane is about 200 km or less, and maximum wind speed near the center is about 50 to 100 m s⁻¹. The paths of hurricanes are largely controlled by the subtropical high pressure areas over the oceans. Initially they move westwards at low

latitudes in the prevailing easterlies, but then often curve polewards around the high pressure center and finally travel in an easterly direction under the influence of the westerly winds of high latitudes (Harvey, 1976).

The frequency of tropical cyclones passing over a specific area is relatively low. Gray (1979) reviews a brief discussion of the character and the effect of the tropical cyclones on the ocean. He found a world average of 80 events per year during a 20 year period (Fig.5.5). They originate in latitudes between 5° to 25°, not at the equator where the Coriolis effect vanishes, but only in longitudes in which the sea is warm, thus allowing the equivalent potential temperature at the surface to reach values high enough for strong convection to be promoted (Gill, 1982).

When tropical storms over very warm surface water ($> 26^{\circ}\text{C}$) are rapidly amplified into intense vortical storms by a certain mechanism¹⁰ under favorable conditions of moisture supply, they become tropical cyclones such as hurricanes or typhoons (Holton, 1979). Thus hurricanes occur more likely during summer season. In fact, more than

¹⁰ *Conditional Instability of the Second Kind (CISK)* -- the process of the cooperative interaction between the cumulus convection and a large-scale perturbation leading to unstable growth of the large-scale system.

70 % of the total tropical cyclones of the Northern Hemisphere during 1958 to 1977 were reported between July and October (Gray, 1979).

The oceanic response to the passage of a hurricane or depression is basically dependent upon the hurricane speed (U) relative to the long gravity-wave speed (c); for a slow-moving disturbance ($U < c$), the atmospheric pressure and the water displacement are out of phase and the response of the ocean is confined to the neighborhood of the hurricane. For a fast-moving disturbance ($U > c$), which is the more usual situation in nature, the pressure and displacement are in phase and the amplified lee waves appear behind the hurricane. When both speeds are the same ($U = c$), the response has the same shape as that of the forcing (Gill, 1982).

Hurricanes which directly hit the Hawaiian Islands such as *Nina* in 1957, *Iwa* in 1982, and *Iniki* in 1992 during a few recent decades (Fig.5.6) have caused great damage and coastal erosion due to the direct storm effects and the surges running up the coastal regions. Unfortunately, no direct measurements of beach profile changes have been taken before and after the hurricanes.

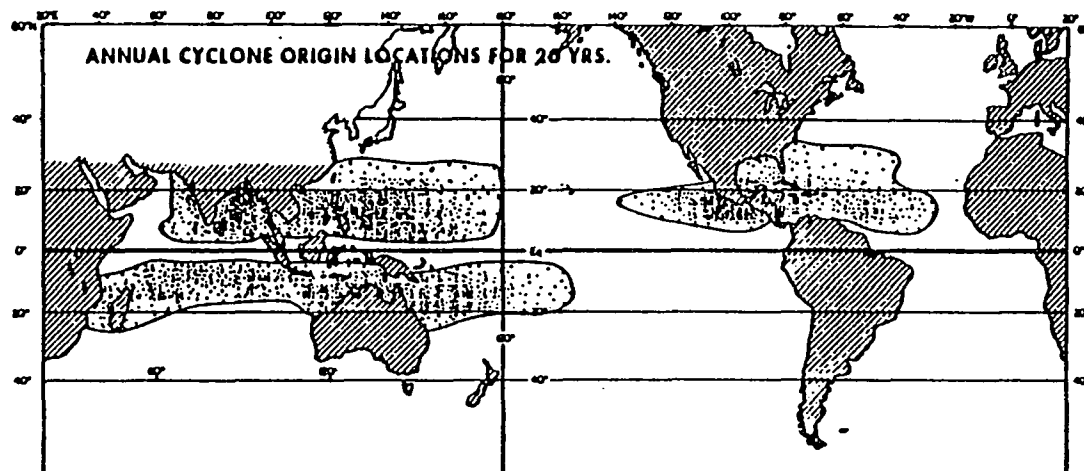


Fig.5.5. The location of the points of origin of tropical cyclones during a 20-year period. (after Gray, 1979)

Run-up height is of particular interest to coastal engineers because it gives the upper limits of inundation of the coastal region and also affects the design and construction of coastal structures.

Hunt (1959) proposes an empirical relationship of the runup height (R_u) to wave height (H_b), deep-water wavelength (λ_o), and beach slope ($= \tan \beta$) such that

$$R_u = \sqrt{H_b \lambda_o} \tan \beta \quad (5.3)$$

The relative runup height (R_u/H_b) may be expressed by

$$\frac{R_u}{H_b} = \sqrt{\frac{\lambda_o}{H_b}} \tan \beta \quad (5.4)$$

The right-hand side of eq.(5.4) is also called 'surf similarity parameter'. Its value determines breaker type¹¹, wave runup, and stability of breakwater units. As an engineering application for a coastal structure, run-up height can be reduced by increasing the roughness and permeability, decreasing the slope, and changing the shape of the structure into a 'berm structure'.

¹¹ Four common classifications are *spilling*, *plunging*, *collapsing*, and *surging breakers* (after Galvin, 1968).

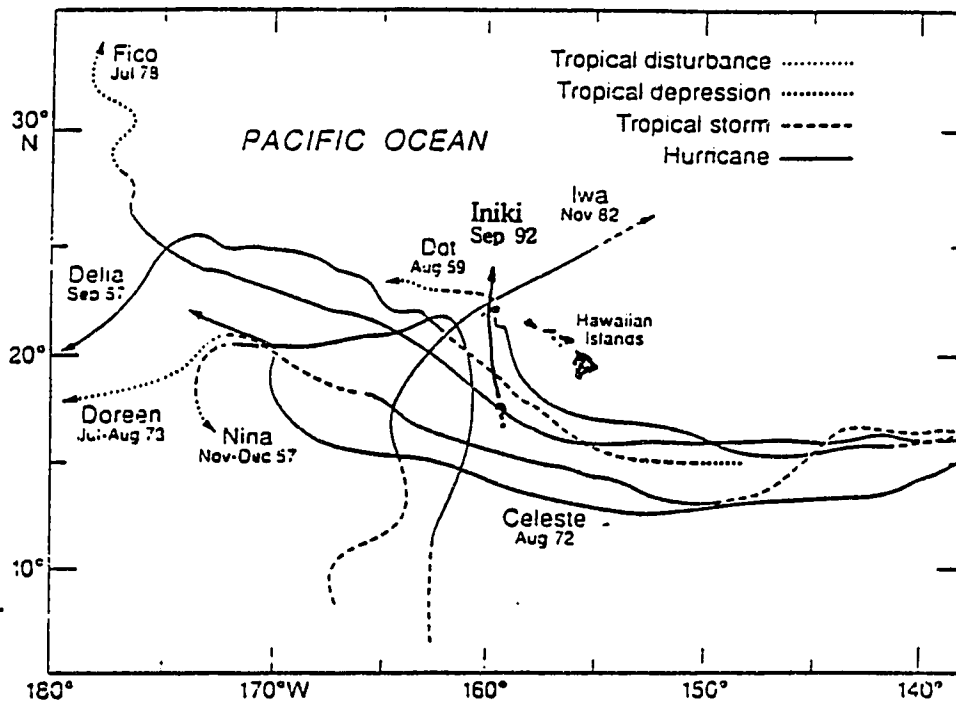


Fig.5.6. Hurricane tracks around the Hawaiian Islands

5.2. SHORT-TERM BEACH EROSION MODELS

Bailard (1984) generalized an energetics-based sediment transport model which had been originally developed for streams by Bagnold (1966). This model is useful for short-term changes of the beach profiles due to its simplicity.

The resulting equation for local longshore and cross-shore transport rates is expressed as functions of local waves, currents, and sediment parameters such that

$$\begin{aligned} \langle q_t \rangle = & \rho C_f \frac{e_b}{\tan \phi} \left(\langle |u_t|^2 u_t \rangle - \frac{\tan \beta}{\tan \phi} \langle |u_t|^3 \rangle i \right) \\ & + \rho C_f \frac{e_s}{w_s} \left(\langle |u_t|^3 u_t \rangle - \frac{e_s}{w_s} \tan \beta \langle |u_t|^5 \rangle i \right) \end{aligned} \quad (5.5)$$

where q_t = instantaneous sediment transport rate
 u_t = instantaneous near-bottom fluid velocity
 C_f = drag coefficient of the bed
 e_b = bedload efficiency factor
 e_s = suspended load efficiency factor
 $\tan \beta$ = bed slope
 ϕ = internal angle of friction for the sediment
 w_s = fall speed of the sediment
 ρ = density of the fluid
 i = unit vector directed upslope
 $\langle \rangle$ = time-averaged quantity

The above sediment transport rates imply the feature that the bedload and suspended load transports consist of primary components directed parallel to the instantaneous fluid velocity vector, and secondary components directed downslope.

Total (near-bottom) velocity u_t is split into an oscillatory and a steady velocity components such that

$$u_t = (\bar{U} \cos \theta + u) i + (\bar{U} \sin \theta + v) j \quad (5.6)$$

And the oscillatory velocity is expressed by the harmonic components such that

$$\bar{u} = u_m \cos \sigma t + u_{m2} \cos 2\sigma t + \dots \quad (5.7)$$

With the assumptions that

- 1) a steady velocity component is relatively small with respect to the maximum amplitude of an oscillatory component ($u/u_m \ll 1$),
- 2) incident wave angle is nearly orthogonal to the shoreline ($\cos \theta \approx 1$),

both local and (spatially) averaged longshore and cross-shore transport rates are obtained.

The resulting cross-shore transport equation becomes

$$\begin{aligned} \langle Q_x \rangle = & \rho C_f u_m^3 \frac{e_b}{\tan \phi} \left(\psi_1 + \frac{3}{2} \delta_u - \frac{\tan \beta}{\tan \phi} u_3^* \right) \\ & + \rho C_f u_m^4 \frac{e_g}{W_g} \left(\psi_2 + 4 u_3^* \delta_u - e_g \frac{u_m}{W_g} \tan \beta u_5^* \right) \end{aligned} \quad (5.8)$$

where

$$\delta_u = \frac{u}{u_m} \quad (5.8.1)$$

$$\psi_1 = \frac{\langle |u|^3 \rangle}{u_m^3}, \quad \psi_2 = \frac{\langle |u|^3 u \rangle}{u_m^4} \quad (5.8.2)$$

$$u_3^* = \frac{\langle |u_e|^3 \rangle}{u_m^3}, \quad u_5^* = \frac{\langle |u_e|^5 \rangle}{u_m^5} \quad (5.8.3)$$

The relative mean velocity δ_u and the wave velocity moments ψ_1, ψ_2 can be estimated from the measured field data and correlation with incident wave characteristics. But u_3^* and u_5^* are assumed to be constants following previous results (Guza and Thornton, 1981; Bailard, 1984).

The oscillatory component of the fluid velocity includes both short-period (*incoming*) waves and longer-period (*reflecting*) infragravity waves, and hence simple Fourier decomposition may not be sufficient to express the oscillatory component.

It seems worthwhile to review Roelvink and Stive (1989) although their idea is not applied in this study. The oscillatory component of the total wave velocity may be decomposed into short and longer waves, that is,

$$u = u_s + u_L \quad (5.9)$$

They discuss the wave velocity moments in terms of these two components. Assuming that 1) the individual waves, u_s , are not correlated to $|u_L|^2$ and $|u_L|^3$, and that 2) $u_L \ll u_s$, they obtain the odd central flow moments such that

$$\langle u|u|^2 \rangle = \langle u_s|u_s|^2 \rangle + 3 \langle u_L|u_s|^2 \rangle \quad (5.10)$$

$$\langle u|u|^3 \rangle = \langle u_s|u_s|^3 \rangle + 4 \langle u_L|u_s|^3 \rangle \quad (5.11)$$

The first terms on the right-hand side are nonzero when there exists an asymmetry about the horizontal plane caused by nonlinearity of the waves. The last terms are nonzero if there exists a correlation between the slowly varying velocity u_e and the short-wave velocity variance u_s^2 . They use separate models for the first and last terms according to a nonlinear, monochromatic theory and a wave envelop interaction for a bichromatic wave train with accompanying bound long wave, respectively.

Despite the simplicity, Bailard's model for cross-shore sediment transport shows some realistic features such that

- 1) gradual onshore sand movement occurs when waves are small, while rapid offshore movement occurs with larger waves.
- 2) the equilibrium wave height is small with steep beaches, while it is larger with flat beaches.
- 3) a beach adjusts to an equilibrium beach slope with the incident wave height over sufficient time.

The limitations of the energetics-based model are that it does not include sediment threshold of motion effects, a variable drag-coefficient, and a different formulation for the rate of energy dissipation in the surf zone.

Steetzel (1990) developed a storm-induced erosion model, modified from Vellinga (1986), for beach and dune profile changes due to storm surges, using a large wave flume.

Cross-shore suspended transport can be computed by integration of the product of the sediment concentration and the particle velocity, which may be expressed as the difference between upper onshore transport (S_u) above the wave trough level (i.e., upper zone) due to the wave-induced flow in the upper layer and lower offshore transport (S_l) below the wave trough level (i.e., lower zone) due to the return flow.

The sediment concentration is assumed constant in the upper zone since the vertical variation of the concentration is very small above the trough level, and the transport can be calculated by

$$S_u = C_d \cdot \int_{z=d_t}^{\bar{z}} u(z) dz = C_d \frac{M}{\rho} \quad (5.12)$$

where C_d = concentration at the mean water level
 M = mass flux above the wave trough level (d_t).

In the lower zone the net offshore transport is obtained from the integral of the product of the mean velocity and mean concentration such that

$$S_1 = \int_{z=0}^{d_c} u(z) \cdot C(z) dz \quad (5.13)$$

Vertical distribution of the sediment concentration is approximately exponentially decreasing from the bottom, which may be expressed by

$$C(z) = C_o \left[1 + \frac{\kappa z}{e_o} \right] \left(-\frac{w_s}{\kappa} \right) \quad (5.14)$$

where

- C_o = reference concentration at the bottom
- w_s = sediment fall velocity
- e_o = reference mixing coefficient
- κ = vertical mixing gradient
- ρ = density of the fluid

The above equation is based on the assumption of mixing coefficient $e(z)$ as a linear function of the level above the bed such that

$$e(z) = e_0 + \kappa z \quad (5.15)$$

And the vertical distribution of the mean particle velocity is described by

$$u(z) = u_0 + \frac{\delta_1}{\kappa} z + \delta_2 \cdot \ln\left(1 + \frac{\kappa z}{e_0}\right) \quad (5.16)$$

where

$$\delta_1 = \frac{1}{\rho} \frac{\partial \overline{\tau}}{\partial z} = \frac{\overline{\tau_t} - \overline{\tau_0}}{\rho \cdot d_t} \quad (5.17.1)$$

$$\delta_2 = \frac{1}{\kappa} \left(\frac{\overline{\tau_0}}{\rho} - \frac{\delta_1}{\kappa} e_0 \right) \quad (5.17.2)$$

and τ_t , τ_0 represent mean shear stress at the wave trough level and at the reference level, respectively.

Now the transport in the lower zone is

$$S_1 = C_0 \frac{e_0}{\kappa} \left(u_0 \cdot I_1 + \frac{\delta_1}{\kappa} \cdot I_2 + \delta_2 \cdot I_3 \right) \quad (5.18)$$

where

$$I_1 = \frac{1}{K_1} (K_2^{K_1} - 1) \quad (5.19.1)$$

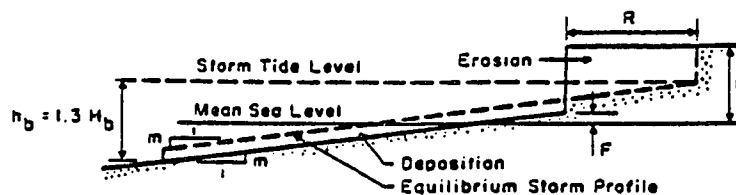
$$I_2 = \frac{1}{K_1} \left[K_2^{K_1} \left(d_t - \frac{e_0}{\kappa} \cdot \frac{K_2}{K_1 + 1} \right) + \frac{e_0}{\kappa} \cdot \frac{1}{K_1 + 1} \right] \quad (5.19.2)$$

$$I_3 = \frac{1}{K_1^2} \left[K_2^{K_1} (K_1 \ln K_2 - 1) + 1 \right] \quad (5.19.3)$$

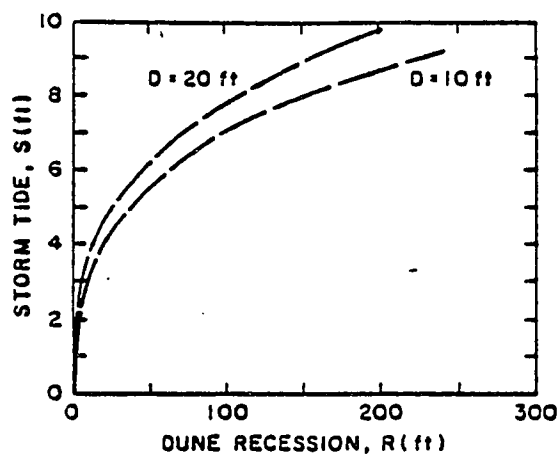
and

$$K_1 = 1 - \frac{W_s}{\kappa}, \quad K_2 = 1 + \frac{\kappa}{e_0} d_t \quad (5.19.4)$$

As an application of the Bruun Rule to a short-term scale, Edelman (1968) proposed a beach-response model before and after a storm with a constant equilibrium profile relative to the instantaneous sea level and a uniform slope depending on sediment characteristics. He assumed the wave-breaking depth as the depth of effective motion. He attempted to generalize the dune erosion as a function of storm surge level and dune height (Fig.5.7).



(a) Edelman's Method I Applied to Idealized Beach Profile.



(b) Dune Erosion Versus Storm Tide for Idealized Profile. $F=0$, $H_b = 1.5 S$.

Fig.5.7. (a) Schematic diagram of the Edelman's (1968) model for an idealized beach profile, and (b) the relationship between dune erosion and storm-surge height.

5.3. SHORT-TERM FLUCTUATION

Short-term events in the order of a few hours to days by tropical storms, hurricanes and tsunamis may worsen the erosion problem since the frequency and severity of the storm surges and the seismic sea waves with rising sea level may be higher and stronger than those at present (IPCC, 1990), and the coastal inundation limit may be further inland. The major damage and loss of life from most hurricanes occur within 100 to 150 km of the landfall position, the point where the low-pressure center crosses the coastline (Fig.5.8). Vertical rise of sea level by hurricanes commonly reaches more than 4 m above the MSL, especially on the continental coasts. The tide-gauge record by hurricane *Camille* in 1969 rose up to a peak-height of 7.5 m around the Gulf of Mexico (Simpson and Riehl, 1981). Although the peak height of sea level on the Hawaiian coasts is not so high as on the continental coasts, tropical storms and hurricanes, may still cause great erosion on the Hawaiian beaches. The effect of the extremely raised sea level due to a big storm usually continues a few days even after the storm passes through.

The frequency of tsunamis (or seismic sea waves) in Hawaii is higher than that of hurricanes; the wave period is less than an hour. Thus their direct effect on beach erosion may or may not be significant. But tsunamis are also accompanied by an oscillatory wave train.

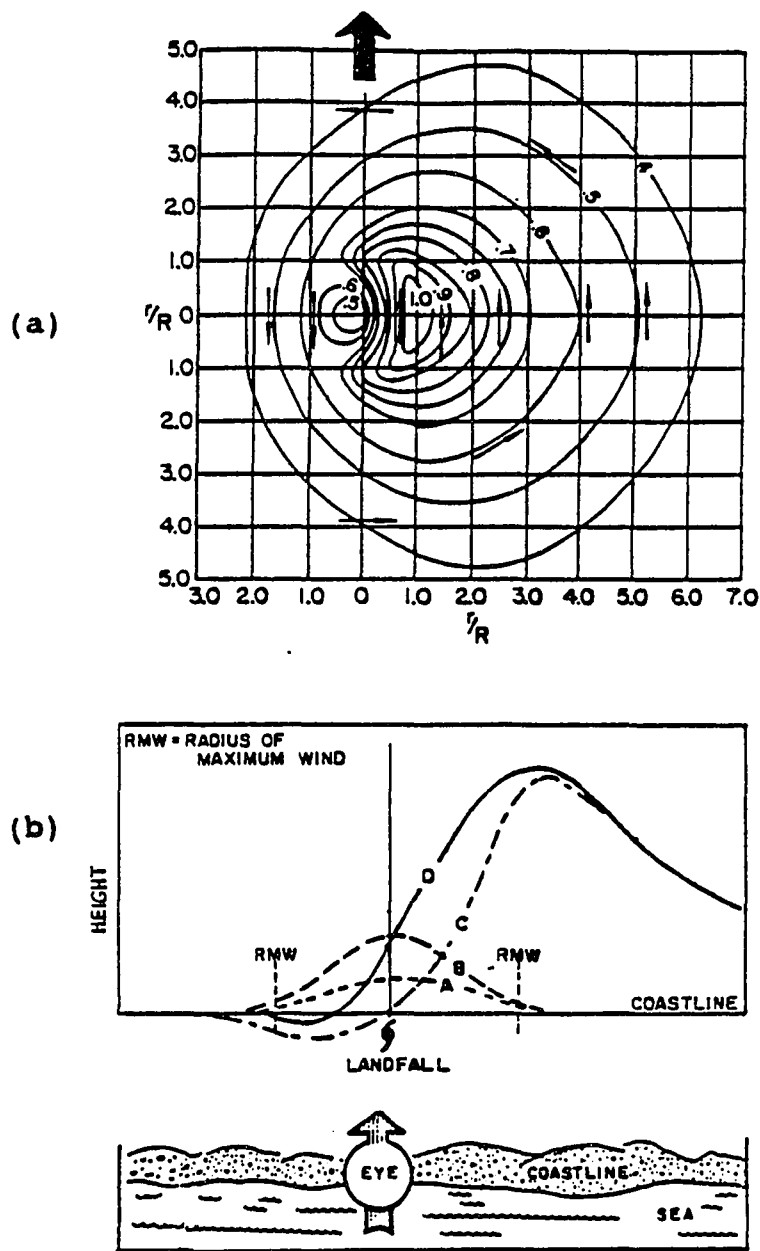


Fig.5.8. (a) Relative significant wave height for a slow-moving hurricane. R : radial distance to maximum significant wave, r : radial distance to point of interest, and (b) components of storm surge at a point of hurricane landfall as viewed from the sea toward the coastline, where A: static inverse barometric effect, B: dynamic inverse barometric effect, C: component resulting from wind stress, D: observed surge profile (after Simpson and Riehl, 1980)

The convolution method (Kriebel and Dean, 1993) gives a simple qualitative result for short-term beach erosion, which is based on the ratio of the erosion time scale to the storm duration. That is, storm duration plays a part in determining the maximum erosion response since the characteristic time-scale of beach erosion (T_s) does not change much, which is a function of beach-face slope, breaking wave height (H_b), and sediment fall speed (w_s) (see eq.(5.20)). Dean (1987) shows that the parameter A in an equilibrium profile with 2/3 power law is a function of sediment fall speed or grain size ($A \approx (w_s^2/g)^{1/3}$).

The erosion time scale (T_s) from the numerical model is given in the form:

$$T_s = C^* \frac{H_b^{3/2}}{g^{1/2} A^3} \left(1 + \frac{h_b}{B} + \frac{mx_b}{h_b} \right)^{-1} \quad (5.20)$$

where

- H_b = wave height at breaking-point,
- C^* = empirical coefficient fitted from numerical tests.

They assume that the beach response to steady-state forcing conditions is approximately exponential in time such that

$$R(t) = R_{\infty} (1 - e^{-t/T_s}) \quad (5.21)$$

where

T_s = characteristic time scale of the exponential response,

R_{∞} = maximum response of the contour (advance or retreat)
that occurs after the system reaches equilibrium.

For a linear beach slope joining the power-law curve as $h = A x^{2/3}$ (Dean, 1977), Kriebel and Dean (1993) propose the maximum erosion potential from the conservation of eroded and deposited sand volumes (see Fig.5.9) such that

$$R_{\infty} = \frac{S \left(x_b - \frac{h_b}{m} \right)}{B + h_b - \frac{S}{2}} \quad (5.22)$$

where S = sea level rise
 B = berm height
 m = linear beach-face slope
 h_b = water depth at wave-breaking point
 x_b = surf-zone width

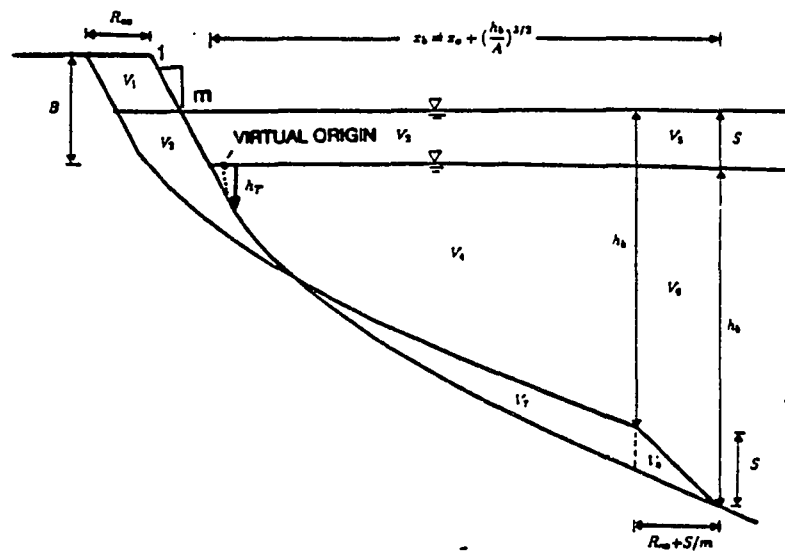


Fig.5.9. Schematic diagram of the maximum potential response (R_m) of modified equilibrium profile to sea level rise. Eroded volume (V_1+V_2) is assumed to be directly deposited to the deeper site (V_7+V_8). h_r is the depth at which linear beach-face slope (m) is tangent to the equilibrium profile with 2/3 power law. B : berm height, S : sea level rise, x_b : surf zone width, h_b : wave-breaking depth (after Kriebel and Dean, 1993).

The time-dependent recession of each contour can be approximated by the convolution method such as

$$R_i(t_j) = \xi R_{i\infty} \int_0^{t_j} f(\tau) e^{-\xi(t_j-\tau)} d\tau \quad (5.23)$$

where

index i is denoted for each sea-level elevation contour,

ξ = characteristic rate parameter ($= 1/T_s$), and

$f(t_j)$ = measured storm-surge hydrograph at time t_j .

For a characteristic erosion time-scale ($T_s = 18.5$ hours) and an idealized storm by the sine-squared function such that

$$f(t) = P \sin^2\left(\frac{\pi t}{T_D}\right), \quad 0 < t < T_D \quad (5.24)$$

maximum erosion occurs by about 10% of the erosion potential for a typical hurricane ($T_D = 6$ hours) near the end of the storm, 40 to 75% of that for a typical storm wave ($T_D = 1$ to 3 days), and about 100% for persistent northeasterlies ($T_D \approx 1$ month) with almost no phase lag, i.e., very close to the time of the peak water level (Fig.5.10).

They have shown that this simple analytic model is in good agreement with the numerical results for the equilibrium response (Kriebel and Dean, 1985).

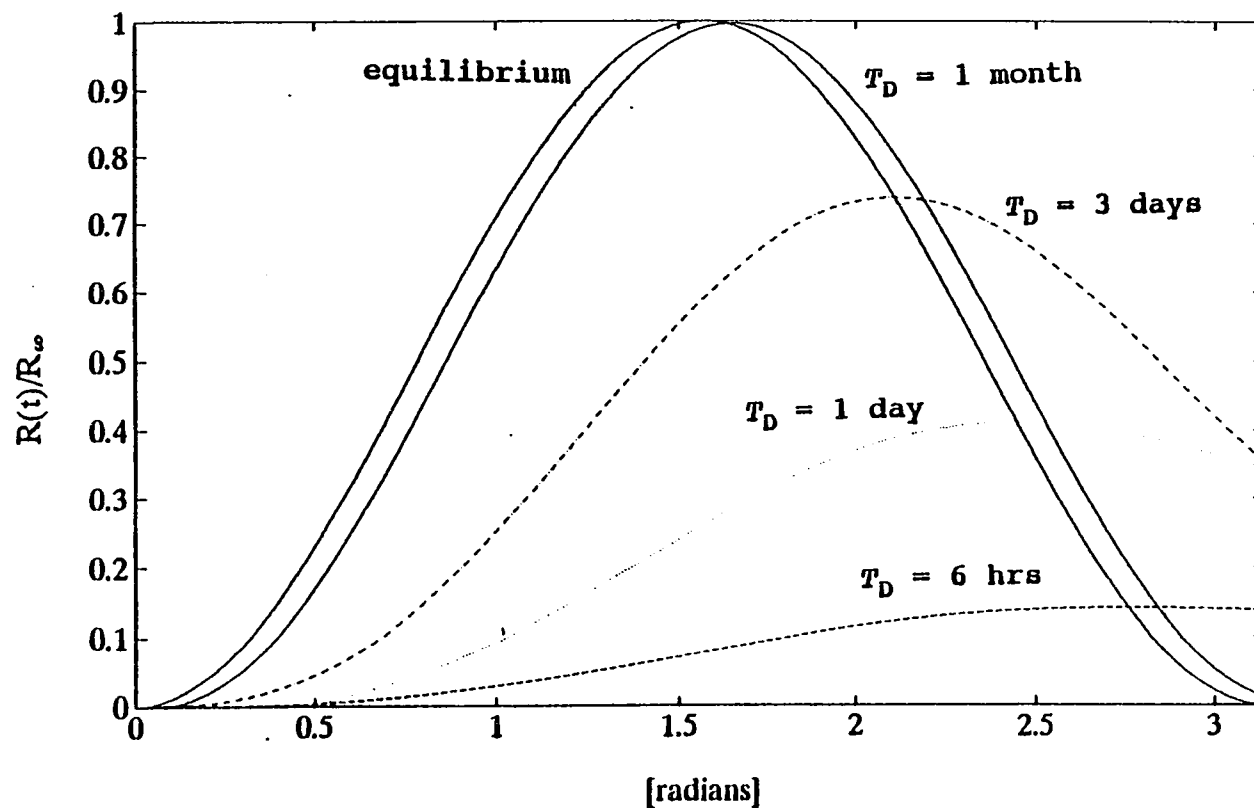


Fig.5.10. Example of amplitude and phase lag of the maximum erosion (a) for a typical hurricane ($T_D = 6$ hrs), (b) for typical storm waves ($T_D = 1$ to 3 days), and (c) for persistent northeasterlies ($T_D = 1$ month) with the erosion time scale of $T_s = 18.5$ hrs, in the Hawaiian Islands.

CHAPTER 6

SHORELINE CHANGES AND BEACH RECOVERY

6.1. SHORELINE CHANGES IN THE HAWAIIAN ISLANDS

Average yearly trends of accretion or erosion of some beaches on the Islands of Kauai, Oahu, Maui, and Hawaii are re-analyzed by taking into account the variation in shoreline position due to the annual cycle in the mean sea level (see Table 3.2 and Table A.2). Then, possible reasons of shoreline dynamics on some selected littoral cells as well as potential errors in calculating shorelines from the previous papers are discussed (Hwang, 1981; Makai Ocean Eng. and Sea Eng., 1991).

Accretion and erosion of beaches are significantly related to the rising and falling trends of MSL. The average linear trends of MSL will be compared with the shoreline changes between two photographs at the same location (time interval is from 5 to 20 years). For a few selected beaches, shoreline changes are corrected with the mean annual cycle of sea level and beach slope; the mean annual cycle obtained from the 80 year time-series of monthly sea levels at Honolulu Harbor can be applied to correct the shoreline change at Waimea Bay, Oahu. In the

same way, the mean annual cycle from about a 40 year time-series of monthly sea levels at Hilo, Hawaii is applied to correct the shoreline change at Hapuna Beach, Hawaii. This assumes that the mean annual cycle of sea level of an island is the same at any place on the island. The calibration of the shoreline changes by interannual fluctuation of sea level is not carried out in this study because it is presently not known at what time of year the highest levels occur in this cycle. Previous analyses of the coastal erosion/accretion in the major Hawaiian Islands show average annual changes based on aerial photographs within a few decades of time (Fig.6.1).

The most serious erosion problems were reported on the Island of Maui, especially on the north shore. More than 70 percent of the total number of transects were eroding. On the Island of Oahu, Waimea Bay Beach ($- 0.95$ m/yr) had the highest erosion rate. Meanwhile, maximum accretion was reported on Kahuku Golf Course Beach ($+ 1.14$ m/yr), as the result of sand dumping. On the Island of Kauai, erosion was reported at about half of the transects. On the west to northwest coast beaches of the island of Hawaii, approximately 60 percent were reported as "eroding".

But there exists a large uncertainty both in photographic measurements by an aircraft and in conversion

of the aerial photographs into base maps. The uncertainty may reverse the mean annual trend of erosion/accretion if the rate of shoreline change is not large. Moreover, when two air photos were not taken in the same month the positions of high water level (HWL), which is usually taken as a shoreline in aerial photography, should be converted into those of the same month to minimize error. Thus the information of the beach slope should be incorporated for an estimate of the shoreline position for the same month of the year. An aerial photograph is an instantaneous snap-shot and therefore cannot be representative for the shoreline in that year.

Consequently, calibration of shoreline position should be carried out, at least based on the mean annual cycle of sea level and beach slope, by converting vertical sea level change into horizontal shoreline change. But the interannual shoreline changes cannot be accurately calibrated up to now, due to the limited knowledge about the prediction of occurrence of the interannual fluctuation of sea level which seems to be largely associated with ENSO events.

One of the most obvious and consistent features of the sea level change in the world oceans is an annual oscillation, which is primarily related to expansion by

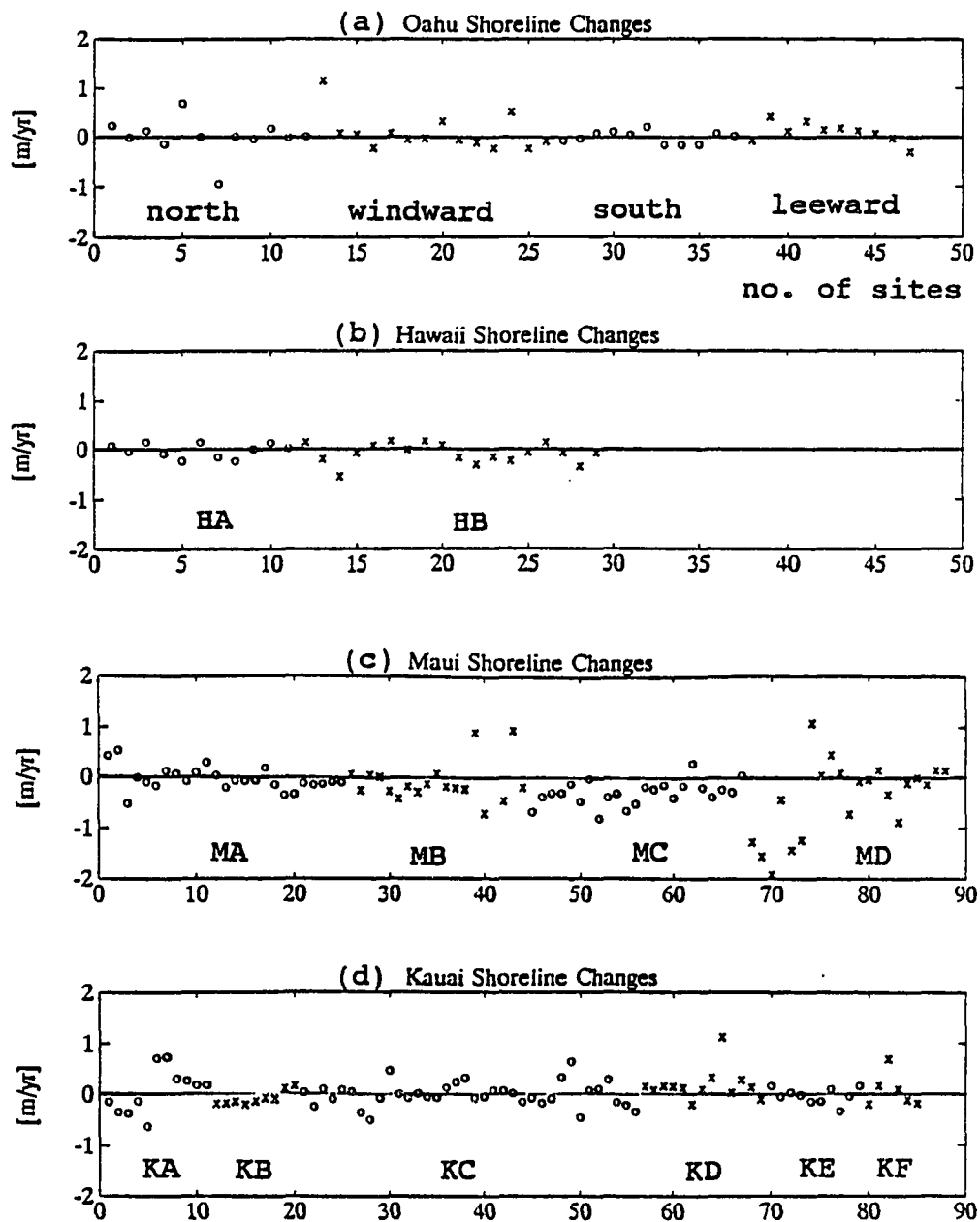


Fig.6.1. Mean annual trend of shoreline changes (in m/yr) on (a) Oahu, (b) Hawaii, (c) Maui, and (d) Kauai. Data are selected from Hwang (1981) for (a), and Makai Ocean Eng. and Sea Eng.(1991) for (b), (c), (d).

heating and contraction by cooling due to the annual variation of solar radiation. Another predominant cause of an annual mean sea level oscillation in synoptic scale is monsoons. For instance, Southeast Asian Monsoons over the coastal regions of the western Pacific, which are primarily northeasterly winds during the winter monsoon (from October to April) and southwesterly winds during the summer monsoon (from May to September), significantly magnify the amplitude of the annual variation of the monthly mean sea level height at the coastal stations (Jeon, 1990).

But the sea-level signals at the island stations away from the coastal regions in the western Pacific are more complex than those at coastal stations. This is because they may include several causes, as well as the steric effect, such as the annual variations of the monsoon and trade wind systems, and the intensity or spatial variation of the equatorial current system, especially of the North Equatorial Current (NEC; between 10°N and 20°N) and the North Equatorial Counter Current (NECC; between 4°N and 10°N) from the western to central Pacific Ocean.

Mean monthly sea levels in the annual cycle at four major Hawaiian Islands are shown in Fig.6.2. (also see Table 2.4). The annual cycle of sea levels implies that the rate of shoreline change based on aerial photographs may result

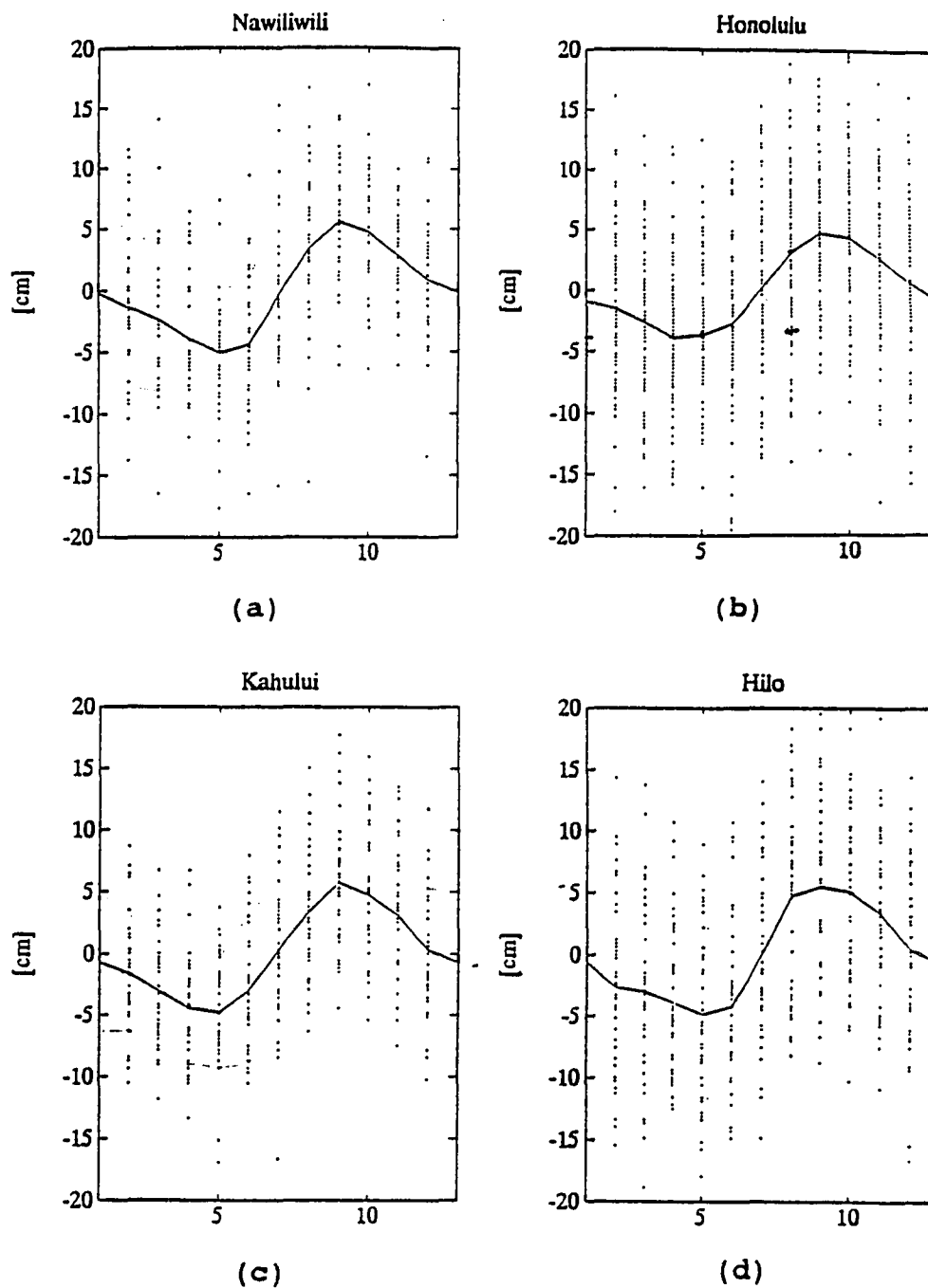


Fig.6.2. Mean annual cycle of monthly sea levels at (a) Nawiliwili, Kauai, (b) Honolulu, Oahu, (c) Kahului, Maui, and (d) Hilo, Hawaii. Data are from PSMSL.

in a larger error range or even a reverse trend of regression and/or transgression unless two air photos used for calculating the shoreline change are taken at least in the same month.

Suppose that one aerial photograph is taken in September (maximum level) some year and the other in April (minimum level) ten years later, and that the shoreline between the two air photos is interpreted as "unchanged". If we further assume that the beach slope is $1/20$ and that the long-term trend of sea level is $+2$ cm/decade with an annual MSL difference of 10 cm at this coast, then the shoreline may be interpreted as "retreated" by 1.6 m (corresponding horizontal distance for the vertical rise of 8 cm). Consequently, interpreting shoreline changes from aerial photography without considering annual sea-level oscillation may cause significantly erratic results. Moreover, interannual sea-level fluctuation could certainly cause the error to be even larger. It makes the prediction of shoreline change difficult that the time span (as well as the sea-level difference) of the interannual fluctuation is somewhat variable, i.e., quasi-periodic.

If the vegetation line in aerial photography, which has been usually represented for the shoreline in Hawaii, is replaced by the mean HWL as used in the U.S. mainland, the influence of season is as clear as in the above reasoning.

6.2 CASE STUDIES

6.2.1. Waimea Bay Beach, Oahu

Waimea Bay is located on the north side of the Island of Oahu, and the beach is often subject to high surf conditions from North Pacific swell (Fig.5.3). The Waimea River, which is usually ponded behind a barrier of sand, drains into the northeastern end of the bay in times of flood (Parker, 1987). There is a sand channel extending steeply into deep water opposite the river mouth, where the offshore sand transport occurs by rip currents. Thus this sand channel fed by rip currents may be an indicative of the mechanism whereby sand moves permanently into deep water. The bay is blocked on both sides by rocky cliffs, which makes it a *littoral cell* where there is no net longshore sediment transport to and from the area (Chamberlain, 1968).

Waimea Bay is chronically eroding with little sand supply to balance the losses from sand mining (from 1949 or possibly earlier to 1967) and offshore transport due to winter storms (Hwang, 1981). But the long-term, annual or interannual trends of sea-level rise may also be important to beach erosion in this area.

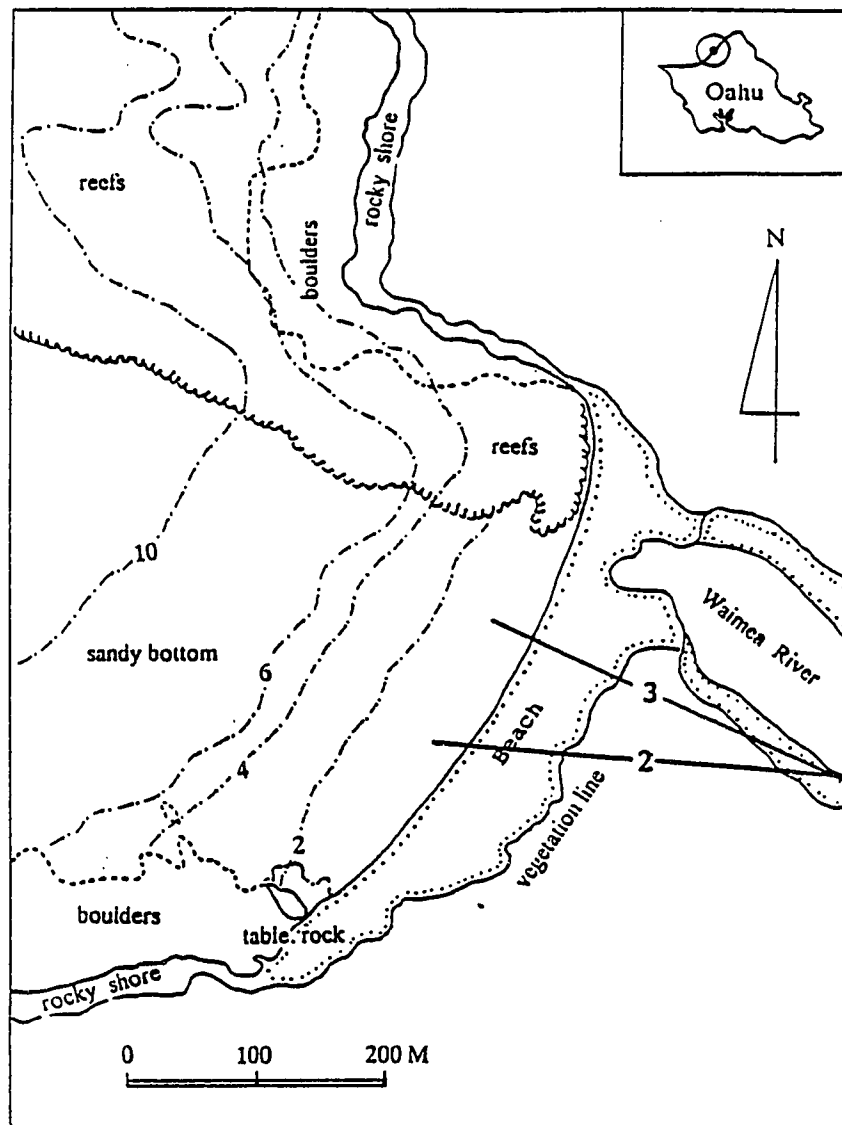


Fig.6.3. Waimea Bay Beach: geography and bottom topography in the nearshore region (transects 2 and 3 are for Table 6.3; transect 1 was not shown in Hwang, 1981).

In previous analyses of the shoreline change from aerial photos (Hwang, 1981), the rates of waterline recession may not have been accurately estimated because of neglecting the effect of the annual oscillation of mean sea level when the photos have been taken in different months of the year.

The average values of the sediment sizes measured along the beach profiles at (a) Waimea Bay, Oahu and (b) Hapuna Beach, Hawaii from previous reports (Moberly and Chamberlain, 1964; Gerritsen, 1978; Parker, 1987) are as follows:

Table 6.1. Average sediment diameter characteristics at the MLW line on (a) Waimea Bay, Oahu, and at (b) Hapuna Beach, Hawaii. Units are in mm and ϕ ($= -\log_2[\text{mm}]$) in parentheses.

(a) Waimea Bay, Oahu						
date	3/62	7/62	10/62	2/63	5/63	8/63*
mm	0.48	0.48	0.74	0.44	0.57	0.61
ϕ	(1.05)	(1.07)	(0.43)	(1.20)	(0.80)	(0.72)
date	1/74	2/74**	9/85	1/86***		
mm	0.62	0.61	0.68	0.70		
ϕ	(0.69)	(0.72)	(0.57)	(0.52)		

(b) Hapuna Beach, Hawaii							
date	4/62	6/62	9/62	1/63	4/63	7/63*	12/73**
mm	0.17	0.17	0.20	0.26	0.19	0.24	0.26
ϕ	(2.58)	(2.56)	(2.33)	(1.94)	(2.43)	(2.04)	(1.94)

Data Sources;

- * 3/62 - 8/63 ; Moberly and Chamberlain (1964),
(Data were averaged from three sites; backshore, MLW line, offshore.)
- ** 12/73, 1/74, 2/74 ; Gerritsen (1978) (data at the MLW line)
- *** 9/85, 1/86 ; Parker (1987) (data averaged from HW, MW, LW)

More than 95% of beach sands on Waimea Bay, Oahu are calcareous sand (CaCO_3) (Moberly and Chamberlain, 1964). This implies that the terrigenous sediment supply from occasional flooding of Waimea River is minor compared to the biogenic component, and that much of the sand found in the bay must be relict sands produced during a lower stand of sea level (Campbell and Hwang, 1982). In general, the primary source of sands of the Hawaiian Beaches is from reef communities. After some Hawaiian fish graze red algae or eat living corals, forams, and echinoids, they puff out the ground debris (pers. comm., Krock, 1993).

The average sediment diameter from LW to HW in Waimea Bay was about 0.6 mm both in winter and summer. But, in general, the average grain size of Hawaiian beach sands is usually larger during winter than in summer (Table 6.2). Coarse materials may result in shorter transport processes due to their larger fall speed if the flow velocity is the same.

Table 6.2. Average grain size of Hawaiian beach sands during winter (December, January, February) and during summer (June, July, August) (after Moberly et al., 1963).

	winter	summer
Kauai	0.56 mm	0.38 mm
Oahu	0.63	0.43
Molokai	0.68	0.55
Lanai	0.39	0.35
Maui	0.50	0.33
Hawaii	0.66	0.45

The long-term trend of beach erosion at Waimea Bay can be partly explained by the Bruun Rule as mentioned in CHAPTER 3. The beach slope of the bottom of an active profile change in a time-scale of a year or less is approximately 8.5 m/170 m (= 1/20). For a time-scale of a few years to decades, it is assumed 15 m/600 m (= 1/40) in this study. The changes of the shoreline (see footnote of Table 6.3) at Waimea Bay from the previous aerial photo analyses (Hwang, 1981) between 1928 and April 1975, and converted values with the mean annual cycle of the sea level at Honolulu Harbor are shown in Table 6.3.

Table 6.3. Changes (in meters) of the shoreline from aerial photographs (data from Hwang, 1981) and converted values (shown in parentheses) applying the mean annual cycle of the sea level at Honolulu Harbor.**

observation period	transect number			average
	1	2	3	
??? ,1928 - May 08,1949	-19.2	*	*	-19.2
	(-19.2-3.3)			(-19.2-3.3)
May 08,1949 - Aug 24,1962	*	*	- 8.5	- 8.5
(May 1962)			(- 5.8)	(- 5.8)
Aug 24,1962 - Apr 22,1967	*	0	- 1.8	- 0.9
(May 1962)		(- 2.8)	(- 4.6)	(- 3.7)
Apr 22,1967 - Jan 23,1971	*	-20.0	-14.0	-17.0
(Apr 1971)		(-18.8)	(-12.8)	(-15.8)
Jan 23,1971 - Apr 11,1975	*	+ 3.4	- 1.5	+ 0.9
(Apr 1971)		(+ 2.2)	(- 2.7)	(- 0.3)

** Vegetation line was used, which may be less influenced by the annual sea-level cycle than when HWL is used as an index computed in the table.

When the mean annual cycle is included, the average trend during the last period (April 1971 - April 1975) can be interpreted as "eroded" instead of "accreted". Then, the overall recession rate of the shoreline becomes approximately from 40 to 110 cm/yr during 1928 to 1967, 450 cm/yr during 1967 to 1971, and about 7.5 cm/yr during 1971 to 1975. With an assumed beach slope ($= 1/40$) and the vertical rise of sea level at Honolulu Harbor ($+1.6$ mm/yr), corresponding recession rate of the shoreline based on Bruun Rule should be 6.4 cm/yr. This value is comparable only with the last period (from 1971 to 1975). Before 1971, the average recession rate of shoreline for 43 years is about 6 to 70 times that by the long-term effect of sea-level rise.

The extreme recession of the vegetation line during 1967 to 1971 should be explained by the erosion due to both sand mining, which was intermittently carried out until 1965, and storm surges. Although the sand mining ceased in 1967, the effect could last until a new equilibrium profile is reached. Consequently, historical information about sand mining on Waimea Bay is needed to more accurately estimate the effect of sea-level rise. At Waimea Beach large changes in beach width can develop over a short time (see Figure 6.2, Gerritsen, 1978).

The interannual (vertical) fluctuation of sea levels at Honolulu Harbor, Oahu and the corresponding (horizontal) shoreline fluctuation at Waimea Bay Beach can be 7 to 20 cm, and 2.8 m to 8 m, respectively (Table 6.4). That is, the interannual fluctuation scale is up to ten times that of the long-term rise of sea levels.

Table 6.4. Interannual rising trends obtained from 12 monthly running means of the monthly mean sea level records at Honolulu, Oahu between 1905 to 1988.

period	total rise		rising rate	
1910 - 1916 (6 yrs)	20	cm	3.33	cm/yr
1918 - 1920 (2 yrs)	17.5	cm	8.75	cm/yr
1929 - 1930 (2 yrs)	10	cm	5.0	cm/yr
1935 - 1936 (1.5 yrs)	7	cm	4.67	cm/yr
1949 - 1944 (3.5 yrs)	11.5	cm	3.29	cm/yr
1955 - 1959 (4 yrs)	17	cm	4.25	cm/yr
1960 - 1962 (2 yrs)	9	cm	4.5	cm/yr
1967 - 1969 (2 yrs)	10	cm	5.0	cm/yr
1973 - 1974 (2 yrs)	10	cm	5.0	cm/yr
1976 - 1981 (5.5 yrs)	12	cm	2.18	cm/yr
1986 - 1988 (3 yrs)	11	cm	3.67	cm/yr

The onset of an El Niño event, if we define it as the year warm water appeared in the equatorial eastern Pacific, between 1950 to 1985 were reported in 1957, 1963, 1965, 1969, 1972, 1976, 1979, 1982 (Graham and White, 1988). With another event in 1986, some seem to match with the rising trends of sea-level at Honolulu, but some do not (see Fig.2.2.(c)). The total period of interannual rising trends is 33.5 years (about 40%) of the total sea-level records.

Short-term sediment transport was calculated using an energetic-based model (Bailard, 1984) for Waimea Bay, Oahu and Hapuna Beach, Hawaii. The average winter and summer wave conditions at the NOAA buoy location, as described in CHAPTER 5, are used in the model. It seems reasonable to adapt the wave climate from the buoy location to the beach sites during winter but not during summer. Although information of wave directionality is lacking, both beaches are located to the north or northwest of the islands, respectively, and the North Pacific swell is predominant during winter. But the trades and the southern swells may not affect these beaches so much as the result of the model output in this study.

The input parameters used in the model for Waimea Beach are as follows:

D_{50}	=	0.59	mm
D_{90}	=	0.90	mm
ρ	=	1.025	g cm^{-3}
ρ_s	=	2.650	g cm^{-3}
w_s	=	7.89	cm s^{-1}
e_b	=	0.130	
e_s	=	0.032	
γ	=	0.8	

Deep-water significant wave height and period are 3.13 m and 7.7 sec during winter, and 1.91 m and 5.7 sec during summer. The ratio of the second to first harmonics of the near-bottom velocity ($= u_{m2}/u_m$) is set as 0.2 (Wang, 1993), and the values of wave velocity moments (u_3^* and u_5^*) are adopted from Bailard (1984).

Time-interval for computing beach profile change and cross-shore transport rate is set 10 seconds and horizontal grid-scale for taking initial bottom profile (Walker, 1974) is 0.76 meter.

The results are shown by the cross-shore sand transport rate [$\text{m}^3/\text{m}/\text{day}$] and bottom profile change in every week for winter and summer wave conditions, respectively (Fig.6.4 and Fig.6.5).

Under winter conditions, sediment initially move toward the onshore region from the offshore region, being accreted at the nearshore region. This process continues in the profile after one week. In two weeks, the nearshore region is again eroded and ready to make an offshore bar. The offshore transport rate becomes large in three weeks, which exceeds about $30 \text{ m}^3/\text{m}/\text{day}$, up to $85 \text{ m}^3/\text{m}/\text{day}$ at 50 m offshore, between the shoreline and over 100 m offshore. These values are much larger than the previous profile surveys across selected Hawaiian beaches at quarterly intervals during 1962 - 1963 (Chamberlain, 1968), where seasonal rates of erosion and accretion of beach sand reservoirs were reported on the order of a few tens of [$\text{m}^3/\text{m}/\text{month}$] (see Table 6.8). Although higher rates on the order of a few hundred [$\text{m}^3/\text{m}/\text{month}$] were reported on north and west coasts, the values of cross-shore transport rates obtained from the model in this study are still high.

The active profile change occurs between the shoreline and about 160 m offshore, which corresponds to about 8.5 m depth. But a slight erosion still happens over 400 m offshore, i.e., below 12 m depth.

The transport processes for the smaller wave height and shorter wave period corresponding to the average summer conditions follow a similar pattern to those for winter conditions. Clear offshore transport occurs after two weeks, then an offshore bar, at a depth less than 2 m and at about 75 m offshore, is formed in four weeks. Offshore transport rate is over $10 \text{ m}^3/\text{m}/\text{day}$ between shoreline and about 60 m offshore in two weeks, and over $20 \text{ m}^3/\text{m}/\text{day}$ between shoreline and about 110 m offshore in three weeks. The overall transport rate is reversed in four weeks, which reaches the maximum ($\approx 5 \text{ m}^3/\text{m}/\text{day}$) where the offshore bar is formed. Although the wave climate at the north shore during summer is more tranquil than what is used in this study, this would give us at least the idea that the sediment transport process occurs in a similar way but with different time and space scales; faster and larger scales for bigger waves, i.e. winter condition, and slower but smaller scales for reduced (summer) wave conditions.

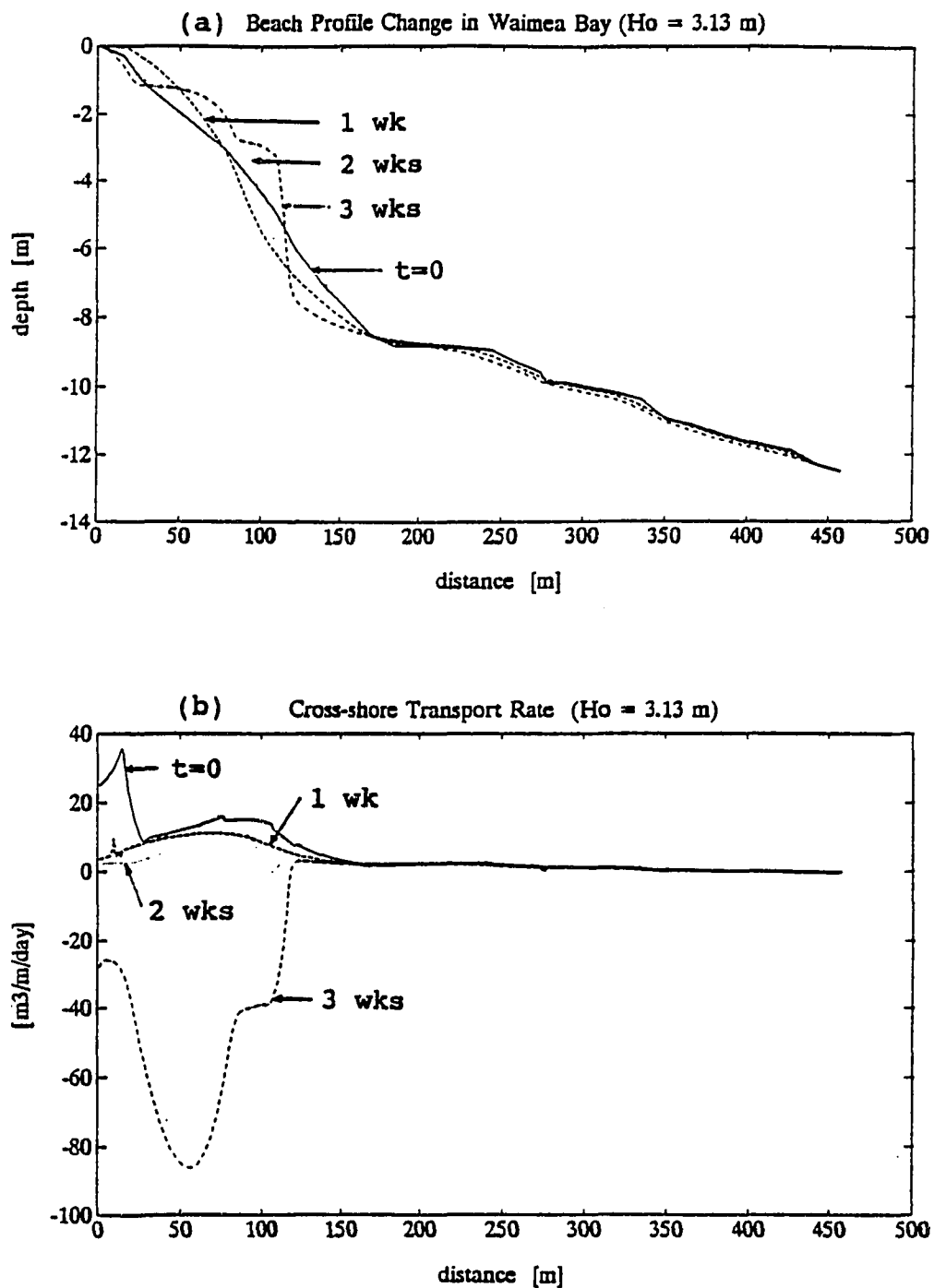


Fig.6.4. (a) Beach profile changes and (b) cross-shore sand transport rates on Waimea Bay Beach, Oahu for winter wave condition by the energetics-based model.

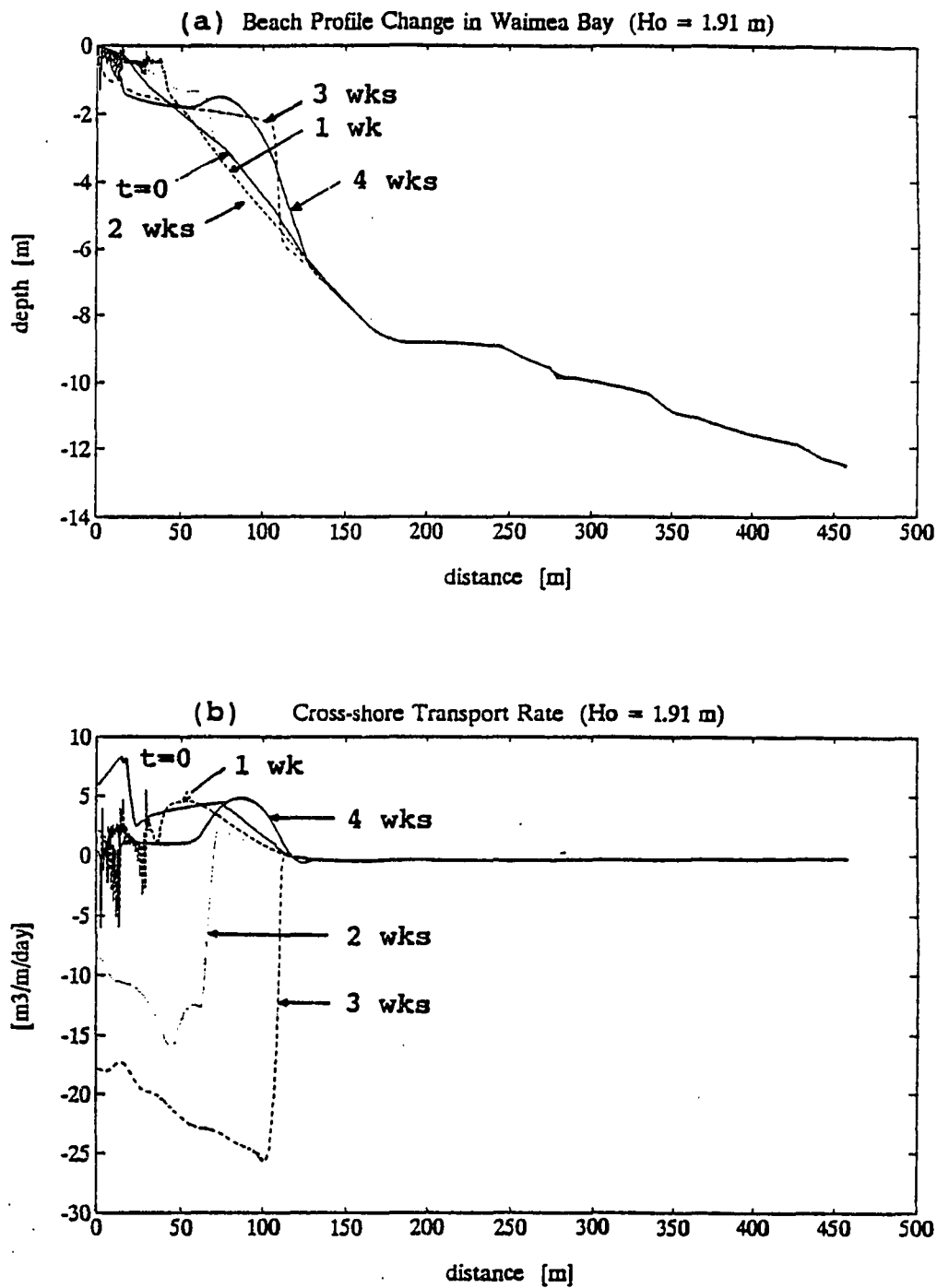


Fig.6.5. (a) Beach profile changes and (b) cross-shore sand transport rates on Waimea Bay Beach, Oahu for summer wave condition by the energetics-based model.

Gerritsen (1978) reported shoreline (MLLW) accretion by about 17 m in the middle of Waimea Bay between January 11 and February 26, 1974. The volume change per unit width above the MLLW reaches about 80 m³/m during the six weeks (see Figure 6.2. Gerritsen, 1978). This accretion occurred during the lowering phase of sea level.

Parker (1987) also measured the beach profile changes above the shoreline between June 2, 1985 and January 23, 1986. She found the shoreline retreats by about 5 to 35 m and the corresponding volume erosion per unit width was 10 to 35 m³/m at 5 transects during the 5 months (from summer to winter). One transect connecting the Waimea River is intentionally omitted in this study (see Figure 15 and 16, Parker, 1987). Mean annual sea level cycle shows that the sea level in June is about 3 cm lower than that in January and 8 cm lower than that in September (maximum). That is, the beach is submerged from June to September, and emerged from September to January by the mean annual sea level cycle. But summer wave conditions are calm, and winter wave conditions are very intense as described in CHAPTER 5.

Consequently, seasonal change of the beach profile may be explained by the combined effects of annual sea level cycle and wave condition rather than the annual change of wave condition only.

6.2.2. Hapuna Beach, Hawaii

Hapuna Beach is located inside Kawaihae Bay on Hawaii's west coast, a few miles south of Mauna Kea Beach. The beach is straight and protected by rocky headlands on both ends forming a littoral cell just like Waimea Bay Beach (Fig.6.6). The beach is approximately 600 m long and 30 to 50 m wide in different seasons. The overall beach slope on Hapuna Beach, Hawaii is fairly even ($\approx 1/20$) and the offshore area consists of rock and coral with numerous sand pockets and some sand channels (Gerritsen, 1978). Due to the gentle slope and finer sand size of the beach, it seems to endure large seasonal change, depending on the wave climate with different seasons.

The shoreline of this beach was interpreted as "eroded" by -9.14 m during about 38 years, which was from aerial photos between March 1950 and May 1988. So the average rate of shoreline change was converted to -0.24 m/yr (Makai Ocean Eng., 1991). This value seems to be reasonably accurate since the mean sea level in March does not deviate much from that in May (minimum level) when considering the mean annual cycle. But if we may convert the shoreline position in May 1988 into that in March 1988, by adding the corresponding horizontal distance (≈ 40 cm) to the mean vertical sea-level difference (≈ 2 cm) between March and May from the beach

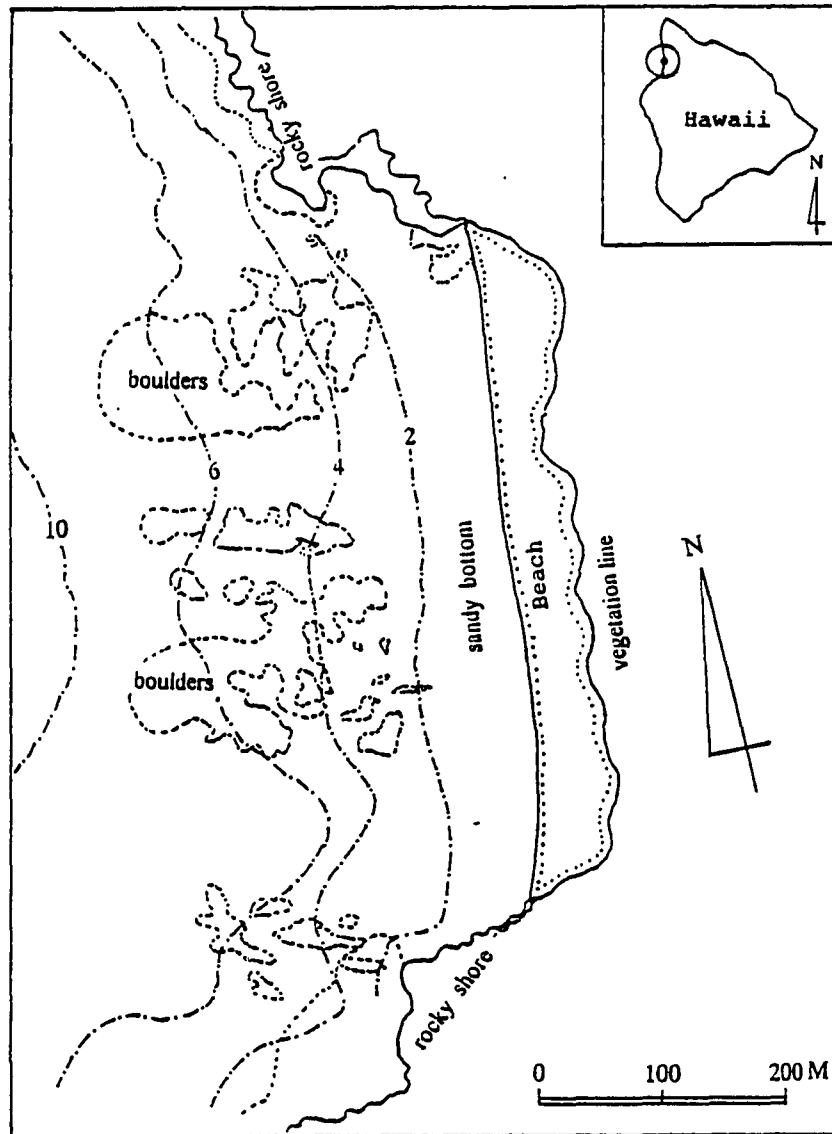


Fig.6.6. Hapuna Beach: geography and bottom topography in the nearshore region.

slope ($= 1/20$), then the shoreline recession rate could be more accurately estimated. In other words, the retreat of shoreline now becomes -9.54 m ($= -9.14 \text{ m} - 0.4 \text{ m}$) or the average recession rate is -25 cm/yr between March 1950 and 1988. The linear trend of the RSL rise from the tide-gauge records at Hilo, Hawaii (see Fig.2.1.(a)) and the corresponding shoreline retreat by the Bruun Rule are $+0.4 \text{ cm/yr}$ and -8 cm/yr , respectively. Comparing this value with the shoreline retreat by aerial photographs, The contribution of the long-term effect of RSL rise by the Bruun Rule is about 30% of the total retreat of the shoreline. Then, the excessive rate of shoreline recession or excessive retreat of shoreline must be explained by other mechanics. That is, the shoreline retreat (R) based on the Bruun Rule would be

$$\begin{aligned}
 R &= S / \tan \beta \\
 &= 4.0 \text{ [mm/yr]} * 38 \text{ [yrs]} * 20 \\
 &= 3.04 \text{ [m]}
 \end{aligned}$$

The excessive retreat of shoreline during this period becomes 6.10 m ($= 9.54 \text{ m} - 3.04 \text{ m}$), which may be associated with the interannual or annual trends of sea-level rise and the short-term events such as storm surges. The interannual rising periods from the tide gauge records at Hilo, Hawaii are as follows (Table 6.5):

Table 6.5. Interannual rising trends obtained from 12 monthly running means of the monthly mean sea level records at Hilo, Hawaii between 1955 to 1988.

period	total rise	rising rate
1955 - 1958 (4 yrs)	11 - 15 cm	2.75 - 3.75 cm/yr
1962 - 1968 (7 yrs)	8 - 10 cm	1.14 - 1.43 cm/yr
1972 - 1973 (2 yrs)	12.5 cm	6.25 cm/yr
1975 - 1977 (3 yrs)	10.0 cm	3.33 cm/yr
1985 - 1988 (2.5 yrs)	8.5 cm	3.40 cm/yr

Vertical sea-level rise and corresponding retreat of shoreline during each rising period is about 8 to 15 cm, and 1.6 to 3 m, respectively. Most of the rising trends match with the occurrences of El Niños: 1957-58, 1965, 1972-73, 1976, 1982-83, 1987-88. It is rather surprising that the signal of 1982-83 El Niño, despite its strong intensity, is not clear in the sea level records at Hilo. The sum of the periods of interannual rising trends of sea level is 18.5 years or about 50% of the total period (from 1950 to 1988). Although a falling trend follows a rising trend in the interannual fluctuation pattern of sea level, some of the transported sediments to the offshore region during the rising period may not return to the onshore region during the following falling period, signifying permanent beach loss.

Because there is nearly no net longshore transport of sediments in a *littoral cell* such as Hapuna Beach, Hawaii, the excessive retreat of shoreline by about 6 m per 38 years is predominantly due to the interannual sea-level fluctuations, and possibly due to storm waves and currents. Even in annual oscillation of cross-shore transports, some of the sediments are permanently lost to the deep offshore region (Campbell and Hwang, 1982).

Consequently, the impact of interannual rises of sea level seems to be more significant than the effect of the long-term linear rising trend in sea level.

Short-term erosion is basically due to wave actions, that is, small onshore drift of Stokes flow above the trough of the wave, offshore (return) flow below the wave trough, and minor transport as bedload due to the combination of gravity and friction.

The input parameters used in the energetic-based model for short-term cross-shore sediment transport are basically the same as in the case of Waimea Bay, Oahu, except the mean sand diameter (≈ 0.21 mm) and the corresponding fall speed.

For one transect in the middle of Hapuna Beach, Hawaii, the beach-profile change and cross-shore sediment transport rate are calculated with three different wave heights and periods in deep water such that

- (1) $H_o = 2 \text{ m} , \quad T = 6 \text{ sec}$
- (2) $H_o = 2.5 \text{ m} , \quad T = 7 \text{ sec}$
- (3) $H_o = 3 \text{ m} , \quad T = 7 \text{ sec}$

The grid step for bottom profile is taken as 7.62 m, and the time step is set as twice the average wave period.

In case (1), initial offshore transport rate is maximum reaching up to 27 m³/m/day at 25 m offshore, and greatly reduced in a month ($\approx 2 \text{ m}^3/\text{m/day}$) and even less thereafter. In other words, most of the transport occurs within a week as seen in Fig.6.7.(1). The depth of active profile change is about 10 m, which seems to continuously erode during the 3 months (= 12 weeks).

In case (2), offshore sediment transport continues from the initial condition until 2 weeks, when maximum offshore transport occurs (up to 180 m³/m/day) at 25 m offshore. Then, the direction of the sediment transport is reversed at the same 25 offshore region, where maximum onshore transport rate is about 120 to 140 m³/m/day, in 4 to 5 weeks. Due to this onshore transport, the bottom is again accreted during this period. The depth of active profile change becomes a little deeper ($\approx 12 \text{ m}$) than the case (1) (Fig.6.7.(2)).

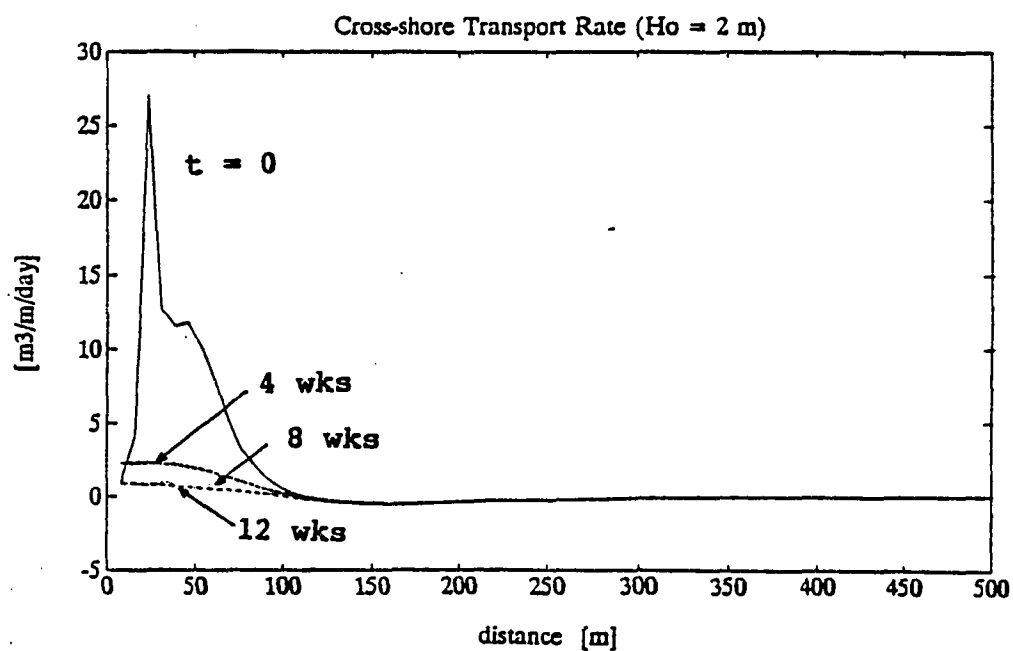
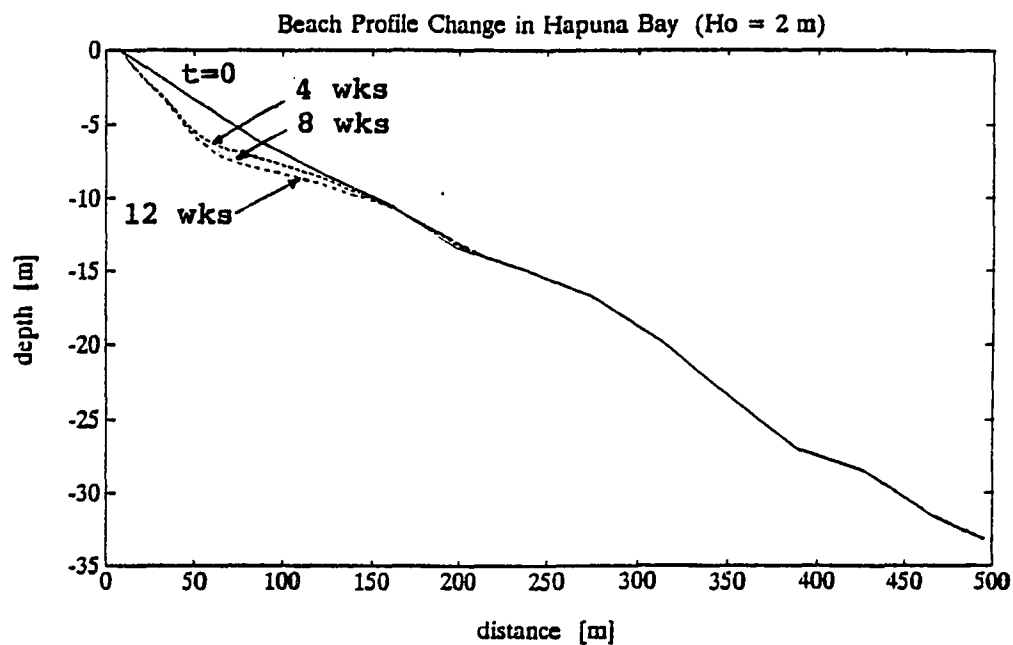
In case (3), maximum offshore transport occurs in a week reaching up to 210 m³/m/day, which makes a small bar at a depth of about 2 m. From the second week, overall erosion occurs between shoreline and 190 m offshore (\approx 13 m depth). It is seen that the eroded material is accreted over deeper region, especially between 270 m and 370 m offshore or the depth range from 16 m and 26 m (Fig.6.7.(3)).

Again, monthly rates of erosion and accretion from the profile surveys during 1962-63 (Chamberlain, 1968) show a smaller order of sand volumes than the model results in this study (Table 6.6).

Table 6.6. Rates of erosion(-) and accretion(+) on (a) Waimea Bay, Oahu and on (b) Hapuna Beach, Hawaii. Data selected from Chamberlain (1968). Unit is in [m³/m/month].

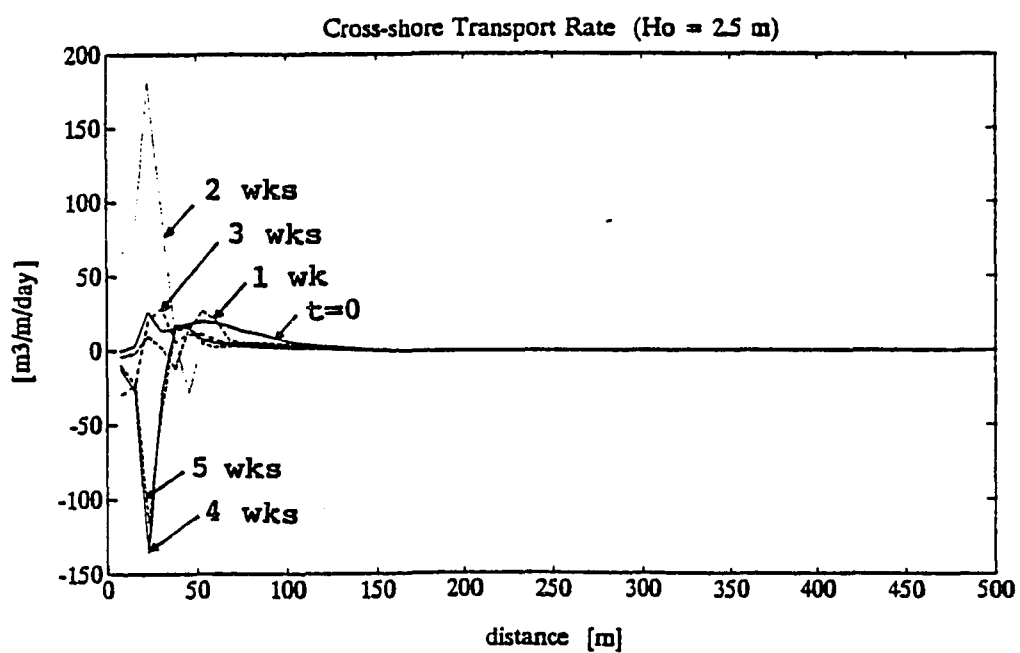
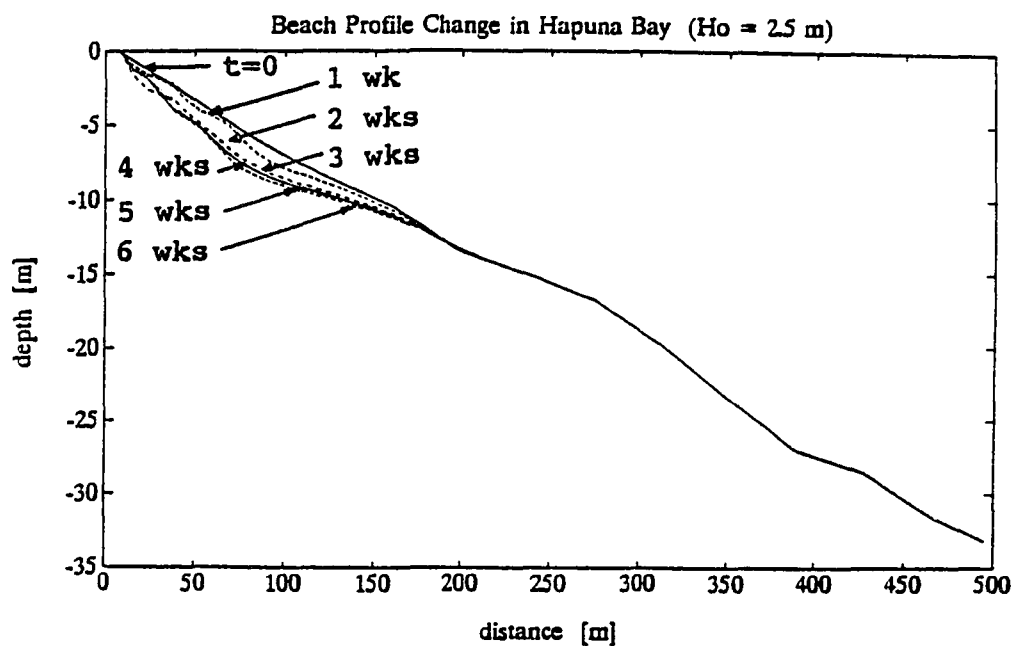
(a) Waimea Bay Beach, Oahu				
5/62-7/62 (2 mo.)	7/62-11/62 (4 mo.)	11/62-3/63 (4 mo.)	3/63-5/63 (2 mo.)	5/63-8/63 (3 mo.)
-18.3	- 7.4	+ 9.3	-74.2	+ 7.6

(b) Hapuna Beach, Hawaii				
4/62-6/62 (2 mo.)	6/62-9/62 (3 mo.)	9/62-1/63 (4 mo.)	1/63-4/63 (3 mo.)	4/63-7/63 (3 mo.)
- 3.4	-11.7	- 0.5	- 6.9	+20.6



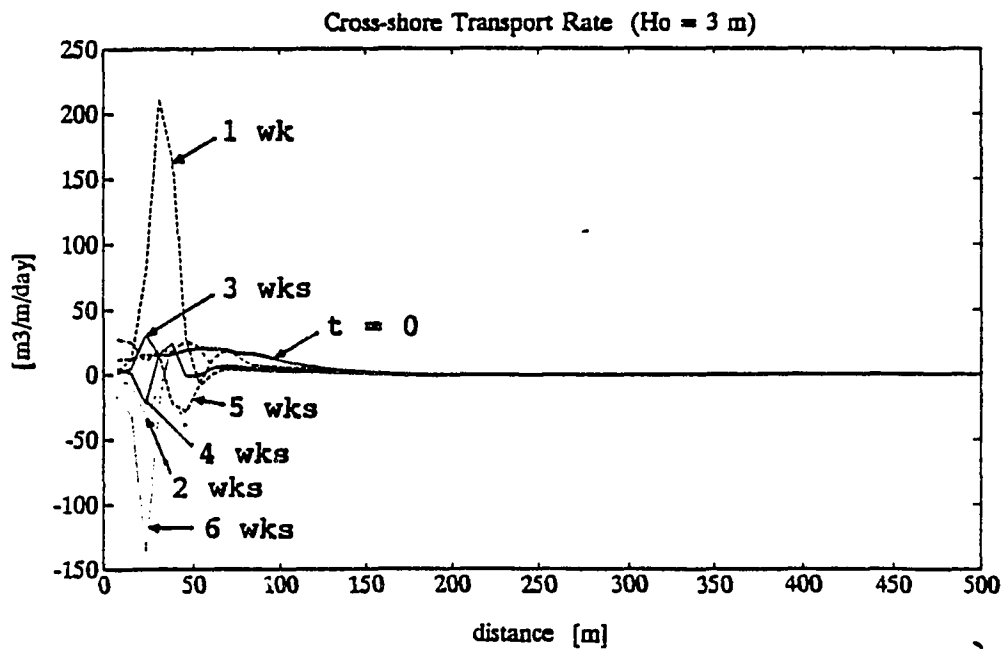
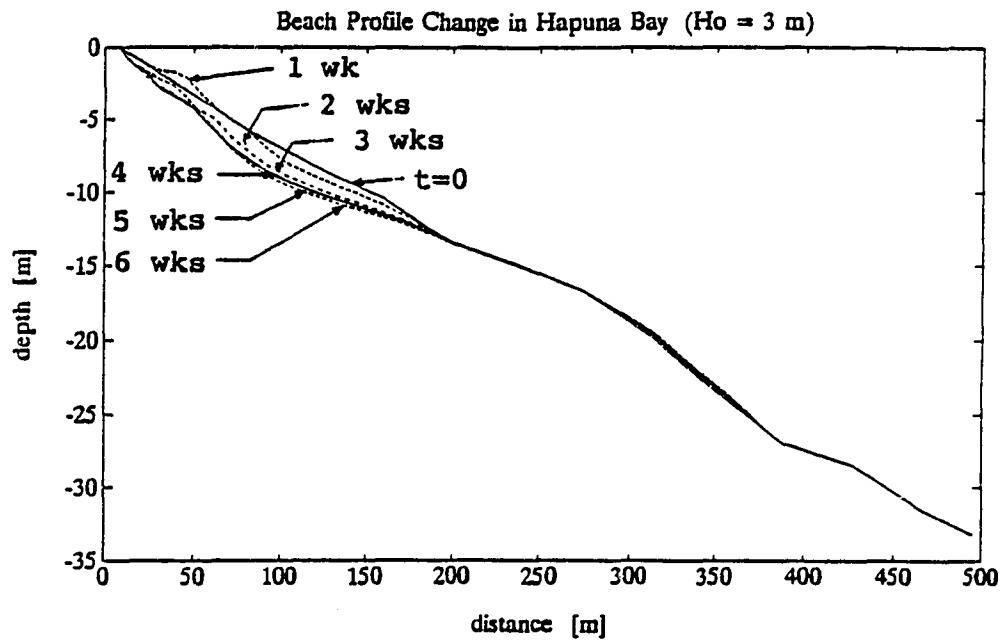
(1) $H_o = 2$ m, $T = 6$ sec

Fig.6.7. Beach profile changes and cross-shore sand transport rates for different wave conditions on Hapuna Beach, Hawaii.



(2) $H_o = 2.5$ m, $T = 7$ sec

Fig.6.7. (continued) Beach profile changes and cross-shore sand transport rates for different wave conditions on Hapuna Beach, Hawaii.



(3) $H_o = 3$ m, $T = 7$ sec

Fig.6.7. (continued) Beach profile changes and cross-shore sand transport rates for different wave conditions on Hapuna Beach, Hawaii.

From the results of cross-shore transport rate and bottom profile change for (a) winter and summer wave conditions on Waimea Bay Beach, Oahu, and (b) 3 different cases of wave height on Hapuna Beach, Hawaii, with the energetic-based model, it can be said that:

'As the deep-water wave height increases, maximum offshore transport occurs earlier and the offshore limit of active profile change becomes deeper. The formation of an offshore bar seems to be an unstable transient stage to adjust the equilibrium profile'.

6.3. BEACH RECOVERY

Beach processes basically show a three-dimensional behavior which combines longshore and cross-shore processes. Longshore sediment transports are generally carried by the wave-induced longshore currents, which show maximum speed near wave-breaking depth (Longuet-Higgins, 1972). In many locations of the Hawaiian Islands wave breaking often occurs a few times instead of once over the long reef bottoms, i.e., highly dissipative and complex shallow bottoms (Fig.6.8).

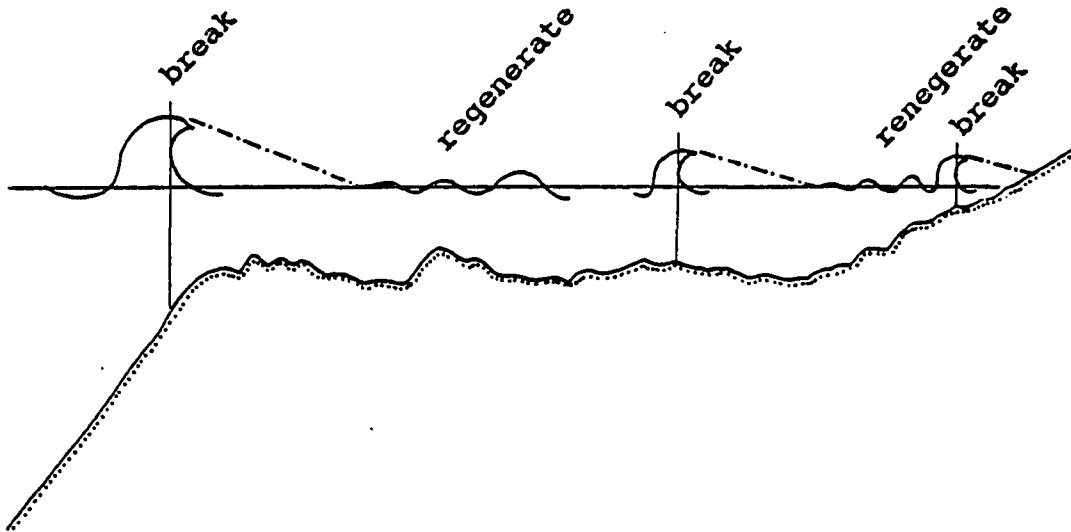


Fig.6.8. Schematic diagram of the complex wave-breaking process over the long reef bottom in the Hawaiian Islands.

Cross-shore sediment transports result from the combined effect of onshore transport near the bottom due to wave asymmetry and offshore transport below the wave trough due to return flow, respectively. During storm-wave conditions, the motion of sediments to the offshore dominates due to strong return flow. Low and mild waves cause sediments to move shorewards and often develop a berm at the uprush level (Gerritsen and Jeon, 1991).

But, after a storm, subsequent mild waves recover the beach only at shallow depths since the smaller wave heights may not sufficiently affect the sediments at deeper depths to which they were transported by the big storm waves. The recovery processes is much slower than the erosion process. Therefore, beach profiles, in general, never reach full equilibrium state within a short time scale due to the continuous variability of the wave-energy level.

Daily tidal motion may also contribute to beach erosion and recovery (or accretion). The effect of beach erosion by storm waves during HW (high water) may be significantly larger than the case during LW (low water), if the tidal difference is large. But the tidal difference in the Hawaiian Islands is usually small (≤ 60 cm) and hence the contribution of daily tidal motion is insignificant relative to that of big storm waves (> 5 m).

Model results show minor recovery only near the foreshore region after deep erosion by model storm waves. An arbitrary storm wave ($H_o = 6$ m, $T = 12$ sec) is exerted for 36 hours on Waimea Bay Beach, Oahu and for 24 hours on Hapuna Beach, Hawaii.

On Waimea Bay Beach, Oahu, overall erosion on the steep shallow region ($h = 0$ to 8 m) and deposition on the gentle deep region ($h = 8$ to 12 m) occurs for model storm waves ($H_o = 6$ m). After 36 hours of the big waves, low wave height ($H_o = 1$ m) is exerted for 60 hours. While there is no active sediment transport below 5 m depth (≈ 100 m horizontal distance from the shoreline), a subsurface bar forms at about 1 m depth and slowly migrates offshore (Fig.6.9). The migration of the bar corresponds to the maximum offshore transport rate around 50 m distance from the shore after 1 day. On Hapuna Beach, Hawaii, a big storm wave ($H_o = 6$ m) for 24 hours causes foreshore erosion and forms a bar at 2 to 3 m depth, which results in accretion down to 9 m depth. Contrary to Waimea Bay Beach, overall deep erosion occurs down to a depth of about 20 m. The recovery rate at shallow depths seems to be very slow even for moderate wave conditions ($H_o = 2$ m) after the storm, due to its steep slope (Fig.6.10).

Consequently, beach recovery by onshore sediment transport in a short-time scale after big storm waves must be carried out by non-breaking long waves.

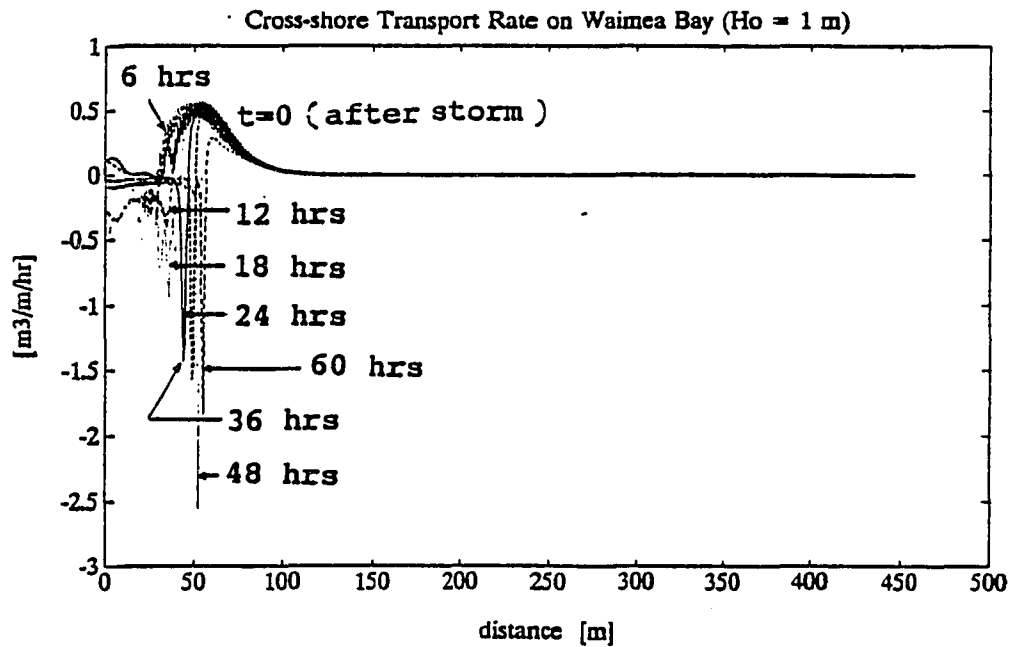
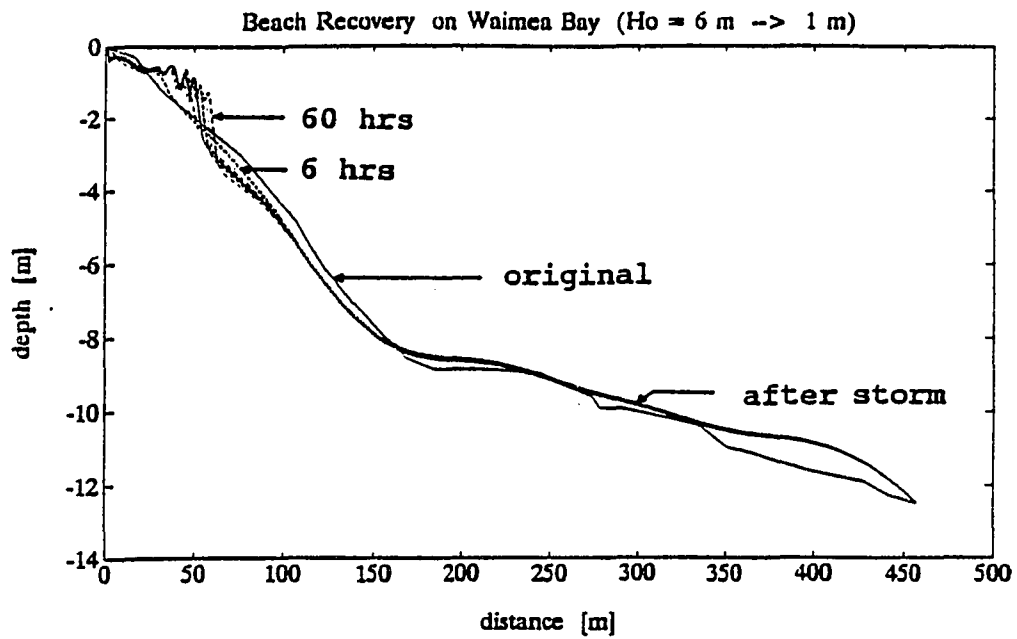


Fig.6.9. Beach profile changes and cross-shore transport rates under a small wave condition ($H_o = 1 \text{ m}$) after an arbitrary big storm ($H_o = 6 \text{ m}$, $t = 36 \text{ hours}$) on Waimea Bay Beach, Oahu.

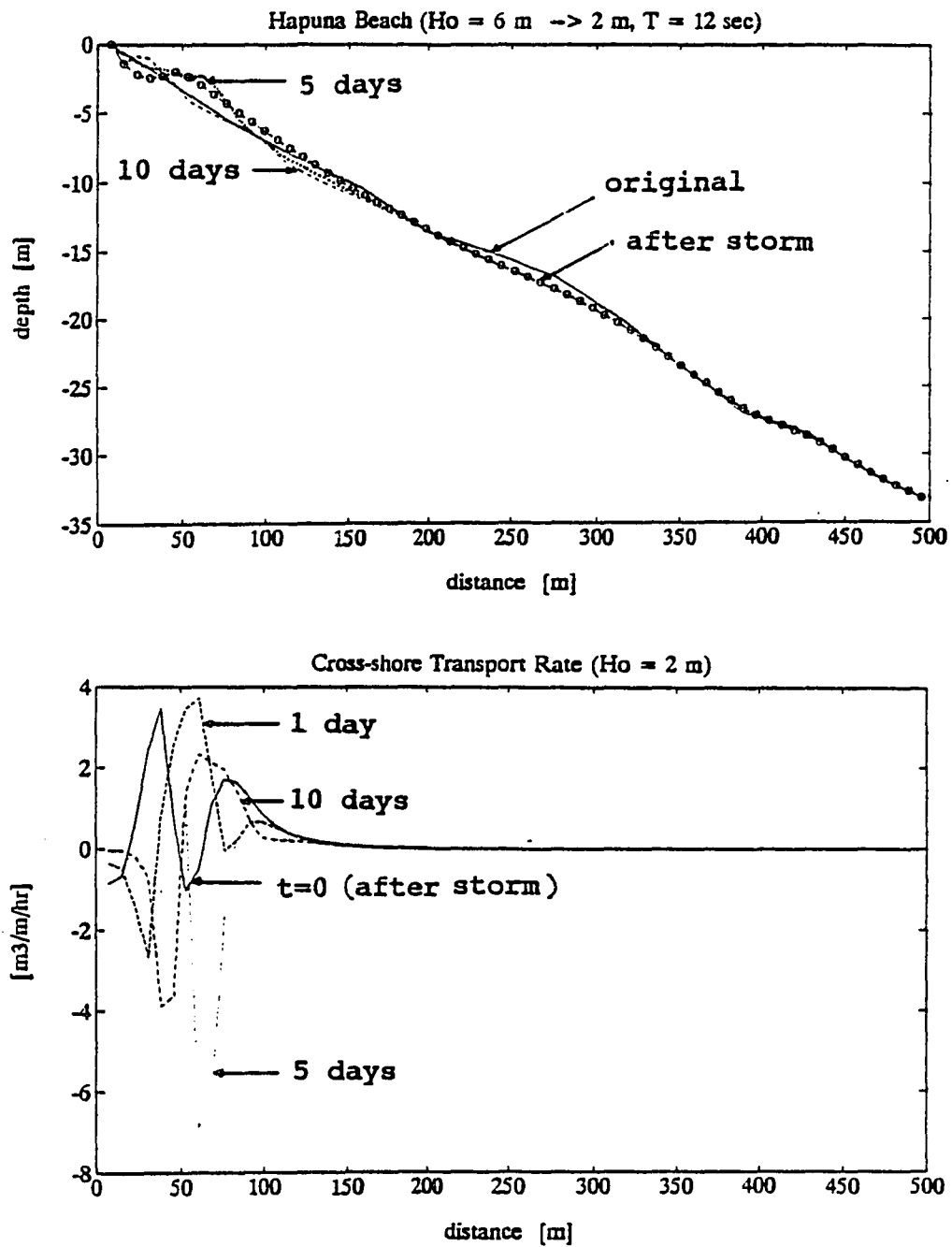


Fig.6.10. Beach profile changes and cross-shore transport rates under a moderate wave condition ($H_o = 2 \text{ m}$) after an arbitrary big storm ($H_o = 6 \text{ m}$, $t = 24 \text{ hrs}$) on Hapuna Beach, Hawaii.

Alternate onshore and offshore sediment transports usually occur in an annual time scale, depending on favorable (or mild) and unfavorable (or high) wave conditions during different seasons. When favorable wave conditions coincide with the lowering phase of the annual cycle in sea level, beach recovery (or onshore transport) rates may be faster. This implies that the rising phase of sea level may result in more erosion or more offshore transport of the eroded materials to greater depths when the rising sea level coincides with unfavorable wave conditions. In general, cross-shore sediment transport in an annual time scale seems to occur alternately between summer and winter seasons, and beach erosion and accretion (or recovery) rates are comparable in the Hawaiian Islands. The seasonal fluctuations in beach sand reservoirs for selected beaches in the Hawaiian Islands during 1962 to 1963 (Moberly, 1968) are shown in Fig.6.11.

In interannual and long-term scales, many of the Hawaiian beaches do not totally recover. That is, they are chronically losing sands to deep water. Moberly (1968) argues about the mechanisms of sand loss to deep water on the Hawaiian beaches -- 1) by waves and currents mainly along sand-bottomed channels, 2) by sedimentation to deep water, 3) by abrasion, 4) by cementation to beachrock, and 5) by storms. Although waves and currents are the primary mechanism of littoral sand transports,

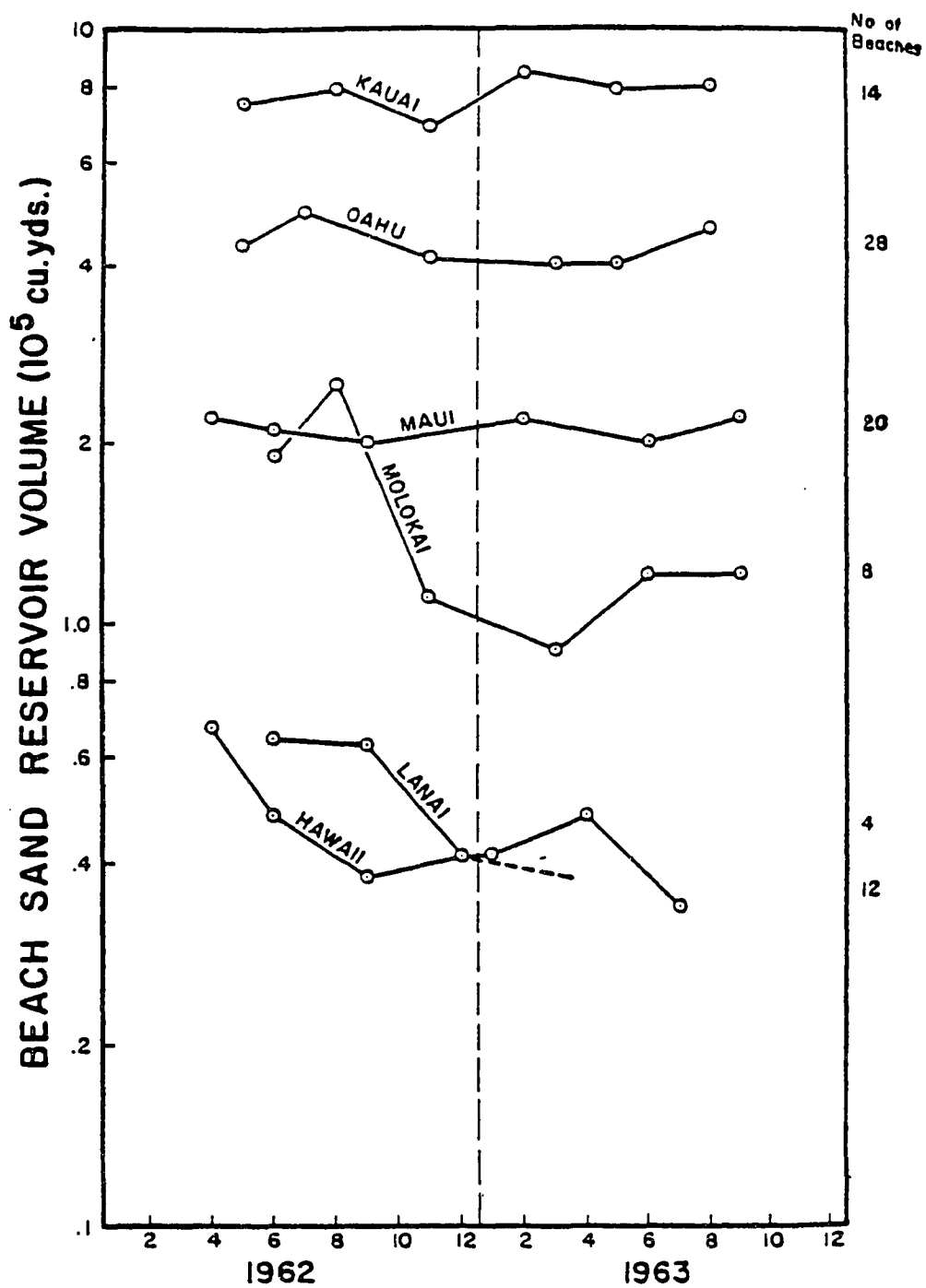


Fig.6.11. Seasonal fluctuations in beach sand reservoirs for 86 selected beaches in the Hawaiian Islands during 1962 to 1963 (after Moberly, 1968).

beach erosion might not have been so serious without continuous rise and fall of sea level in an interannual time scale since elevated sea level makes it possible for waves to transport more beach sands to deep water which can never be fully returned even after sea level falls. As the time scale of sea level fluctuation becomes longer, the rate of beach recovery seems to be lower.

In this study, it is hypothesized that the beach recovery rate (χ) exponentially decreases as a function of the period of sea-level fluctuation such that

$$\chi = A * \exp\left(-\frac{t}{T_c}\right) \quad (6.1)$$

where A = beach-erosion coefficient (≤ 1) as a function of underlying geology, sediment characteristics
 t = period of sea-level fluctuation (in months)
 T_c = characteristic time scale of the chronic beach erosion

Although this hypothesis is crude in its dynamics and critically dependent upon the characteristic time scale (T_c), it may represent the chronic beach erosion in a fairly reasonable manner when T_c is properly chosen from historical aerial photographs at littoral cells. For the case studies

at Waimea Bay Beach, Oahu, and at Hapuna Beach, Hawaii, T_c was applied as 100 months (≈ 8.3 years), based on the aerial photographs at the separate sandy beaches of the major four Hawaiian Islands (Hwang, 1981; Makai Eng. & Ocean Eng., 1991). This value is approximately twice the average ENSO period.

Then, the beach recovery rate in annual oscillation ($t = 12$ months) and in interannual fluctuation ($t \approx 4$ years) can be calculated as

$$\chi_{1yr} = \exp\left(-\frac{12}{100}\right) \approx 0.89 \quad (6.2)$$

and

$$\chi_{4yr} = \exp\left(-\frac{48}{100}\right) \approx 0.62 \quad (6.3)$$

It means that sediment losses by the sea-level fluctuation with periods of 1 year and 4 years are about 10% and 40%, respectively. If we further assume that the sea-level record at Honolulu can be applied to Waimea Bay Beach, Oahu (which is fairly reasonable; see Fig.3.1) and the record at Hilo to Hapuna Beach, Hawaii (which may be deviated a little), then the net shoreline retreat by the sea-level fluctuations with different time scales are calculated as follows:

$$\begin{array}{rcl}
 (1) \text{ shoreline retreat} & = & \text{SLR} * \beta \\
 (2) \text{ shoreline accretion} & = & \text{SLR} * \beta * \chi \\
 \hline
 (1) - (2); \text{ net retreat} & = & \text{SLR} * \beta * (1 - \chi)
 \end{array}$$

where

SLR = vertical rise in sea level

β = beach-face slope

χ = beach recovery rate

When applying long-term trend of sea-level rise, interannual and annual fluctuations with beach recovery rates, the contribution of each component to horizontal beach retreat can be estimated as in Table 6.7.

The contributions of long-term rise in relative sea level is not significant at either beach; 4% at Waimea Bay Beach, Oahu and 8% at Hapuna Beach, Hawaii. But, if global warming is accelerating in the near future, thermal expansion of seawater would contribute more to long-term rise in relative sea level.

The effect of sea-level fluctuation on beach erosion has not been studied as much as that of waves. But sea-level fluctuation may cause significant beach erosion, especially with an interannual (or even longer) periods. Annual oscillation of sea level as well as annual wave climate are the primary cause of alternating cross-shore

sediment transport. However, the question of the portion of sediment loss in annual onshore/offshore transport might not have attracted the attention of most coastal geologists and engineers probably because it could not be reasonably measured, relative to the amplitude of annual oscillation.

The contributions of sea level changes (long-term rise, interannual, and annual components) and waves (short-term) to the shoreline retreat were estimated as about half and half, respectively, at both beaches. The shoreline retreat by sea-level change only can be formulated by

$$R(t) = R_1(t) + R_2(t) + R_3(t) \\ = \frac{L}{H} * t * \left[S + S_1 \left(1 - A_1 \exp \left(-\frac{t_1}{T_c} \right) \right) + S_2 \left(1 - A_2 \exp \left(-\frac{t_2}{T_c} \right) \right) \right] \quad (6.4)$$

where

$R(t)$ = shoreline retreat

$R_1(t)$ = retreat by long-term sea-level rise

$R_2(t)$ = retreat due to interannual sea-level fluctuation

$R_3(t)$ = retreat due to annual sea-level oscillation

S = vertical sea-level rise

S_1 = mean height of the interannual fluctuation

S_2 = mean height of the annual oscillation

A_1 = coefficient for the annual oscillation with time t_1

A_2 = coefficient for the interannual fluctuation with the quasi-period t_2

Table 6.7. Contributions of sea-level changes and waves to shoreline retreat at (1) Hapuna Beach, Hawaii, and at (2) Waimea Bay Beach, Oahu, based on the hypothesized beach recovery rate and measured aerial photographs.

(1) Hapuna Beach, Hawaii ($\beta = 1/15$)

	SLR (vertical)	E/A (horizontal)	Net Retreat
long-term rise	0.4 cm/yr	-0.06 m/yr	-0.06 m/yr
interannual fluc.	14 cm/4 yr (3.5 cm/yr)	-0.53 m/yr +0.32 m/yr	-0.21 m/yr
annual oscillation	10 cm/yr	-1.50 m/yr +1.35 m/yr	-0.15 m/yr
short-term effects			-0.37 m/yr
Total			-0.79 m/yr

(2) Waimea Bay Beach, Oahu ($\beta = 1/20$)

	SLR (vertical)	E/A (horizontal)	Net Retreat
long-term rise	0.2 cm/yr	-0.04 m/yr	-0.04 m/yr
interannual fluc.	16.8 cm/4 yr (4.2 cm/yr)	-0.84 m/yr +0.50 m/yr	-0.34 m/yr
annual oscillation	9 cm/yr	-1.80 m/yr +1.62 m/yr	-0.18 m/yr
short-term effects			-0.39 m/yr
Total			-0.95 m/yr

Here it is assumed that there is no longshore transport and that the beach slope is always the same during the erosion process. On the other hand, the irregularity of the period (or the quasi-periodicity) of the interannual fluctuation of sea levels makes it difficult to predict beach erosion. When the (mean) period of ENSO events is assumed as 4 years, the shoreline retreats at an isolated beach with different slopes can be calculated as follows:

Table.6.8. Calculated shoreline retreats for different beach-face slopes with sea-level changes ($S = 2$ cm/10 yrs, $S' = 10$ cm/yr, $S'' = 16$ cm/4yrs are assumed here.)

β	$R_1(t)$	$R_2(t)$	$R_3(t)$	$R(t)$
1:5	1.0 cm/yr	5.7 cm/yr	7.6 cm/yr	14.3 cm/yr
1:6	1.2	6.8	9.1	17.1
1:7	1.4	7.9	10.7	20.0
1:8	1.6	9.0	12.2	22.8
1:10	2.0	11.3	15.2	28.5
1:20	4.0	22.6	30.5	57.1
1:30	6.0	33.9	45.7	85.6
1:40	8.0	45.2	61.0	114.2
1:50	10.0	56.5	76.2	142.7
1:75	15.0	84.8	114.3	214.1
1:100	20.0	113.0	152.4	285.4

In addition, potentially accelerating global warming in the near future will definitely cause the long-term effect to contribute more to beach erosion.

CHAPTER 7

COASTAL ZONE MANAGEMENT

Human activities such as the building of ill-designed coastal structures or sand mining, etc., may be significant factors affecting coastal erosion in the Hawaiian Islands, especially on Oahu and on Maui.

Harbor construction often requires dredging or widening of a navigation channel, which may change natural sand-bypassing systems and groins or breakwaters may interrupt the transport of littoral material. These coastal structures may change the patterns of wave propagation and energy dissipation and cause serious leeside erosion.

Removal of beach material for nourishing other beaches or for constructing structures and buildings, and mining of subsurface sand resources may result in erosion by changing the equilibrium profile. One serious reason for the chronic erosion on Waimea Bay, Oahu is the sand mining which has been carried out intermittently from 1949 to 1965 (Hwang, 1981).

Building seawalls, bulkheads, and revetments for coastal protection may also cause erosion problems when they are not properly constructed with consideration of all the important design factors (Gerritsen and Jeon, 1991).

7.1. ARTIFICIAL BEACH NOURISHMENT

Through natural nourishment beaches maintain a near equilibrium state. Artificial nourishment as an alternative could be applied to protect or to reduce beach erosion as intermittant or continual processes. It is usually economically attractive and environmently more acceptable.

There are some requirements for artificial nourishment such that:

- 1) the grain size of nourished materials must be equal or somewhat larger than that of original sands to prevent the nourished beach from losing sands too fast;
- 2) nourished materials should not be calcified to avoid formation of hard surfaces;
- 3) for recreational beaches, color should match the original beach sands.

It seems worthwhile to discuss methods of artificial nourishment although some of them are not directly related to the natural beach systems. They can be summarized as follows:

- 1) direct placement by trucking and dredging,
- 2) dumping sands at one site (or stock-piling),
- 3) dumping sands at the shallow subsurface bottom (2 to 3 m)

3) dumping sands on the shallow subsurface bottom (2 to 3 m)
(or offshore dumping).

This method has the advantages of providing wave-breaking and of providing a source for onshore sediment motion during low-swell conditions. However, a portion of the dumped sands may be lost to deep water during severe storms.

4) sand bypassing with

- pumping plant to transfer sands from accretionary side of the groin to the other eroding side through pipe line,

- sediment trap in the harbor and dredging intermittently,

- weir portion to allow sands to be deposited in the harbor through low level portion (weir) of the jetty, and dredging intermittently,

- a vertically mobile bed by fluidization in the harbor entrance to stir up deposited sediments and to allow outflux during ebb tide,

- a jetty interrupting the littoral drift and forming a sand spit from its end, which is dredged intermittently,

- asymmetric offshore breakwater to the harbor in order to allow sediments to be deposited and to be dredged intermittently.

7.2. HARD SOLUTIONS

Offshore breakwaters in shallow water parallel to shore are frequently used as a hard solution against beach erosion. Since they induce deformation of the shoreline due to wave refraction and diffraction, the length of the breakwater as related to the distance from the shoreline must be carefully considered. Low-level or permeable breakwaters may be used to prevent the formation of tombolo : extreme shoreline deformation which causes the offshore breakwater to be connected to the beach.

Groins to protect beaches from erosion may under certain conditions be accepted such as when lee-side erosion can be avoided or at least accepted. A groin constructed at the boundary of a sandy beach and rocky shoreline will usually not cause a beach-erosion problem. Where there is a periodic reversal of longshore transports depending on the direction of wave approaches, the fill between two groins may oscillate from one end of the compartment to the other. Multiple transitional groins with gradually reduced lengths may be used in order to avoid an abrupt change between protected and unprotected beach to reduce erosion of the downdrift beach.

Revetment may be used to protect dunes from storm-tide damage. There are two types of revetments:

1) Sloping revetments include

- rubble mound
- concrete blocks
- placed stones, e.g., Kalama Beach (Maui),

Hilo Harbor (Hawaii)

- asphalt concrete
- stepped revetment.

2) Vertical types include

- vertical gravity seawall, e.g., Mokuleia (Oahu); West Maalaea Bay, Waimahaihai Beach, and Honokowai Beach (Maui)
- steel bulkhead
- concrete sheet piling
- bulkhead with anchor.

A revetment is usually constructed (with toe protection) considerably above MHW (mean high water), out of the normal reach of the waves. In order to reduce the height of wave runup on smooth slopes, ripples may be added. In case of bulkhead revetment, the backside may be eroded by wave overtopping during severe storms which may even form a lagoon. Design factors are different from case to case. We must consider all the important design factors quantitatively in order to obtain suitable DWL (design water level) and other design parameters for a certain case.

7.3. MANAGEMENT STRATEGIES

Loss of beaches or coastal areas has both direct and indirect consequences for coastal communities, requiring abandonment and adjustment of property and, in extreme cases, posing a danger to life (Carter, 1988). Basically there are three kinds of coastal-zone-management strategies:

1) *retreat* In accordance with rising sea level and more disastrous coastal hazards by storm surges or tsunamis in the future, all the residential areas are shifted inland and a buffer system with natural or appropriate artificial dunes, *etc.*, is created. This strategy is most for undeveloped coastal zones; regulations are the primary management controls. It is different from a temporary evacuation such as during a tsunami warning, in the sense that a coastal buffer-zone is permanently preserved by legal controls.

2) *status quo* with shore protection For developed coastal zones which endure erosion, coastal structures such as breakwaters, revetments, or groins have been constructed to protect further erosion. This method often causes shoreline deformation and other erosion problems due to the dynamic impact of the structures. It may be combined with artificial nourishment.

3) *beach nourishment* For developed beaches that have not been hardened, extending coastal zones temporarily seawards by artificial beach nourishment could be applied. Since the first rule of coastal management should always be "to work with, rather than against, the natural system" (Carter, 1988), extending beaches by intermittent sand replenishments must be carefully evaluated, based on the nearshore circulation system, wave climate, sediment characteristics, bottom topography, and environmental concerns etc.

Hwang and Fletcher (1992) suggest developing the concept of *Beach Management District* (BMD)¹² for the strategies 2) and 3) above. Through the cooperation of landowners, the counties and the State, it may be possible to develop and finance alternatives such as for example offshore structures, sand replenishment, or a field of permeable groins. The success of this program has varied with the type of district established and with the level of cooperation from the State and from local governments.

Lastly, it is recommended that the State of Hawaii should establish 'the Office of Beach Restoration' for measuring beach profiles at a regular basis and for monitoring and nourishing major Hawaiian beaches.

¹² BMD includes the overlay district, the improvement district, and the special taxing district. See Hwang and Fletcher (1992) for further reference.

CHAPTER 8

CONCLUSIONS

Long-term relative sea levels at selected island stations in the North Pacific between the equator and about 30°N are examined in association with different time scales of motions. Coastal response to these sea level dynamics with different time scales are discussed in detail, based on aerial photographs of shoreline changes. Wave climate around the Hawaiian Islands as well as surf conditions on Oahu are analyzed for simulating cross-shore beach erosion processes with an energetics-based sediment transport model.

Tide-gauge records from the selected island stations in the North Pacific (between the equator and 30°N) show the following:

- (1) The mean annual cycle of sea level is the strongest signal at most of the stations, reaching about 10 cm in the mean annual height difference. The mean annual sea level cycle and alternate annual wave conditions are the main causes of the cross-shore oscillation of sediment transport, with is some permanent loss of sediments to deep water.

(2) Long-term linear regressions show a trend of relative sea level rise of +1 to +5 cm/decade at most of the sea level stations, primarily resulting from local tectonism such as volcanic loading, plate movement with reef evolution and subduction at the plate boundaries. Continual volcanic loading at Kilauea, Hawaii results in consequential subsidence of the Hawaiian Islands. Hence the Island of Hawaii subsides with fastest rate (+ 2.5 mm/yr), the neighboring island Maui with slower rate (+ 1.0 mm/yr), and the Islands of Oahu (+0.15 mm/yr) and Kauai (+ 0.33 mm/yr) with slowest rate. The slightly falling trend of sea level at Midway atoll (- 0.6 mm/yr) is associated with reef evolution and plate movements. A secondary reason for the rising sea level up to the present may be contributions from the thermal expansion of sea surface waters by global warming (+ 1.4 mm/yr). The rate of submergence is the sum of the rate of subsidence and the global rate of sea-level rise. It is likely that in the future sea-level trend would accelerate by the increasing rate of greenhouse gases into the atmosphere up to 6 mm/yr. Although various GCMs (general circulation models) have simulated present and future atmosphere and oceans and support the accelerating trend of sea level rise, there still exist a primary uncertainty about the feedback mechanism of clouds before transferring the "potentially increasing thermal energy" to the ocean surface.

(3) Energy density distribution of monthly sea level values shows a strong peak at about a four year period in the Hawaiian Islands. A unique spectral peak with 25 to 30 year period is shown at Honolulu, Oahu, due to its relatively longer time-series (> 85 years). Interannual fluctuations from the time-series smoothed by twelve-month running means show clear signals with periods between 2 and 7 years, which are closely associated with ENSO events. Sea level rise and fall with an interannual time scale may be an important factor for serious erosion problems, which seems to affect beach erosion up to five to ten times the long-term linear trend. As the time scale of sea level fluctuation becomes longer, beach erosion rate would be higher (or beach recovery rate would be lower).

Reanalysis of previous aerial photographs of shoreline changes in association with sea level fluctuations in the Hawaiian Islands suggests the followings:

(4) Among the four major Hawaiian Islands (Hawaii, Maui, Oahu, and Kauai), Maui seems to endure the most serious problem of chronic beach erosion.

(5) In order to more precisely interpret long-term or interannual shoreline changes from aerial photographs, measurements must be carried out at least in the same month

of the year. This will remove the errors from different sea levels on the annual cycle and from different wave conditions in different months.

(6) Measurements at different times of the year may lead to incorrect interpretations, even to reverse trends of erosion/accretion of shoreline changes, unless the potential errors included in aerial photographic measurements and mapping procedures are systematically corrected.

(7) From aerial photographs it has been found that Waimea Bay Beach on the north shore of Oahu has been seriously eroded over the last decades; Hapuna Beach on the northwest coast of Hawaii also eroded but to a lesser degree. The primary reason for the erosion at Waimea Beach seems to be the sand mining at Waimea Bay during 1949 to 1965.

Wave data analyses and an energetic-based cross-shore sediment transport model give results as follows:

(8) Short-term change of beach profiles is basically caused by wave conditions (wave height and period) in addition to the effects of changes in MSL (mean sea level) height.

(9) The average of significant wave height from NOAA buoy (51001) during winter (December, January, and February) exceeds 3 m and the average wave period is about 8 seconds, while both wave height and period are greatly reduced during summer (June, July, and August) ($H_0 \approx 2$ m, $T \approx 6$ sec). This is because relatively mild trade winds (northeasterlies) prevail most of the year including summer and stronger North Pacific swells (northwesterlies) control the wave climate in winter.

(10) The surf conditions on the north and south shores of Oahu are distinctly different; while the surf height on the north shore is calm during summer and usually very high during winter, it is fairly low on the south shore in both seasons.

(11) Calculated beach profile changes at Waimea Bay Beach, Oahu and on Hapuna Beach, Hawaii by a cross-shore sediment transport model show similar patterns for different wave conditions, except erosion to greater depth for higher wave height. At Hapuna Beach, Hawaii, it is shown that higher waves result in faster offshore transport and a greater depth of the active zone.

(12) Beach recovery processes are usually much slower than erosion processes, especially after big storm waves. Deep

erosion during storm waves can not be recovered by favorable (or mild) waves of much longer duration. The erosion may be partly recovered by non-breaking long waves such as long-period swells, but eroded material may be permanently lost to deep water.

Even in sea-level fluctuations at longer time scales beach sediments cannot be fully recovered. As a hypothesis it is proposed that the beach recovery rate exponentially decreases as the period of sea-level fluctuation increases.

(13) The formation and migration of a bar at shallow depths presents an unstable transient feature, which results as the bottom tries to adjust to an equilibrium state during a period of high waves. In this process standing infragravity waves may play a role. Because of the time it takes to reach equilibrium conditions and of the continuous variability of the wave energy level and its directionality, equilibrium conditions are hardly ever reached in the field.

APPENDICES

A.1. DENSITY OF SEAWATER

The density of seawater is a function of temperature, salinity and pressure: the parameters temperature and salinity nonlinearly affect density, which increases by approximately 1 kg m^{-3} for a change of temperature of $- 5^{\circ}\text{C}$, for a change of salinity of $+ 1 \text{ psu}$ (practical salinity unit) or for a change of pressure of $+ 2,000 \text{ kPa}$.

In the open ocean, temperature ranges from $- 2^{\circ}\text{C}$ to $+ 30^{\circ}\text{C}$, salinity from 30 to 38 psu and sea pressure from 0 to about 10^5 kPa at a depth of 10,000 m. Salinity may fall down to 0 near estuaries or melting ice. The density of seawater at atmospheric pressure varies from about $1,000 \text{ kg m}^{-3}$ for almost fresh water to about $1,028 \text{ kg m}^{-3}$ for the densest ocean water.

Thermal expansion coefficient correspondingly increases as temperature increases and hence volume expansion rate of surface seawater at 31°C in the tropics is about 6 times larger than that at 0°C (Table A.1).

Table A.1. Temperature-dependency of the density of standard seawater ($S = 35$ psu) at an atmospheric pressure ($P = 0$), and corresponding thermal expansion coefficient (α), gradients of P and α with respect to salinity (S).

P (bar)	S (psu*)	T (°C)	σ_t^{**} (kg m ⁻³)	α (10 ⁻⁷ K ⁻¹)	$\partial P/\partial S$	$\partial \alpha/\partial S$
0	35	-2	28.187	254	0.814	33
0	35	0	28.106	526	0.808	31
0	35	2	27.972	781	0.801	28
0	35	4	27.786	1021	0.796	26
0	35	7	27.419	1357	0.788	23
0	35	10	26.952	1668	0.781	20
0	35	13	26.394	1958	0.775	17
0	35	16	25.748	2230	0.769	15
0	35	19	25.022	2489	0.764	14
0	35	22	24.219	2734	0.760	12
0	35	25	23.343	2970	0.756	11
0	35	28	22.397	3196	0.752	9
0	35	31	21.384	3413	0.749	8

* psu = practical salinity unit

** $\sigma_t = \rho$ (density) - 1,000 in [kg m⁻³].

A.2. MEAN ANNUAL TREND OF SHORELINE CHANGES IN THE HAWAIIAN ISLANDS

Table A.2. Mean annual trend of shoreline changes [m/yr] on
(a) Oahu (data from Hwang, 1981), (b) Hawaii, (c) Maui, and
(d) Kauai (data from Makai Ocean Eng. and Sea Eng., 1991).
(see also Fig.6.1)

(a) Oahu

North	Windward	South	Leeward
0.22	1.12	-0.08	-0.07
-0.01	0.08	-0.11	0.41
0.12	0.04	0.08	0.11
-0.14	-0.23	0.10	0.31
0.68	0.07	0.04	0.13
0.0	-0.05	0.20	0.17
-0.94	-0.04	-0.17	0.12
0.01	0.31	-0.17	0.06
-0.03	-0.06	-0.16	-0.03
0.17	-0.11	0.08	-0.31
-0.01	-0.24	0.02	
0.01	0.50		
	-0.24		
	-0.09		

(b) Hawaii

HA	HB
0.06	0.14
-0.03	-0.20
0.16	-0.55
-0.09	-0.07
-0.24	0.06
0.14	0.17
-0.16	-0.02
-0.24	0.16
0.0	0.08
0.13	-0.17
0.02	-0.31
	-0.16
	-0.24
	-0.06
	0.13
	-0.08
	-0.35
	-0.07

* (+); accretion, (-); erosion

Table A.2. (continued) Mean annual trend of shoreline changes [m/yr] on (a) Oahu (data from Hwang, 1981), (b) Hawaii, (c) Maui, and (d) Kauai (data from Makai Ocean Eng. and Sea Eng., 1991). (see also Fig.6.1)

(c) Maui

MA	MB	MC	MD
0.41	0.05	-0.68	-1.26
0.52	-0.26	-0.38	-1.54
-0.52	0.04	-0.31	-1.90
-0.02	0.0	-0.31	-0.44
-0.11	-0.27	-0.41	-1.42
-0.18	-0.42	-0.48	-1.22
0.11	-0.19	-0.02	1.06
0.05	-0.29	-0.81	0.04
-0.09	-0.13	-0.38	0.44
0.08	0.06	-0.31	0.08
0.28	-0.19	-0.65	-0.72
0.02	-0.22	-0.52	-0.08
-0.21	-0.23	-0.19	-0.04
-0.08	0.89	-0.23	0.14
-0.07	-0.71	-0.15	-0.33
0.17	2.18	-0.40	-0.87
-0.15	-0.46	-0.17	-0.12
-0.35	0.92	0.27	0.00
-0.34	-0.21	-0.21	-0.14
-0.35		-0.38	0.14
-0.34		-0.25	0.13
-0.12		-0.29	
-0.15		0.04	
-0.13			
-0.10			
-0.10			

* (+); accretion, (-); erosion

Table A.2. (continued) Mean annual trend of shoreline changes [m/yr] on (a) Oahu (data from Hwang, 1981), (b) Hawaii, (c) Maui, and (d) Kauai (data from Makai Ocean Eng. and Sea Eng., 1991). (see also Fig.6.1)

(c) Kauai

KA	KB	KC	KD	KE	KF
-0.14	-0.19	0.03	0.14	0.16	-0.20
-0.34	-0.18	-0.25	0.06	-0.05	0.16
-0.37	-0.15	0.09	0.15	0.03	0.67
-0.13	-0.21	-0.09	0.14	-0.02	0.09
-0.63	-0.15	0.09	0.11	-0.16	-0.12
0.69	-0.09	0.05	-0.21	-0.14	-0.18
0.72	-0.10	-0.35	0.09	0.10	
0.30	0.10	-0.50	0.31	-0.33	
0.26	0.15	-0.08	1.09	-0.04	
0.17		0.46	0.02	0.16	
0.17		0.00	0.28		
		-0.08	0.12		
		0.02	-0.11		
		-0.05			
		-0.06			
		0.12			
		0.24			
		0.32			
		-0.08			
		-0.05			
		0.06			
		0.06			
		0.02			
		-0.15			
		-0.07			
		-0.17			
		-0.10			
		0.32			
		0.62			
		-0.46			
		0.06			
		0.10			
		0.28			
		-0.17			
		-0.23			
		-0.35			

* (+); accretion, (-); erosion

A.3. SEDIMENT FALL SPEED

Sediment fall speed is a function of the grain size, shape of the falling object, and of the viscosity of the fluid. Stokes (1945) first derived the equation of the fall speed (w_s) for low Reynolds numbers ($Re < 1$). For a single spherical object settling through a motionless fluid, the drag force on the sphere is

$$\begin{aligned} F_{drag} &= C_D A \frac{1}{2} \rho U^2 \\ &= C_D \pi \left(\frac{D}{2} \right)^2 \rho \frac{1}{2} w_s^2 \\ &= C_D \frac{\pi}{8} \rho D^2 w_s^2 \end{aligned} \quad (A.1)$$

where A represents projected area of the body on to a plane normal to U , and U is the same as w_s .

Drag coefficient (C_D) for low Reynolds numbers ($Re < 1$) is

$$\begin{aligned} C_D &= \frac{F_{drag}}{\frac{1}{8} \pi \rho D^2} \\ &= \frac{3 \pi \mu D U}{\frac{1}{8} \pi \rho D^2} \\ &= \frac{24}{R_e} \quad \left(\text{where } R_e = \frac{\rho D U}{\mu} \right) \end{aligned} \quad (A.2)$$

When the immersed weight (weight - buoyancy of the fluid) is balanced by the drag force, the settling velocity will be determined. The immersed weight (I) of a sphere is

$$\begin{aligned} I &= \frac{4}{3} \pi \left(\frac{D}{2} \right)^3 (\rho_s - \rho) g \\ &= \frac{1}{6} \pi D^3 (\rho_s - \rho) g \end{aligned} \quad (\text{A.3})$$

Since $F_{\text{drag}} = I$, we have

$$\begin{aligned} w_s &= \frac{D^2}{18 \mu} (\rho_s - \rho) g \\ &= \frac{g}{18 \nu} \left(\frac{\rho_s}{\rho} - 1 \right) * D^2 \end{aligned} \quad (\text{A.4})$$

where dynamic viscosity $\nu = \mu/\rho$. This is usually called the 'Stokes law'. The corresponding value of the Reynolds number for a sphere falling down with the fall speed is

$$R_o = \frac{g}{18 \nu^2} \left(\frac{\rho_s}{\rho} - 1 \right) * D^3 \quad (\text{A.5})$$

From a comparison of the observed and calculated fall speeds of spheres of known size, Stokes law for the drag is tolerably accurate for most purposes when $R_o < 1$, and there is no detectable error when $R_o < 0.5$ (Batchelor, 1967).

Meanwhile, there have been several attempts to express a sediment fall speed as a function of shape factor as well as size in a practical way. Maude and Whitmore (1958) suggest that a sediment fall speed follows the relationship such that

$$w_s = w_o (1 - C)^b \quad (\text{A.6})$$

where w_o is fall speed of a single grain, C is the volumetric particle concentration, and b is a function of particle size and shape. It was empirically obtained that $b = 4.65$ for small particle and that $b = 2.32$ for large one. Peirce and Williams (1966) have shown for four different muds that the settling speed is proportional to $(1 - C)^5$. Hallermier's (1981b) empirical fitting for the fall speed of common natural grains is consistent with the above results (see Shore Protection Manual, 4-18, 4-21).

REFERENCES

- Anders, F.J. and M.R. Byrnes (1991) Accuracy of shoreline change rates as determined from maps and aerial photographs. *Shore and Beach*, 58(2), 17-26.
- Bagnold, R.A. (1966) An approach to the sediment transport problem from general physics. U.S. Geological Survey Prof. Paper, 422-I.
- Bailard, J. (1981) A simplified model for longshore sediment transport. *Coastal Eng. Conf.*, 1444-1470.
- Bailard, J. (1984) Simple model for surfzone sediment transport. *Naval Civil Eng. Lab. Tech. Note*, Port Hueneme, CA 93043.
- Barnett, T.P. (1983) Recent changes in sea level and their possible causes. *Climatic Change*, 5(1), 16-37.
- Barnett, T.P. (1984) The estimation of global sea level change: a problem of uniqueness. *J. Geophys. Res.*, 89 (C5), 7980-7988.
- Barnett, T.P. (1988) Global sea-level change. In: Climate variations over the past century and the greenhouse effect: a report based on the first climate trends workshop, Washington D.C. National Climate Program Office/NOAA, Rockville, Maryland, 7-9.
- Barstow, S.F., H.E. Krogstad, K. Torsethaugen, and T. Audunson (1985) Procedures and problems associated with the calibration of wave sensors, page 55-82, In: Evaluation, Comparison and Calibration of Oceanographic Instruments. *Graham & Trotman Ltd.*, London, pp267.
- Barth, M.C. and J.G. Titus (1984) Greenhouse Effect and Sea Level Rise. (Ed.) Van Nostrand Reinhold Co., New York, pp325.
- Batchelor, G.K. (1967) An Introduction to Fluid Dynamics. *Cambridge Univ. Press*, London and New York.
- Bodge, K.R. (1992) Representing equilibrium beach profiles with an exponential expression. *J. Coastal Res.*, 8(1), 47-55.

- Braatz, B.V. and D.G. Aubrey (1987) Recent relative sea-level change in eastern north America. *Soc. Econ. Paleont. Mineral.*, 47, 29-46.
- Broomfield, P. (1976) Fourier analysis of time series: and introduction. New York, John Wiley & Sons, 129-137.
- Bruun, P. (1954) Coastal erosion and development of beach profiles. *U.S. Army Beach Erosion Board of Tech. Memorandum*, No.44, U.S. Army Corps of Engineers, Waterway Exp. Station, Vicksburg, Mississippi.
- Bruun, P. (1962) Sea-level rise as a cause of shore erosion. *J. Water. Harb. Div.*, Proc. of ASCE, 88(WW1), 117-130.
- Bruun, P. (1988) The Bruun rule of erosion by sea-level rise: a discussion on large-scale two- and three-dimensional usages. *J. Coastal Res.*, 4(4), 627-648.
- Caldwell, P., K. Wyrski, and S. Nakahara (1989) TOGA Sea Level Center: Data from the Pacific. JIMAR contribution no.89-202, Univ. of Hawaii, pp34.
- Campbell, J.F. (1972) Erosion and accretion of selected Hawaiian beaches, 1962-1972. *HIG-72-20*, The University of Hawaii Sea Grant Program, *UNIHI-SEAGRANT-TR-72-02*.
- Campbell, J.F. and D.J. Hwang (1982) Beach Erosion at Waimea Bay, Oahu, Hawaii. *Pac. Sci.*, 36, 35-43.
- Carter, R.W.G. (1988) Coastal Environments -- An Introduction to the Physical, Ecological and Cultural Systems of Coastlines. *Academic Press*, London, pp617.
- Chamberlain, T. (1968) The Littoral Sand Budget, Hawaiian Islands. *Pac. Sci.*, xxii, 161-183.
- Coastal Engineering Research Center (1984) Shore Protection Manual. (4th ed.), Dep. of the Army, U.S. Army Corps of Engineers, Washington, D.C. 20314.
- Dean, R.G. (1977) Equilibrium beach profiles: U.S. Atlantic and Gulf coasts. Department of Civil Eng., Tech. Rep. No.12, Univ. of Delaware, Newark, Delaware.
- Dean, R.B. and E.M. Maurmeyer (1983) Models for beach profile response. In: Komar, P.D. (ed.), *CRC Handbook of Coastal Processes and Erosion*. CRC Press, Boca Raton, pp151-166.
- Dean, R.G. (1991) Equilibrium beach profiles: characteristics and applications. *J. Coastal Res.*, 7(1), 53-84.

- Douglas, B.C. (1991) Global sea level rise. *J. Geophys. Res.*, 6981-6992.
- Dubois, R.N. (1975) Support and refinement of the Bruun rule on beach erosion. *J. Geol.*, 83, 651-
- Edelman, T. (1968) Dune erosion during storm conditions. *Proc. Coastal Eng. (ASCE)*, New York, 719-
- Emery, K.O. and D.G. Aubrey (1991) Sea Levels, Land Levels, and Tide Gauges. *Springer-Verlag New York Inc.*, pp 237.
- Fletcher, C.H. (1992) Sea-level trends and physical consequences: applications to the U.S. shore. *Earth Science Review*, 33, 73-109.
- Folkert, M.B. and R.V. Woodle (1973) Status of environmental sensing systems for unattended ocean buoys., 162-176, in *Environmental Data Buoy Technology Workshop*, Kingston.
- Galvin, C.J. (1968) Breaker type classification on three laboratory beaches. *J. Geophys. Res.* 73(12), 3651-3659.
- Gerritsen, F. (1978) Beach and surf parameters in Hawaii. *Sea Grant Tech. Rep. UNIHI-SEAGRANT-TR-78-02*, Univ. of Hawaii, pp178.
- Gerritsen, F. and D. Jeon (1991) Nearshore Processes and Littoral Drifts. (unpublished manuscript). Dept. Ocean Eng., Univ. of Hawaii, pp130.
- Gill, A.E. (1982) Atmosphere-Ocean Dynamics. International Geophys. Series, vol. 30, *Academic Press*, New York, pp662.
- Gornitz, V., S. Lebedeff, and J. Hansen (1982) Global sea level trend in the past century. *Science*, 215, 1611-1614.
- Gornitz, V. and S. Lebedeff (1987) Global sea-level changes during the past century. *Soc. Econ. Paleont. Mineral.*, 47, 3-16.
- Graham, N.E., and W.B. White (1988) The El Niño cycle: a natural oscillator of the Pacific ocean-atmosphere system. *Science*, 240, 1293 - 1302.
- Gray, W.M. (1979) Hurricanes: their formation, structure and likely role in the tropical circulation. In: 'Meteorology over the Tropical Oceans' (D.B. Shaw, ed.), pp151 - 218, *Royal Meteor. Society*, London.

- Guilcher, A. (1988) Coral Reef Geomorphology. *John Wiley & Sons Ltd.*, Chichester, pp228.
- Guza, R.T. and E.G. Thornton (1981) Velocity moments in the surf zone. Contract Rep. to Naval Civil Eng. Lab., pp56.
- Hanson, H. and N.C. Kraus (1989) GENESIS: Generalized model for simulating shoreline change. Rep.1. Tech. Ref., prepared for US Army Corps of Engineers, Washington, D.C. 20314-1000.
- Hayden, B., W. Felder, J. Fisher, D. Resio, L. Vincent, R. Dolan (1975) Systematic variations in inshore bathymetry. *Tech. Rep. No. 10*, Dept. of Environmental Sci., Univ. of Virginia, Charlottesville, Virginia.
- Harvey, J.G. (1976) Atmosphere and Ocean: Our Fluid Environments. 1st ed., *Academic Press*, pp143.
- Hallermeier, R.J. (1981a) Seaward limit of significant sand transport by waves: An annual zonation for seasonal profiles. *Coastal Eng. Tech. Aid No. 81-2*, Coastal Eng. Res. Center, Vicksburg, Mississippi.
- Hallermeier, R.J. (1981b) Terminal settling velocity of commonly occurring sand grains. *Sedimentology*, 28,
- Holton, J.R. (1979) An Introduction to Dynamic Meteorology. 2nd ed., *Academic Press*, pp391.
- Hwang, D.J. (1981) Beach changes on Oahu as revealed by aerial photographs. *HIG-81-3*, Hawaii Inst. of Geophys., Univ. of Hawaii.
- Hwang, D.J. and C.H. Fletcher (1992) Beach management plan with beach management districts. Hawaii Coastal Zone Management Program, pp192.
- Inman, D.L., W.R. Gayman, and D.C. Cox (1963) Littoral sedimentary processes on Kauai, a subtropical high island. *Pac. Sci.*, 17(1), 106-130.
- Intergovernmental Panel on Climate Change (1990) Climate Change: The IPCC Scientific Assessment. J.T.Houghton, G.T.Jenkins, and J.J.Ephraums (Ed.), *Cambreidge Univ. Press*.
- Jenkins, G.M. and D.G. Watts (1968) Spectral Analysis and Its Applications. *Holden-Day, Inc.*, San Francisco, pp525.

- Jeon, D. (1990) Mean annual variations of the thermal structure in the South China Sea. M.S. Thesis, Dept. Oceanography, Univ. of Hawaii, Honolulu, Hawaii 96822.
- Kidson, C. (1986) Sea-level changes in the Holocene. p27-64 In *Sea-level Research: a manual for the collection and evaluation of data*. O.v.d. Plassche (Ed.), Geo Books, Regency House, 34 Duke St., Norwich.
- Kinsman, B. (1984) Wind Waves -- their generation and propagation on the ocean surface, *Dover Publ. Inc.*, New York, pp676.
- Komar, P.D. (1976) Beach Processes and Sedimentation. *Prentice-Hall, Inc.*, New Jersey. pp429.
- Komar, P.D. (1986) The 1982-83 El Niño and erosion on the coast of Oregon. *Shore and Beach*, 3-12.
- Komar, P.D. and D.B. Enfield (1987) Short-term sea-level changes and coastal erosion. *Soc. Econ. Paleont. Mineral.*, 47, 17-27.
- Komar, P.D., N. Lanfredi, M. Baba, R.G. Dean, K.Dyer, T. Healy, A.C.Ibe, J.H.J. Terwindt, B.G. Thom (1991) The response of beaches to sea-level changes: a review of predictive models. *J. Coastal Res.*, 7(3), 895-921.
- Kriebel, D.L. and R.G. Dean (1985) Numerical simulation of time-dependent beach and dune erosion. *Coast. Eng.*, 9, 221-245.
- Kriebel, D.L. and R.G. Dean (1993) Convolution method for time-dependent beach-profile response. *J. Water. P. Coast. Ocean Eng.*, 119(2), 204-226.
- Laevastu, T., d.E. Avery, and D.C. Cox (1964) Coastal currents and sewage disposal in the Hawaiian Islands. *HIG-64-1*, Hawaii Inst. of Geophys., Univ. of Hawaii, pp101.
- Lambeck, K. and S.M. Nakiboglu (1984) Recent global changes in sealevel. *Geophys. Res. Letters*, 11(10), 959-961.
- Larson, M. (1991) Equilibrium profile of a beach with varying grain size. *Coastal Sediments '91 (ASCE)*, pp905-919.
- Lisitzin, E. (1974) Sea-Level Changes. *Elsevier Publ. Co.*, Amsterdam, pp286.

- Longuet-Higgins, M.S. (1972) Recent progress in the study of longshore current. In: Waves in beaches and sediment transport, *Academic Press*, 203-248.
- Madden, R.A. and V. Ramanathan (1980) Detecting climate change due to increasing carbon dioxide. *Science*, 209, 763-768.
- Makai Ocean Eng., Inc. and Sea Eng., Inc. (1991) Aerial photograph analysis of coastal erosion on the Islands of Kauai, Molokai, Lanai, Maui and Hawaii. Honolulu, Hawaii, pp200.
- Maude, A.D. and R.L. Whitmore (1958) A generalized theory of sedimentation. *British J. Appl. Phys.*, 9, 477-482.
- Moberly, R.J. (1968) Loss of Hawaiian Littoral Sand. *J. Sed. Petrology*, 38(1), 17-34.
- Moberly, R.J., T. Chamberlain (1964) Hawaiian Beach Systems. *HIG Rep. HIG-64-2*, Hawaii Inst. of Geophys., Univ. of Hawaii.
- Moberly, R.J., D.C. Cox, T. Chamberlain, F.W. McCoy, Jr., and J.F. Campbell (1963) Coastal Geology of Hawaii. *HIG Rep. No 41.*, Hawaii Inst. of Geophys., Univ. of Hawaii, pp216.
- Moberly, R.J., J.F. Campbell, and W.T. Coulbourn (1975) Offshore and other sand resources for Oahu, Hawaii. *Sea Grant Tech. Rep. UNIHI-SEAGRANT-TR-75-03.* also as *HIG-75-10*, Hawaii Inst. of Geophys., Univ. of Hawaii, pp36.
- Moberly, R.J. and F.T. Mackenzie (1985) Climate change and Hawaii: significance and recommendations. *HIG-85-1*, Hawaii Inst. of Geophys., Univ. of Hawaii, pp33.
- Nakiboglu, S.M., K. Lambeck, and P. Aharon (1983) Postglacial sealevels in the Pacific: implications with respect to deglaciation regime and local tectonics. *Tectonophysics*, 91, 335-358.
- Noda, E.K. and Associates, and DHM Inc. (1989) Hawaii shoreline erosion management study. Hawaii Coastal Zone Management Program, Office of State Planning.
- Parker, S. (1987) Seasonal Changes in Beach Characteristics on the Island of Oahu, Hawaii. M.S. Thesis, Univ. of Hawaii, pp 122.
- Patzert, W.C. (1969) Eddies in Hawaiian Waters. *HIG-69-8*, Hawaii Inst. of Geophysics, Univ. of Hawaii.

- Peirce, T.J. and D.J.A. Williams (1966) Experiments on certain aspects of sedimentation of estuary muds. *Proc. Inst. Civil. Eng.*, 34, 391-402.
- Peltier, W.R. and A.M. Tushingham (1989) Global sea level rise and the greenhouse effect. *Science*, 244, 806-810.
- Penland S. and K.E. Ramsey (1990) Relative sea-level rise in Louisiana and the Gulf of Mexico: 1908-1988. *J. Coastal Res.*, 6(2), 323-342.
- Pickard, G. and W.J. Emery (1982) Descriptive Physical Oceanography -- An Introduction. (4th ed.) Pergamon Press, pp249.
- Pilkey, O.H., R.S. Young, S.R. Riggs, A.W. Sam Smith, H. Wu, and W.D. Pilkey (1993) The concept of shoreline profile of equilibrium: a critical review. *J. Coastal Res.*, 9(1), 255-278.
- Pruszek, Z. (1993) The analysis of beach profile changes using Dean's method and empirical orthogonal functions. *Coastal Eng.*, 19, 245-261.
- Rayner, R.F. and S.J. Archer (1985) Evaluation and calibration of oceanographic instruments -- the user's view., 23-34, in Evaluation, Comparison and Calibration of Oceanographic Instruments, vol. 4, Graham & Tritman Ltd., pp267.
- Roelvink, J.A. and M.J.F. Stive (1989) Bar-generating cross-shore flow mechanisms on a beach. *J. Geophys. Res.*, 94(C4), 4785-4800.
- Schwartz, M.L. (1965) Laboratory study of sea-level rise as a cause of shore erosion. *J. Geol.*, 73, 528-
- Schwartz, M.L. (1967) The Bruun theory of sea-level rise as a cause of shore erosion. *J. Geol.*, 75, 76-
- Scott, G.A.J. and G.M. Rotondo (1983) A model for the development of types of atolls and volcanic islands on the Pacific lithosphere plate. *Atoll Res. Bull.*, 260, pp33.
- Shoshany, M. and A. Degani (1992) Shoreline detection by digital image processing of aerial photography. *J. Coastal Res.*, 8(1), 29-34.
- Simpson, R.H., and H. Riehl (1980) The hurricane and its Impact. Blackwell, Oxford.

- Steetzel, H.J. (1990) Cross-shore transport during storm surges. *Proc. 22th Coastal Eng.*, 1922-1934.
- Stokes, G.G. (1845) *Trans. Camb. Phil. Soc.*, 8, 287.
- Sturges, W. (1987) Large-scale coherence of sea level at very low frequencies. *J. Phys. Oceanogr.*, 17, 2084-2094.
- Thieke, R.J. and R.J. Sobey (1990) Cross-shore wave transformation and mean flow circulation. *Elsevier Sci. Pub.*, Amsterdam, *Coastal Eng.*, 14, 387-415.
- Trupin, A., and J. Wahr (1990) Spectroscopic analysis global tide gauge sea-level data. *Geophys. J. International*, 100, 441-453.
- Vellinga, A.P. (1986) Beach and dune erosion during storm surges. Ph.D. thesis, Delft Univ. of Technology, Delft, The Netherlands.
- Walker, J.R. (1974) Recreational Surf Parameter. *Tech. Rep.*, UH-Look Lab-73-30, Dept. Ocean Eng., Univ. of Hawaii.
- Wang, N. (1993) Sediment transport and nearshore circulation. Ph.D dissertation, Univ. of Hawaii.
- Wigley, T.M.L. and S.C.B. Raper (1992) Implications for climate and sea level of revised IPCC emission scenarios. *Nature*, 351, 293-300.
- Wong, K.W. (1980) Basic mathematics of photogrammetry. In: C.C.Slama (ed.), *Manual of Photogrammetry*, 4th Ed., American Soc. Photogr., Falls Church, VA, pp1056.
- Woodworth, P.L. (1991) The permanent service for mean sea level and the global sea level observing system. *J. Coastal Res.*, 7(3), 699-710.
- Wyrteki, K. and S. Nakahara (1984) Monthly maps of sea level anomalies in the Pacific: 1975-1981. *HIG-84-3*, Hawaii Inst. of Geophys., Univ. of Hawaii.
- Wyrteki, K., B.J. Kilonsky, and S. Nakahara (1988) The IGOS sea level pilot project in the Pacific. JIMAR contribution no. 88-0150, Univ. of Hawaii.
- Wyrteki, K. (1990) Sea Level Rise: The Facts and the Future. *Pac. Sci.*, 44(1), 1-16.